

STUDY ON CRUSTAL STRUCTURE OF JAPANESE ISLAND ARCS AS REVEALED FROM MAGNETIC AND GRAVITY FIELD ANALYSIS †

Yoshio UEDA*

CONTENTS

ABSTRACT

CHAP. I. INTRODUCTION

CHAP. II. DESCRIPTION OF THE METHOD FOR MAGNETIC AND GRAVITY FIELD ANALYSIS

- 2.1 Two-dimensional inversion method to derive magnetic basement relief
from magnetic anomaly using Fourier expansion method
- 2.2 Inversion method to derive magnetic basement relief from magnetic
anomaly based on Fourier transform method
- 2.3 Definition of magneto-gravity response function
- 2.4 Definition of magneto-gravity response filter
- 2.5 Response of gravity to topography
- 2.6 Correlation analysis in the space domain

CHAP. III. CRUSTAL STRUCTURE OF KURILE AND HONSYU ARCS AS REVEALED FROM MAGNETIC AND GRAVITY FIELD ANALYSIS

- 3.1 Airborne magnetic survey by the Hydrographic Department of Japan(JHD)
- 3.2 Data processing of airborne magnetic survey data
- 3.3 Gravity anomaly data used in the present study
- 3.4 General features of magnetic anomaly profiles over the Japanese Islands
and their adjacent seas
- 3.5 Hokkaido and northeast Honsyu
- 3.6 Central Honsyu
- 3.7 Southwest Honsyu
- 3.8 Discussions and concluding remarks of chapter III

CHAP. IV. CRUSTAL STRUCTURE OF THE IZU--OGASAWARA(BONIN) ARCS AS REVEALED FROM MAGNETIC AND GRAVITY FIELD ANALYSIS

- 4.1 Data description
- 4.2 Geological settings

† Received 17th November 1993.

* 海上保安学校 Maritime safety school

- 4.3 Characteristic features of magnetic and gravity anomalies
- 4.4 Characteristics of the crustal structure
- 4.5 Estimation of ρ/J ratio at the Moho boundary
- 4.6 Discussions and concluding remarks of chapter IV

CHAP. V. CRUSTAL STRUCTURE OF THE RYUKYU ARC AND ITS ADJACENT SEAS AS REVEALED FROM MAGNETIC AND GRAVITY FIELD ANALYSIS

- 5.1 Data description
- 5.2 Geological settings
- 5.3 Characteristic features of gravity anomalies
- 5.4 Characteristic features of magnetic anomaly and the magnetic basement structure derived from it
- 5.5 Pseudo-gravity analysis
- 5.6 Bulk magnetization of the Ryukyu Arc
- 5.7 Two-dimensional magneto-gravity response analysis
- 5.8 Discussions and concluding remarks of chapter V

CHAP. VI. CRUSTAL STRUCTURE OF THE DAITO RIDGE AS REVEALED FROM MAGNETIC AND GRAVITY FIELD ANALYSIS

- 6.1 Background
- 6.2 Data description
- 6.3 Gravity-topography response analysis
- 6.4 Magneto-gravity response analysis
- 6.5 Three-dimensional gravity and magnetic basements of the Daito ridge
- 6.6 Discussions and concluding remarks of chapter VI

CHAP. VII. DISCUSSIONS AND CONCLUSIONS

ABSTRACT

This paper consists of seven chapters, ① introduction, ② description of the method for magnetic and gravity field analysis, ③ crustal structure of Kurile and Honsyu arcs as revealed from magnetic and gravity field analysis, ④ crustal structure of the Izu-Ogasawara (Bonin) Arcs as revealed from magnetic and gravity field analysis, ⑤ crustal structure of the Ryukyu Arc and its adjacent seas as revealed from magnetic and gravity field analysis, ⑥ crustal structure of the Daito ridge as revealed from magnetic and gravity field analysis, and ⑦ discussions and conclusions.

In succession of chapter I, the methods used in the present study are explained in chapter II with the results of the numerical examples, i.e. (1) two-dimensional inversion of magnetic anomaly to obtain the magnetic basement relief using the Fourier expansion method, (2) three-dimensional inversion method based on Oldenburg's two-dimensional formula, (3) definition of the magneto-gravity response function to derive the magnetization direction and ρ/J ratio of the source body, (4) definition of magneto-gravity response filter to extract the magnetic anomalies correlative with gravity anomalies.

The method of correlation analysis in the space domain is also described to obtain the magnetization intensity and ρ/J ratio of the source bodies. The new method described in (3) and (4) will enable us to derive an inclination of magnetization vector without any assumption of the shape and location of the source body. These methods can also discriminate between the magnetic anomaly produced by the upper boundary and that by the lower boundary of the magnetized layer.

In chapter III, magnetic basement structures of Kurile and Honsyu arcs consistent with gravity field are presented by selecting typical anomalies such as the Sanriku-Isikari linear anomaly (SILA) in the northeast Honsyu, the Kusiro-Nemuro linear anomaly (KNLA) in the coastal region of the southeastern part of Hokkaido, the southwest Honsyu linear anomaly (SWHLA) in the inner region of southwest Honsyu, and the broad negative anomalies in the outer region of central Honsyu. The model for SILA derived reveals a good agreement between the Conrad surface and the magnetic basement uplift. The model for KNLA also shows the magnetic layer corresponding to the density boundary within the crust. The negative broad magnetic anomaly of the central part of Honsyu seems to be ascribed to the seismic velocity boundary in the crust. A considerably large dimension of the magnetic source is required for SWHLA, but the associated Bouguer gravity anomaly is featureless.

The magnetic basement models presented above reveal the magnetic sources in the upper crust with low ρ/J ratio as well as those in the lower crust with appreciable density contrast as is the case of SILA and KNLA. The former source may be the granitic rocks of magnetite series or serpentinite suites of high magnetic susceptibility. The magnetic structures of northeast Honsyu and Kurile arcs are consistent with lithological model inferred from the magnetization of xenolith samples.

In chapter IV, the magnetic basement model covering the Izu-Ogasawara Arc is completed from the geological/geophysical considerations. Different features of magnetic basement are confirmed between the northern and the southern part of the Izu-Ogasawara Arc with the border at the Sofugan tectonic line (Yuasa, 1992). The magnetic massives of the inner forearc highs of the northern arc show relatively low ρ/J ratio correlative to acidic to andesitic buried bodies. The magnetic anomalies of the Nisi-Sitito ridge are well explained by the normal magnetization of topographic uplifts.

The bulk magnetization per unit km^2 along the Quaternary volcanic front of the southern arc becomes 2.3 times as strong as that of the northern arc. These features may be explained by the stable location of the volcanic front in the southern arc as inferred from old volcanic edifices overlapped by the Quaternary volcanic ones.

In chapter V, the magnetic basement model over the Ryukyu Arc and its adjacent seas is completed from the geological/geophysical considerations. This model reveals the existence of the segmented large magnetic massives having low ρ/J ratio beneath the Tunghai Shelf break. Besides, the Miocene volcanic basement block located in the trenchward side of the Quaternary volcanic front suggests the southeastward migration of the central Ryukyu.

In chapter VI, the magnetization of the Daito ridge is discussed based on the magneto-gravity response analysis. The inclination of the magnetization vector derived shows a good agreement with the present field direction, contrary to the shallow inclination derived from the DSDP sediment core

previously. The above features suggest that the magnetization of the Daito ridge is caused by an enhanced magnetic susceptibility or viscous remanent magnetization.

Throughout the present study, the characteristic features of the crust are made apparent for the Japanese Island Arcs from the viewpoint of the magnetic, gravity and topographic features. Especially, the distribution of the magnetic massives with low ρ/J ratio becomes apparent, i.e. in the inner zone of southwest Honsyu Arc, the forearc area of the northern part of the Izu-Ogasawara Arc, and the eastern margin of the Tunghai Shelf. The granitic to andesitic rocks rich in magnetite seem to be the most plausible candidate as the source body. Until now, the granitic rock of magnetite series have been thought to be produced in the back-arc side of the arc-trench system. The present study, however, proposes the other case outcropping in the forearc region of the Izu-Ogasawara Arc. Forearc magnetism in the initial stage of subduction and dehydration process of the subducting plate may be related with the origin of these magnetic sources in the forearc region.

The magnetic and gravity field analyses on the Izu-Ogasawara and Ryukyu arcs suggest that the undulation of the Moho boundary may be the source of the regional trend of the surface magnetic anomalies. Present study also reveals the significant contribution of magnetic susceptibility to the observed magnetic anomalies. This mechanism may arise from enhanced initial susceptibility at high temperature and/or the enhanced viscous remanent magnetization of the deep-seated source. The experimental results concerning the enhanced susceptibility may give a significant constrain for constructing the magnetic structure of the crust in the Japanese Islands and the surrounding areas.

CHAPTER I. INTRODUCTION

The main point of this paper is that it handles almost all the magnetic, gravity and topographic data available around Japan and processes them by a new and unified method.

The Japanese Island Arcs consist of several arcs such as Kurile, Honsyu, Ryukyu, and Izu-Ogasawara arcs. These arcs face subducting plate boundaries, being characterized by thick continental crust. They are also accompanied by active volcanism, seismicity and high heat flow in the back-arc region. The Daito ridge is also a remnant old-island arc as inferred from the existence of the thick continental crust. Although the plate tectonics has paved the way to the understanding of the global tectonic history, there still remain unsolved subjects related to the regional

tectonics and the origin of the characteristic features of the continental crust of the arcs.

To clarify the structure of these islands arcs is an important clue for understanding petro-physical properties of the crust, rock magnetism of deep seated source body, geological structures and petrological/chemical condition at depth, as well as for the construction of the tectonic framework of the arcs.

In recent years, the data base of topography and magnetic/gravity anomaly has become available through the Japan Oceanographic Data Center (JODC) as the results of enormous surveys conducted by the organizations in charge of mapping the geophysical data. The data base has enabled us to compile regional/global map of topography, magnetic and gravity field anomalies. These maps are helpful for understanding

the geological/geophysical features of the island arcs, but, the potential field anomaly map itself is insufficient to understand the crustal structure in the quantitative manner. For instance, the magnetic body of the same shape with the same magnetization intensity produces different magnetic anomalies when the body is placed at different geographic position due to skewness effect depending on ambient field directions.

To elucidate the crustal structure of the island arcs using these data bases is an indispensable subject for understanding the physical/chemical state of the crust as well as its compositional state. For this purpose, it is urged to establish a comprehensive analysis method incorporating magnetic, gravity and topographic data. In response to the above circumstances, this paper presents several new ideas for comprehensive analysis method of magnetic and gravity anomalies using the topographic data and shows the magnetic structure of the Japanese Island Arcs and the Daito ridge through geological and geophysical interpretations.

The analytical methods developed in this study are the synthetic analysis of magnetic and gravity anomalies using magneto-gravity response function and the extraction of magnetic anomalies correlative with gravity anomalies using magneto-gravity response filter. These new methods enable us to obtain the direction of magnetization vector without assuming the geometry and location of the source body. Two-dimensional and three-dimensional magnetic inversion method to calculate magnetic basement from magnetic anomalies are presented with some numerical examples. The correlation analysis in space domain is also formulated for calculation of the density over magnetization ratio ρ/J

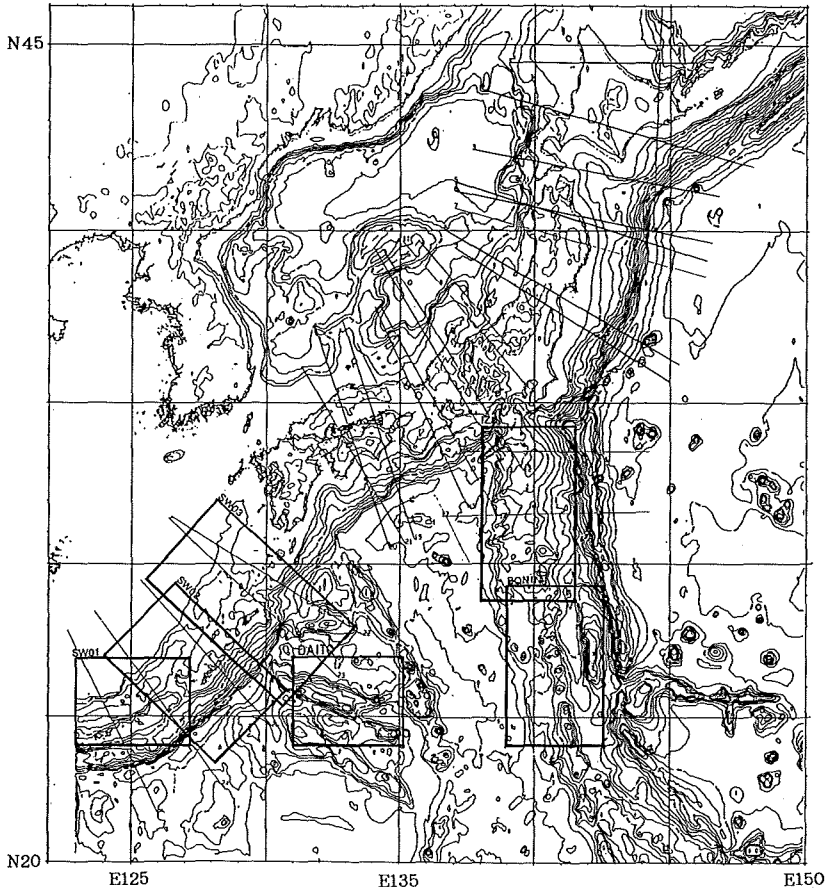
and magnetization intensity of the topographic uplift.

The above methods will be applied for the representative transections over the Kurile and Honsyu Arcs and for the areal survey data covering the Izu-Ogasawara Arc, the Ryukyu Arc and its adjacent seas, and the Daito ridge, as shown in Fig.1.1, to clarify the characteristic features of the continental crust.

The data source of magnetic transections of the Kurile and Honsyu Arcs are from the results of airborne magnetic surveys conducted by the Hydrographic Department of Japan (JHD) from 1984 to 1985 (JHD, 1988). The above magnetic data provide long transections crossing these arcs free of secular variation field, which attracts the author to analyze these magnetic profiles by the newly developed magneto-gravity response method to elucidate the crustal structure of the arcs. The areal data used for the present study are based on MGD77 data files supplied from JODC. The original data were also measured by JHD as part of the continental shelf survey project covering the seas in the vicinity of the Japanese Island Arcs and its marine economical zones. The MGD77 data files are composed of the digital data of water depth, magnetic anomaly, and free-air gravity anomaly, as well as those of the date of survey and ship's location. These data enable us to calculate the grid data covering the regional areas shown in Fig.1.1.

Regional magnetic anomaly maps covering the Japanese Islands and their adjacent seas have been compiled by several authors (Segawa and Oshima, 1975; Okubo et al., 1985; Oshima, 1987). These maps reveal that the continental crust also produces conspicuous linear magnetic anomalies with large amplitude comparable with oceanic

Fig.1.1 Location map of the profiles and areal survey data used for present study.



magnetic lineations, as seen over northeast Honshu and the continental shelf in the south offing of southeast Hokkaido. Segawa and Oshima (1975) named these anomalies the continental linear anomalies. But, the origin of these anomalies is still of debate. Magnetic modelling of the continental linear magnetic anomaly over northeast Honshu (Sanriku-Isikari linear anomaly: SILA) has been cited as the palaeomagnetic evidence showing the clockwise rotation of northeast Honshu. However, there remain some ambiguities of magnetization direction due to arbitrary assumption of the location and shape of the source body. In addition to the above continental linear anomalies, distribution of distinguished magnetic anomalies originated from the continen-

tal crust will be made apparent through the present study as shown in the inner part of southwest Honshu, in the forearc region of the Izu-Ogasawara Arc, and in the eastern margin of the Tunghai shelf of the East China Sea. The broad negative anomalies also become apparent in the outer region of central Honshu. These continental magnetic anomalies are helpful to investigate the crustal structure and rock magnetism at depth. Magneto-gravity response analysis of these continental anomalies may offer more convincing constraints for the origin and palaeomagnetic implications of these magnetic anomalies because of more objective assumptions involved in the analysis.

As to the Izu-Ogasawara Arc, the different

geophysical and petrochemical features between the northern and southern Izu-Ogasawara Arc bordered at the Sofugan Tectonic line are proposed by Yuasa and Murakami (1985). The above different features may be related to the different state of mantle materials as inferred from the distinct change of the subducting plate angle between the northern and southern arcs. Besides, the different tectonic history may also be plausibly assigned as suggested by Yuasa and Nohara (1992). The recent fulfilment of geophysical surveys may give a significant contribution to the tectonics of the Izu-Ogasawara Arc. The following two different models have been proposed for the tectonic history of the Izu-Ogasawara Arc. Uyeda and Miyashiro (1974) ascribed the origin of the arc to the N-S trending transform fault of the Kula-Pacific Plate. On the other hand, Seno and Maruyama (1984) to the W-E trending subduction zone in the Philippine basin at the Eocene age. The palaeomagnetic measurements of the igneous rocks sampled from the Ogasawara ridge (Haston and Fuller, 1991) is in favour of the latter model. The above easterly deflected magnetization, however, should be confirmed by the potential field analysis in a more convincing way. To study this subject, the assumption of normal magnetization of the uplifts of the Nisi-Sitito ridge and the Ogasawara ridge is examined based on the correlation analysis in space domain.

Concerning the Ryukyu Arc and its adjacent seas, zonal arrangement of geological structures have been proposed by several authors (Hatae, 1955; Konishi, 1965; Kizaki, 1978). These zonations also assume that the topographic depressions of the Tokara channel and the Kerama Gap as the left lateral faults segmenting the

Ryukyu Arc, which may be related to the south-eastward migration of the Ryukyu Arc. Preliminary magnetic zonation was assumed by Ueda (1986) to assess the above geological zonation of the Nansei-Syoto islands covering the Ryukyu Arc. Dense sea-bottom surveys conducted by JHD also made apparent the detailed features of topography, magnetic, and gravity anomalies of the Ryukyu Arc and its adjacent seas (Oshima et al., 1988; Okuma et al., 1991; Kasuga et al., 1992). These results have provided more convincing magnetic zonations covering the Ryukyu arc-trench system and the Tunghai shelf region, taking into account the topographic and gravity features.

The magnetic modelling of the Okinawa Trough given by Oshida et al. (1992) indicates that the anomalies are not the spreading linear anomalies but the reflection of the magnetized layers of P-wave velocity 3.6-6.4 km/s. But, the upheaved Bouguer gravity anomaly over the Okinawa Trough is not taken into account in their model. In the present study, an alternative model to explain both magnetic and gravity features in a consistent way is proposed.

The Daito ridge is thought to be a remnant old-island arc as inferred from crystalline schist and acidic plutonic rocks discovered from the ridge (Shiki et al., 1979). The gravity analysis on the Daito ridge (Segawa, 1976) also clarify the thick continental crust showing isostatic compensation. In spite of the above aspects, conspicuous magnetic anomalies are associated with the Daito ridge (Kasuga et al., 1986). The magneto-gravity response analysis on the Daito ridge may clarify the significant role of enhanced magnetic susceptibility and/or viscous remanent magnetization instead of thermal remanent magnetization.

Through the present study, the characteristic features of the crustal structure of the Japanese Island Arcs will be summarized and their tectonic implications will be made more apparent. The magnetic structure thus derived may contribute significantly to the establishment of the lithological model of the crust when combined with rockmagnetism of xenolith samples. The magnetic property of the crust is also constrained by the fugacity (O_2)-temperature equilibrium condition as well as mineral composition. These conditions are closely related with dehydration process of the subducting plate (Tatsumi, 1989). The new aspect of the existence of the magnetic sources of low ρ/J ratio may offer the basic constraint for the construction of the tectonic framework and magmatism in the deep crust. The significant role of the enhanced magnetic susceptibility and/or viscous remanent magnetization of the deep-seated magnetic sources will be discussed based on the derived magnetic structural models. The magnetic signals of the Moho boundary are also described for the case of the Izu-Ogasawara Arc and the Okinawa Trough. These results may be significant for understanding petrophysical, petrological features of the lower crust above the Moho boundary.

CHAPTER II. DESCRIPTION OF THE METHOD FOR MAGNETIC AND GRAVITY FIELD ANALYSIS

2.1 Two-dimensional inversion method to derive magnetic basement relief from magnetic anomaly using Fourier expansion method

2.1.1 Theoretical background

Let us consider a rectangular coordinate system

with the positive z -axis pointing downward. Then, magnetic potential in free space is given by

$$\phi_m = \int_V \mathbf{J} \cdot \text{grad}(1/r) dv, \quad (1)$$

where \mathbf{J} represents magnetization vector and v the volume of a source body.

According to Kato (1975a,b), a pseudo-gravity potential ϕ_{pg} , and pseudo gravity F_{pg} are defined as

$$\phi_{pg} = \int_V (\mathbf{J}/r) dv, \quad F^{PG} = \partial \phi_{pg} / \partial z. \quad (2)$$

Then, gravity potential (ϕ_g) is given by $\phi_g = \phi_{pg} \cdot \rho \cdot G_c / J$ and gravity anomaly (F^G) by $F^G = F^{PG} \cdot \rho \cdot G_c / J$, where G_c is the gravitational constant.

The magnetic potential ϕ_m and the magnetic anomaly field F^M are related with the pseudo-gravity ϕ_{pg} by

$$\phi_m = \phi_{pg} / \partial \beta, \quad F^M = \partial \phi_m / \partial \alpha = \partial^2 \phi_{pg} / \partial \alpha \partial \beta, \quad (3)$$

where α, β represent the direction of magnetic field and magnetization respectively.

Consider a two-dimensional coordinate system shown in Fig. 2.1, where Z -axis is positive downward and X -axis in the profile direction. Then, a pseudo-gravity δF^{PG} due to a horizontal plate at depth Z and with the thickness δZ is given by

$$\delta F^{PG}(Z) = 2\pi J \delta Z, \quad (4)$$

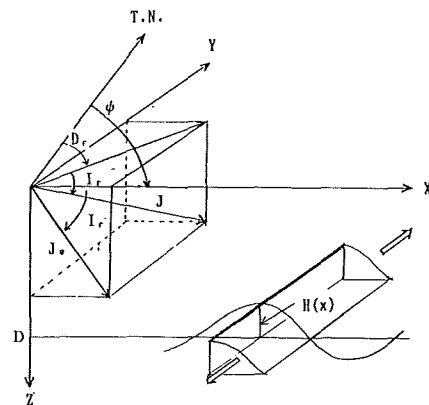


Fig. 2.1 Coordinate system of two-dimensional magnetic analysis.

where J is magnetic moment per unit volume.

As the magnetic moment varies in the X -direction, $J(x)$ can be expressed in terms of Fourier expansion series:

$$\begin{aligned} J(x) &= \sum_m (a_m J \cos mx + b_m J \sin mx) \\ &= \sum_m J_m \end{aligned} \quad (5)$$

where $m = 2\pi M / \lambda_0$, M is wavenumber, and λ_0 is basic wavelength. Equation (4) can be expressed by the Fourier term of wavenumber m in the following way:

$$\delta F_m^{PG}(Z) = 2\pi J_m \delta Z, \quad (6)$$

Then, the pseudo-gravity at ground level ($z=0$) is given by

$$\delta F_m^{PG}(0) = 2\pi J_m \cdot e^{-mz} \cdot \delta Z, \quad (7)$$

The magnetic anomaly due to a plate with the upper and the lower depths at Z_1, Z_2 is calculated through vertical integration of Eq. (7) as follows:

$$\begin{aligned} F_m^{PG}(0) &= \int 2\pi J_m \cdot e^{-mz} \cdot dZ \\ &= 2\pi J_m \cdot (e^{-mz_1} - e^{-mz_2}) / m, \end{aligned} \quad (8)$$

From Eq. (8) magnetic moment of wavenumber m becomes

$$J_m = m F_m^{PG}(0) / \{2\pi(e^{-mz_1} - e^{-mz_2})\} \quad (9)$$

The distribution of the magnetic moment of a horizontal layer with a finite thickness $\delta\xi$ can be transformed to the relief of magnetic basement with constant magnetization J_0 on the assumption that the product $\delta\xi \cdot J(x)$ is equal to $J_0 \cdot H(x)$, where $H(x)$ represents the relief of magnetic basement with constant magnetic moment J_0 .

From this relation, $H(x)$ becomes

$$H(x) = \pm \delta\xi \cdot J(x) / J_0, \quad (10)$$

where a positive sign is adopted for derivation of an upper surface and a negative sign for derivation of a lower boundary (Ueda and Kato, 1991).

2.1.1.2 Algorithm

Let the magnetic anomaly profile be denoted by $F(x)$. This can be expressed in terms of Fourier expansion series as

$$F(x) = \sum_m (a_m \cos mx + b_m \sin mx) \cdot e^{mz} \Big|_{z=0}, \quad (11)$$

where, the observed plane is defined as $z=0$.

After Kato (1975a, 1975b), the above equation can be expressed as a matrix product as

$$F(x) = \{A_m\} \{\Delta_m\} e^{mz} \Big|_{z=0}, \quad (12)$$

where, $\{A_m\} = (a_m, b_m)$, $\{\Delta_m\} = (\cos mx, \sin mx)^T$.

The first derivation of $F(x)$ along the direction cosine vector $\alpha(l, m, n)$ is given by

$$\begin{aligned} \partial F(x) / \partial \alpha &= \partial F(x) / \partial x \cdot l + \partial F(x) / \partial z \cdot n \\ &= \sum \{A_m'\} \{\Delta_m\} e^{mz} \Big|_{z=0}, \end{aligned} \quad (13)$$

where l is positive in the X direction, n is positive downward, and Y -axis is normal to the X - Z plane. In the above equation, the coefficient vector $\{A_m'\}$ is related to $\{A_m\}$ by

$$\{A_m'\} = m \begin{pmatrix} n \\ l \end{pmatrix} \{A_m\}^T = \{D_m\} \{A_m\}. \quad (14)$$

The above matrix $\{D_m\}$ is called, "differential operator". If the direction cosine vector (l, m, n) is parallel to the present magnetic field, l and n are given by

$$l = \cos(I_0) \cos(\psi - D_0), \quad n = \sin(I_0) \quad (15)$$

where I_0, D_0 are inclination and declination of the present field and ψ is the azimuth of the X -axis. Furthermore, an effective inclination I_0' is related to the direction cosine by

$$\tan I_0' = n/l, \quad (n^2 + l^2)^{1/2} = |\sin I_0 / \sin I_0'|. \quad (16)$$

Using the above relation, it becomes apparent that the differential operator multiplies the amplitude by a factor of $m \cdot |\sin I_0 / \sin I_0'|$ and shifts the phase by $\delta\theta = \pi/2 - I_0'$.

On the other hand, we can derive the integral operator $\{I_m\}$ from the inverse relation of

$$\{E\} = \{D_m\} \cdot \{I_m\} \quad (17)$$

where $\{E\}$ denotes a unit matrix. From the above equation, the integral operator becomes

$$\{I_m\} = 1/m \cdot (n^2 + l^2) \begin{pmatrix} n \\ l \end{pmatrix}. \quad (18)$$

Taking Eq. (16) into consideration, the integral operator multiplies the amplitude by a factor of $|\sin I_0' / m \sin I_0|$ and shift the phase by

$$\delta\theta = I_0' - \pi/2.$$

From Eq. (3), we can derive Fourier coefficients of the pseudo-gravity $\{A_m^{PG}\}$ from Fourier coefficients of magnetic anomaly field $\{A_m\}$ by conducting the double integration along polarized direction $\beta(L, M, N)$ and magnetic field direction $\alpha(l, m, n)$ and then single differentiation in the downward direction. These operations are expressed in terms of the operators as

$$\{A_m^{PG}\} = m \{I_m\}_{L,N} \{I_m\}_{l,n} \{A_m\}. \quad (19)$$

Total amount of phase shift by the above operations becomes

$$\delta\theta = I_0' + I_r' - \pi. \quad (20)$$

This parameter has the same form as the skewness parameter defined by Schouten and Mccamy (1972).

Referring to Eq. (9), Fourier coefficients $\{A_m^J\}$ of the magnetic moment distribution on the horizontal tabular body with a constant thickness $z_2 - z_1$ become

$$\begin{aligned} \{A_m^J\} &= m \{A_m^{PG}\} / \{2\pi(e^{-mz_1} - e^{-mz_2})\}, \\ &= m^2 \{I_m\}_{L,N} \{I_m\}_{l,n} \{A_m\} / \{2\pi \\ &\quad (e^{-mz_1} - e^{-mz_2})\}. \end{aligned} \quad (21)$$

Using the above coefficients, we can obtain the distribution function of magnetic moment $J(x)$ as

$$J(x) = \sum_m \{A_m^J\} \{\Delta_m\}. \quad (22)$$

Let denote the upper surface and the lower boundary of a magnetic layer by $DU(x)$ and $DL(x)$, and their mean depth by UP_0 and BT_0 , respectively. It is reasonable to separate magnetic anomaly into two components by filtering; one is relatively short-wavelength anomalies attributable to the upper surface of the causative magnetic layer and the other relatively long-wavelength ones attributable to the lower boundary. Referring to Eq. (10), the relief $DU(x)$ and $DL(x)$ become

$$DU(x) = UP_0 - \delta\xi \cdot JU(x)/J_0, \quad \lambda_{U1} < \lambda_{UP} < \lambda_{U1}$$

$$DL(x) = BT_0 + \delta\xi \cdot JL(x)/J_0, \quad \lambda_{L0} < \lambda_{UP} < \lambda_{L1} \quad (23)$$

where $JU(x)$, $JL(x)$ are magnetic moments corresponding to the upper and lower boundary derived from bandpassed anomalies.

The topographic uplifts with wavelengths shorter than 160km are considered to be sustained by the elasticity of the crust, but those with wavelengths longer than 160km are compensated for by isostasy (Hagiwara, 1979). In the present study, it is tentatively assumed that high-pass filtered anomalies with the wavelengths shorter than 160km can be ascribed to the undulation of the upper surface and the low-pass filtered anomalies with the wavelengths longer than 160km to the lower boundary of the magnetic layer. Such operation is easily conducted by incorporating filtering algorithm. In the application of this method, the optimum window parameter may be determined by trial and error while adjusting cut-off wavelengths. Equation (23) is an approximation to convert the distribution of magnetic moment with a finite thickness to the undulation of the magnetic layer of constant magnetization intensity. Because this approximation ignores the contribution from the second and higher order terms of the relief to the Fourier components of magnetic anomaly (Parker, 1972), the relief obtained by the above method is somewhat different from the real relief from the exact point of view. So, the exact magnetization intensity should be re-evaluated by the least squares method. For this purpose, the magnetic layer derived from the above procedure is approximated by the sequence of horizontal tabular bodies as shown in Fig. 2.2. The magnetic anomalies of total force caused by these tabular bodies can be expressed as a sum of each contribution as

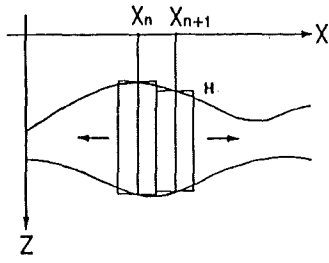


Fig.2.2 Approximation of the magnetic layer by the sequence of horizontal tabular bodies.

follows:

$$A(x) = \sum_n J_x K_1(x, x_n, z_n) + J_z K_2(x, x_n, z_n) \\ = \sum_n J (K_1 \cos I_r' + K_2 \sin I_r') \quad (24)$$

where K_1 and K_2 are parameters related to the model geometry, I_r' is an effective inclination of magnetization vector, x_n, z_n are coordinates of the four corners of the n -th tabular body (Johnson, 1969). The magnitude of J can be determined by the least squares algorithm from the observed $F(x)$ and calculated $A(x)$ anomalies. In the above calculation, a standard deviation and goodness-of-fitting ratio GFR (Uyeda and Richards, 1966) defined by the following Eq. (25), (26) are calculated to confirm the accuracy of the model derived.

$$\sigma = (\sum_n (A(x_i) - F(x_i))^2 / N)^{1/2}, \quad (25)$$

$$GFR = \sum_n |F(x_i)| / \sum_n |A(x_i) - F(x_i)|. \quad (26)$$

where N is the total number of data.

2.2 Inversion method to derive magnetic basement relief from magnetic anomaly based on Fourier transform method

2.2.1 Basic formula

Parker(1972) contrived the calculation method of potential field caused by a layer of uneven topography based on FFT algorithm. Let us consider a cartesian coordinate with z -axis pointing downward as shown in Fig.2.1. In the following explanation, we assume that the mean depth

to a source material is D , that the relief $h(x, y)$ is measured upward relative to a reference level of $z=D$ plane and that an observed plane is located in the X - Y plane at $z=0$. According to Parker (1972), the Fourier transform of gravity anomaly $G(u, v)$ is related to that of the relief of uneven layer as:

$$G(u, v) = 2\pi G_c \rho e^{-wD} \cdot \sum_{n=1} w^{n-1} / n! H_n(u, v) \quad (27)$$

where $H_n(u, v)$ denotes the Fourier transform of the n -th degree of a relief given by $h^n(x, y)$ and w is $(u^2 + v^2)^{1/2}$. Parker(1972) also demonstrated that the summation of the Fourier transform components converges under the condition of $\text{Max} \{h(x, y)\} / D < 1$ independently of wavenumber w . Oldenburg(1974) rearranged Eq.(27) to yield an iterative procedure for inverting two-dimensional gravity profiles. Here is shown the iterative formula for calculating the three-dimensional relief $h(x, y)$ from areal gravity field as:

$$H(u, v) = G(u, v) \cdot e^{wD} / (2\pi G_c \rho) - \sum_{n=2} w^{n-1} / n! \cdot H_n(u, v) \\ = G(u, v) \cdot e^{wD} / (2\pi G_c \rho) - \varepsilon(0), \quad (28)$$

where $\varepsilon(0)$ is a small term, which is usually neglected in a thin-layer approximation. This iterative algorithm at first begins under the assumption of $\varepsilon(0) = 0$, and then the newest estimation of $\varepsilon(0)$ iteratively obtained is subtracted from the first term for the derivation of updated relief $h(x, y)$. The above iteration is carried out until $h(x, y)$ converges. In practice, there exist the lower limit of ρ_{\min} and the upper limit of the reference depth D_{\max} in order to have the iteration converged. In relation to these conditions, Oldenburg(1974) incorporated low-pass filter algorithm to eliminate divergence of the result in the high frequency range, which is caused by downward continuation by the factor of e^{wD} as seen in the

term of Eq. (28).

For the inversion of magnetic anomaly to magnetic relief, we use pseudo-gravity defined in Eq. (2) instead of gravity field and replace the product $\rho \cdot G_c$ by J . In this case, the iteration formula corresponding to Eq. (28) becomes

$$\begin{aligned} H(u, v) &= G_{pg}(u, v) \cdot e^{wD} / (2\pi J) - \sum_{n=2} W^{n-1} / n! \cdot \\ &H_n(u, v) \\ &= G_{pg}(u, v) \cdot e^{wD} / (2\pi J) - \varepsilon(0), \end{aligned} \quad (29)$$

where $G_{pg}(u, v)$ is the Fourier transform of pseudo-gravity.

The Fourier transform of $G_{pg}(u, v)$ is deduced from the Fourier transform of magnetic field $F(u, v)$ as follows (Hagiwara, 1980; Kubota et al., 1989):

$$G_{pg}(u, v) = -w \cdot 1 / (lu + mv - inw) \cdot 1 / (Lu + Mv - iNw) \cdot F(u, v). \quad (30)$$

The combination of Eq. (29) and Eq. (30) gives the formula of magnetic inversion for the derivation of magnetic basement relief.

2.2.2 Numerical example

To know the criterion on which the above magnetic inversion method can be applied to the field analysis, a numerical examination is conducted using the magnetic anomalies caused by three-dimensional uplift. Figure 2.3(a) shows the three-dimensional uplift giving rise to magnetic anomaly illustrated in Fig. 2.3(b). The magnetic anomalies are calculated based on Parker's inversion formula, where the magnetization is assumed as $J=7.0A/m$, $D_r=-70^\circ$, $I_r=-15^\circ$ and the ambient magnetic field direction is $D_0=-3.5^\circ$, $I_0=35^\circ$ respectively. The magnetic anomaly was then processed according to the inversion algorithm of Eq. (29), (30). The inversion was conducted under different JT and ITR , where JT means the maximum of n adopted for the estimation of $H_n(u, v)$ and ITR iteration number. The

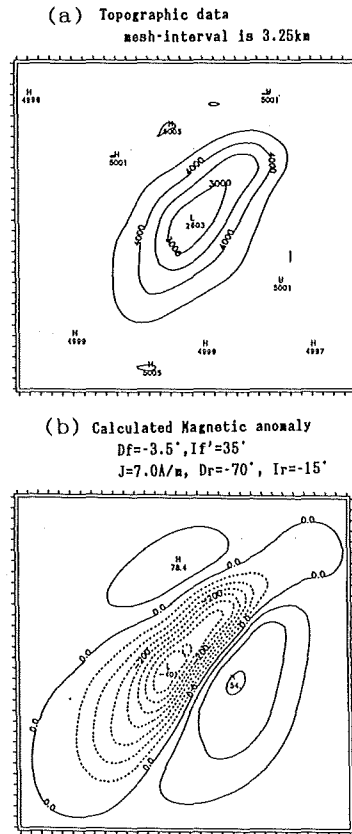


Fig. 2.3 Numerical test of 3-D iteration method using Oldenburg's formula.

results of numerical experiment are shown in Figs. 2.4 to 2.6. Figure 2.4(a) is the uplift obtained under the condition $JT=1$ and $ITR=1$, which corresponds to the thin-layer approximation. The calculated uplift under the above condition differs considerably from the original model. The difference amounts to 0.45km around the summit area as shown in Fig. 2.4(b). This disagreement exceeds 20% of the elevation of the real uplift. Figures 2.5 and 2.6 give the result for $JT=2$, $ITR=2$ and $JT=2$, $ITR=3$, respectively. If compared with Fig 2.4, the difference from the real uplift decrease significantly. For the case of $JT=2$, $ITR=3$, especially, the relative error is suppressed below 2% of the elevation of the input model. The inversion up to degree $JT=3$ was also

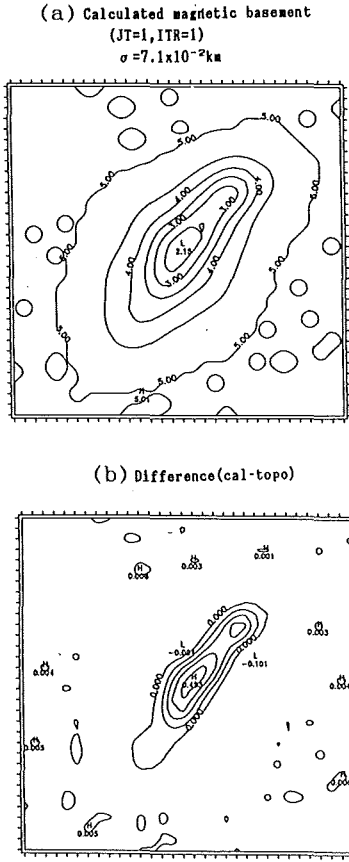


Fig.2.4 Calculated magnetic basement for input data shown in Fig.2.3(a).

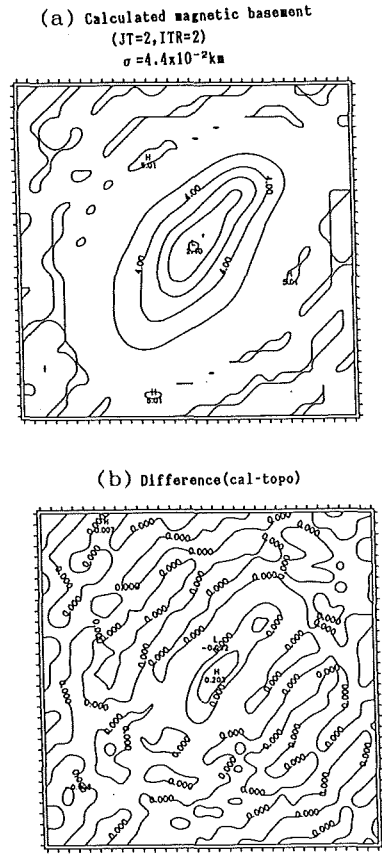


Fig.2.5 Calculated magnetic basement for input data shown in Fig.2.3(a).

attempted, but it proved to be a failure because of divergence of the result. Taking the above experiments into consideration, we adopt JT=2, ITR=3 for further inversion to obtain magnetic basement relief.

2.3 Definition of magneto-gravity response function

2.3.1 Two-dimensional magneto-gravity response function

(1) Derivation of formula

As already shown in the previous section, magnetic potential ϕ_m is related to gravity potential by Poisson's formula:

$$\phi_m = J / (G_c \cdot \rho) \partial \phi_g / \partial \beta \quad (31)$$

where the symbols have the same meaning as mentioned before.

In case of two-dimensional geometry of the source shown in Fig.2.1, these parameters vary only in the x-direction. Assuming that a function $f(x, z)$ is magnetic anomaly profile at altitude $Z = z$, and let $F(u, z)$ be the Fourier transform of $f(x, z)$, then:

$$f(x, z) = 1/2\pi \int F(u, z) \cdot e^{iux} du \quad (32)$$

where u is a wavenumber of the transformed function.

By differentiating Eq. (32) in the x-direction, we obtain

$$\partial f(x, z) / \partial x = 1/2\pi \int iu \cdot F(u, z) \cdot e^{iux} du. \quad (33)$$

This relation indicates that differential opera-

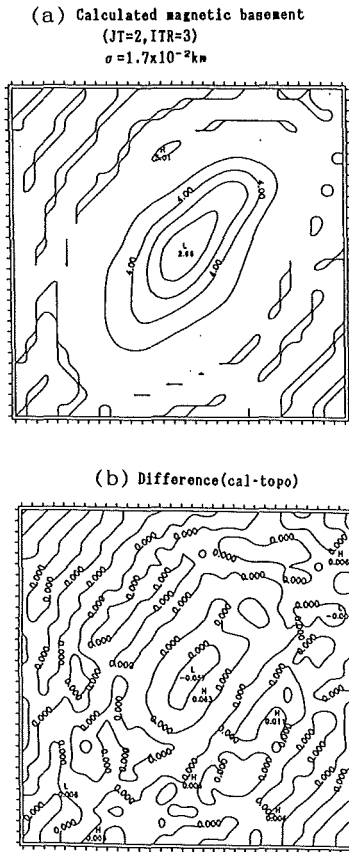


Fig.2.6 Calculated magnetic basement for input data shown in Fig.2.3(a).

tion in the x-direction inspace domain corresponds to multiplying the Fourier transform of the original function by iu (Oosaki, 1976; Kubota et al., 1989). Besides, potential field $f(x, z)$ must satisfy the relation

$$\nabla^2 f = \partial^2 f / \partial^2 x + \partial^2 f / \partial^2 z = 0. \quad (34)$$

This is equivalent to

$$\partial^2 F(u, z) / \partial^2 z = u^2 \cdot F(u, z). \quad (35)$$

Solving Eq. (35) under the condition of convergence ($z \rightarrow -Z$), we can breakdown the function of $F(u, z)$ as

$$F(u, z) = F(u) \cdot e^{uz}. \quad (36)$$

This equation implies that differential operation in the z -direction in space domain corresponds to multiplying the original Fourier transform by u in the frequency-domain. It is also apparent that the

integral operation in the x -direction in space domain results in dividing the original Fourier transform by iu .

By differentiating Eq(31) in the magnetic field direction, we obtain

$$f = \partial \phi_m / \partial \alpha = J / (G_c \cdot \rho) \partial^2 \phi_g / \partial \alpha \partial \beta. \quad (37)$$

Using the Fourier transform of magnetic anomaly and gravity potential, differential form of Eq. (37) can be expressed by:

$$F(u) = J / (G_c \cdot \rho) \cdot (iuL + nu) \cdot (iuL + Nu) \cdot \Phi_g(u). \quad (38)$$

As the Fourier transform of gravity field is related to that of gravity potential by $G(u) = u \cdot \Phi_g(u)$, Eq. (38) becomes

$$F(u) = J / (G_c \cdot \rho) \cdot (il + n) \cdot (iL + N) \cdot u \cdot G(u). \quad (39)$$

From this equation, Fourier transform $G(u)$ is given by

$$G(u) = - (G_c \cdot \rho) / J \cdot 1 / (1 - in) \cdot 1 / (L - iN) \cdot 1 / u \cdot F(u). \quad (40)$$

This equation is a formula to convert Fourier transform of magnetic anomaly to that of gravity anomaly (Ueda, 1990).

Now that,

$$\begin{aligned} (l^2 + n^2)^{1/2} &= | \sin I_o / \sin I_o' | \\ (L^2 + N^2)^{1/2} &= | \sin I_r / \sin I_r' | \end{aligned} \quad (41)$$

we get:

$$\begin{aligned} 1 - in &= (l^2 + n^2)^{1/2} \cdot e^{-iI_o'} \\ &= | \sin I_o / \sin I_o' | \cdot e^{-iI_o'} \\ L - iN &= (L^2 + N^2)^{1/2} \cdot e^{-iI_r'} \\ &= | \sin I_r / \sin I_r' | \cdot e^{-iI_r'}. \end{aligned} \quad (42)$$

Now, a combination of Eq(40) and Eq(41), (42) yields:

$$\begin{aligned} G(u) &= C \cdot 1 / u \cdot | \sin I_r' \cdot \sin I_o' | / | \sin I_r \cdot \sin I_o | \cdot \\ &\quad \exp \{ i(I_r' + I_o' - \pi) \} \cdot F(u) \\ &= \text{RES}(u) \cdot F(u), \end{aligned} \quad (43)$$

where $C = G_c \cdot \rho / J$, $G_c = 6.672 \times 10^{-8} \text{cm}^3 / \text{g} \cdot \text{sec}^2$.

Equation (43) gives the response function in frequency domain which yields gravity field as an

output from magnetic field as an input. The effective inclination of magnetization vector can be estimated from the phase factor (δ) of Eq (43) as:

$$I_r' = \delta - I_0' + \pi \quad (44)$$

without any assumption on the size and shape of the source body.

In the case of three-component magnetic field, Eq (44) is reduced to:

$$\begin{aligned} I_r' &= \delta + \pi \text{ for horizontal component,} \\ I_r' &= \delta + \pi/2 \text{ for vertical component.} \end{aligned} \quad (45)$$

Besides, the above method offers the frequency dependence of the effective inclination of magnetization vector. The effective inclinations in long-wavelength zone may be related to the magnetization of relatively deep-seated sources or relatively shallow sources with large horizontal dimension and those in short-wavelength zone related to the shallow-seated sources with intermediate to small dimension. In addition to the above features, the response function method enables us to judge whether the magnetic anomalies originated from the upper boundary or the lower boundary of the magnetic source layer. When the lower boundary of the causative layer polarized in the present magnetic field direction contributes to surface magnetic anomalies, the effective inclination of magnetization of I_r' may shift by about 180° from the value of I_0' of the present magnetic field, because of a negative density contrast of the lower boundary. This feature is especially useful for elucidating magnetic characteristics of the Moho boundary.

(2) Numerical example

To confirm the accuracy of the method in 2.3.1, numerical experiments are conducted. Figure 2.7(a) shows a tabular model and its calculated magnetic and gravity anomalies. The

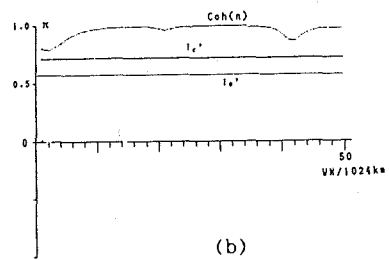
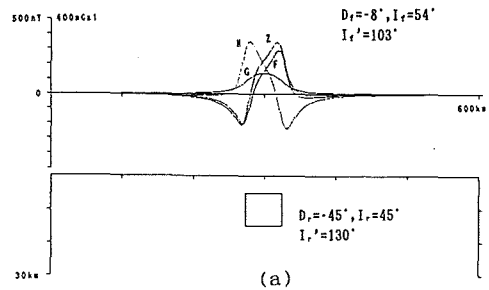


Fig.2.7 Numerical examples of two-dimensional magneto-gravity response analysis.

- (a): Magnetic and gravity anomaly profiles of a two-dimensional tabular body, which is used as numerical test data for verification of response function method. G:gravity anomaly, H:horizontal component, Z:vertical component, F:total intensity anomaly. Parameter of this model are listed in Table 2.1.
- (b): Effective inclination of magnetization vector (I_r') for the model shown in (a). I_0' :effective inclination of magnetic field, Coh:coherence between gravity and magnetic anomalies.

model parameter are listed in Table 2.1. Using the 256 calculated equi-distance data (4km interval), effective inclinations of magnetization are estimated. The results are indicated in Fig.2.7(b). It should be noted that the derived effective inclination I_r' precisely agrees with the assumed value 130° .

Table 2.1 Parameters for calculation of magnetic and gravity anomalies for Fig.2.7.

Parameters of model	Value
Top, bottom and width	5km, 15km, 50km
Dec & Inc of magnetic field	-8°, 54'
Effective inc. of field	103'
Dec & Inc of magnetization	-45°, 45'
Effective inc. of magnetization	130'
Magnetization intensity	3.0×10^{-3} emu/cc
Effective magnetization	2.75×10^{-3} emu/cc
Density contrast	0.4g/cc
Azimuth of profile	101'

Figure 2.8 shows another example of numerical experiment. The model parameters are listed in Table 2.2. In the case of this example, the deep-seated source(model B) and the shallow source(model A) have different effective inclination $I_r' = 103^\circ$ and $I_r' = 120^\circ$, respectively. With the same procedure, the derived I_r' are plotted against the wave-number as shown in Fig.2.8(b). It is noticeable that the value of I_r' becomes very close to the value of $I_r' = 103^\circ$ in the long-wavelength zone, which gradually approaches the value of 120° in the short-wavelength zone, although considerable differences occur in the intermediate zone. The derived value in the long-wavelength zone corresponds to the effective inclination of magnetization of the deep-seated source and those in short-wavelengths to shallow source. These numerical experiments may ensure the plausibility of response function method when applied to the field data.

2.3.2 Three-dimensional magneto-gravity response function

(1) Derivation of formula

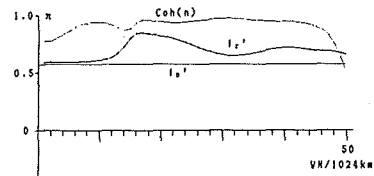
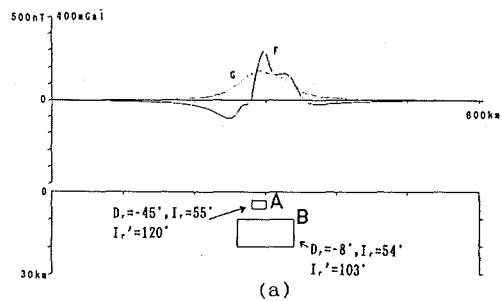
Let us consider a three-dimensional coordinate system shown in Fig.2.9. The relation between the Fourier transforms of areal magnetic and gravity field are given by

$$G(u, v) = -1 \cdot C \cdot w \cdot 1 / (lu + mv - inw) \cdot 1 / (Lu + Mv - iNw) \cdot F(u, v) \quad (46)$$

where u, v are wavenumbers defined by $2\pi/\lambda_x, 2$

Table 2.2 Parameters for calculation of magnetic and gravity anomalies for Fig.2.8.

Parameter	model A	model B
Top depth	3km	10km
Bottom depth	6km	20km
Width	20km	80km
Dec of magnetization	-45°	-8°
Inc of magnetization	55°	54°
Effective Inc I_r'	120°	103°
Magnetization intensity(emu/cc)	0.004	0.003
Effective intensity(emu/cc)	0.0038	0.0025
Dec & Inc of magnetic field	-8°, 54°	
Effective Inc of magnetic field	103°	
Azimuth of profile	101°	



(b)

Fig.2.8 Numerical examples of two-dimensional magneto-gravity response analysis.

(a): Magnetic and gravity anomaly profiles caused by two sources of two-dimensional tabular bodies, which are used as numerical test data for verification of response function method. G:gravity anomaly, F:total intensity anomaly. Parameter of this model are listed in Table 2.2.

(b): Effective inclination of magnetization vector (I_r') for the model shown in (a). I_0' :effective inclination of magnetic field, Coh:coherence between gravity and magnetic anomalies.

π/λ_y in the X and Y direction and $w = (u^2 + v^2)^{1/2}$, $C = G_c \cdot \rho / J$, respectively. $\alpha(l, m, n)$ and $\beta(L, M, N)$ are direction cosine of the present magnetic field and the magnetization vector, respectively. This formula is deduced from the original equation given by Hagiwara (1980) and Kubota et al. (1989) with minor modifications. The direction cosines are given by:

$$\begin{aligned}
 l &= \cos(I_o) \cdot \cos(D_o) \\
 m &= \cos(I_o) \cdot \sin(D_o) \\
 n &= \sin(I_o) \\
 L &= \cos(I_r) \cdot \cos(D_r) \\
 M &= \cos(I_r) \cdot \sin(D_r) \\
 N &= \sin(I_r)
 \end{aligned} \quad (47)$$

Here, we define the angle θ_l and θ_r as shown in Fig. 2.9, then

$$\begin{aligned}
 Lu + Mv &= (u, v) \cdot (L, M) \\
 &= w \cdot |\cos I_r| \cdot \cos(\theta_r)
 \end{aligned} \quad (48)$$

Hence, $Lu + Mv - iNw$

$$\begin{aligned}
 &= (u^2 + v^2)^{1/2} \cdot (L^2 + M^2)^{1/2} \cdot \{ \cos(\theta_r) - iN / \\
 &\quad (L^2 + M^2)^{1/2} \} \\
 &= w \cdot \cos(I_r) \cdot \{ \cos(\theta_r) - i \cdot \tan(I_r) \} \\
 &= w \cdot \cos(I_r) \cdot \{ \cos(\theta_r) / \cos(I_r') \} \cdot e^{-iI_r'} \quad (49)
 \end{aligned}$$

here,

$$\begin{aligned}
 |\tan(I_r')| &= |\tan(I_r) / \cos(\theta_r)| \\
 &\geq |\tan(I_r)|
 \end{aligned} \quad (50)$$

Combination of eq. (46) to (50) yields:

$$\begin{aligned}
 G(u, v) &= C/w \cdot \cos(I_r') \cdot \cos(I_o') / \{ \cos(I_r) \cdot \cos \\
 &\quad (I_o) \cdot \cos(\theta_r) \cdot \cos(\theta_l) \} \cdot \\
 &\quad \exp \{ i(I_r' + I_o' - \pi) \} \cdot F(u, v) \quad (51) \\
 &= \text{RES}(u, v) \cdot F(u, v)
 \end{aligned}$$

where $\text{RES}(u, v)$ is magneto-gravity response function.

As I_o' is a known parameter, the value of I_r' can be estimated from phase factor δ of Eq. (51) as follows:

$$I_r' = \delta - I_o' + \pi \quad (52)$$

From Eq. (50), it is seen that the magnitude of

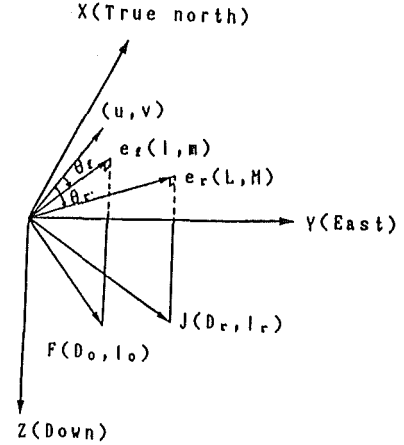


Fig. 2.9 Three-dimensional coordinate system for derivation of magneto-gravity response function. Abbreviations shown in figure are as follows,

F: magnetic field direction, J: magnetization vector, (u, v) : a wavenumber vector with component of (u, v) , where $u = 2\pi/\lambda_x$, $v = 2\pi/\lambda_y$, unit in radian/km, e_r : horizontal projection of magnetization vector of unit length with horizontal component of (L, M) , e_l : horizontal projection of magnetic field vector of unit length with horizontal component of (l, m) .

I_r' becomes minimum when the direction of the wavenumber vector (u, v) coincides with the azimuth of magnetization vector projected on a horizontal plane under the condition that $(u^2 + v^2)^{1/2} = \text{constant}$. Thus, theoretically it is possible to determine the declination of magnetization vector by finding the direction of the wavenumber vector which gives the minimum magnitude of effective inclination I_r' . Then, the minimum magnitude of I_r' corresponds to the inclination I_r of magnetization vector.

(2) Numerical example

To examine the effectiveness of practical application of the above method, numerical experi-

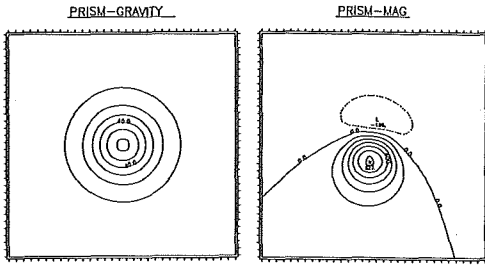
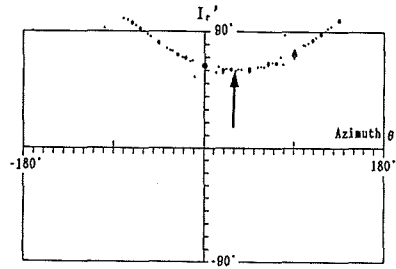


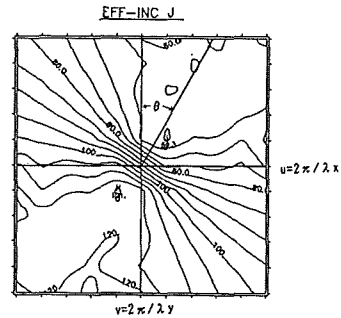
Fig.2.10 Gravity and magnetic anomalies caused by a prism body.

Density contrast is 1.0g/cm^3 , magnetic field direction is $D_r=0^\circ$, $I_r=45^\circ$ and polarized vector is $D_r=30^\circ$, $I_r=60^\circ$, $J=5.0\text{A/m}$, Top and bottom are 5km and 15km , horizontal dimension is $5\text{km}\times 5\text{km}$ and observed height is 0km .

ments are conducted by using the calculated magnetic/gravity anomalies caused by prismatic bodies. The calculated gravity and magnetic total intensity anomalies are shown in Fig.2.10. The assumed magnetization of the prism model is $J=5\text{A/m}$, $D_r=30^\circ$, $I_r=60^\circ$ and density contrast is 1.0g/cm^3 . The phase factor of magneto-gravity response function is evaluated based on Eq. (51), and the estimated value of the effective inclination of I_r' is plotted against the azimuth of wave vector as shown in Fig.2.11. It is found that the effective inclination has the minimum value of 60° at the azimuth direction of 30° . These values correspond to the assumed inclination and declination of the magnetized vector. Another numerical experiment is also conducted using the calculated magnetic anomaly shown in Fig.2.12(a), which is originated from the same prism with different magnetization of $D_r=-15^\circ$, $I_r=-30^\circ$. From the result shown in Fig.2.12(b), it is recognized that the effective inclination derived has the negative sign and takes the minimum magnitude of -30° around the azimuth of -15° . These numerical examples manifests the effectiveness



(a)



(b)

Fig.2.11 Numerical example of three-dimensional magneto-gravity response analysis.

- (a): The values of effective inclination (I_r') of magnetization vector against azimuth of wavenumber vector of (u, v) . The value of I_r' becomes the minimum value of 60° at the azimuth of 30° . These values coincide with the inclination and declination of magnetization vector of a source body.
- (b): Effective inclination (I_r') of magnetization are plotted in the two-dimensional coordinate system defined by wavenumber u and v . Effective inclination of magnetization vector becomes the minimum value of 60° at the azimuth of 30° .

of response function method for determining three-dimensional magnetization direction as well as two-dimensional case mentioned in the previous section.

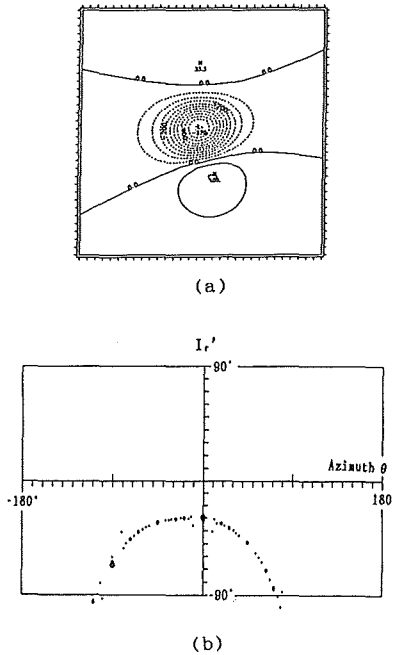


Fig.2.12 Numerical example of three-dimensional magneto-gravity response analysis.

- (a): Magnetic anomaly caused by a prism body. Magnetic field direction is $D_0=0^\circ$, $I_0=45^\circ$ and magnetization vector of the prism body is $D_r=-15^\circ$, $I_r=-30^\circ$, $J=5.0\text{A/m}$. Top and bottom depth of the prism are 5km and 15km, horizontal dimension is $5\text{km}\times 5\text{km}$ and observed height is 0km.
- (b): The values of effective inclination (I_r') of magnetization vector against azimuth of wave number vector of (u, v) . The value of I_r' becomes the maximum value of -30° at the azimuth of -15° . These values agree with the inclination and declination of magnetization vector of a source body.

2.4 Definition of magneto-gravity response filter

2.4.1 Derivation of basic formula

Here we would like to introduce an idea that magnetic anomalies f consist of two components, one (f_g) that is correlated with the gravity anomaly and the other (f_n) that is uncorrelated as:

$$f = f_g + f_n.$$

From the relationship given by Eq. (43) and Eq. (51), f_g can be evaluated by a convolution integration as (Clarke, 1971; Ueda, 1992):

$$f_g(x, y) = \iint h(x_0, y_0) \cdot g(x - x_0, y - y_0) dx_0 dy_0 \quad (53)$$

where $h(x_0, y_0)$ is an impulse response.

By calculating the Fourier transform of both side of Eq. (53), we have:

$$\begin{aligned} F(u, v) &= F_g(u, v) + F_n(u, v) \\ &= \Phi(u, v) \cdot G(u, v) + F_n(u, v) \end{aligned} \quad (54)$$

where $F(u, v)$, $F_g(u, v)$, $F_n(u, v)$ denote the Fourier transform of f, f_g, f_n and $\Phi(u, v)$ is a transfer function of the unknown filter $h(x_0, y_0)$. In the present paper, $1/\Phi(u, v)$ is defined as response function as given by Eq. (51).

Because f_n does not correlate with g , the cross-spectrum $S_{f \cdot g}$ between magnetic and gravity field become:

$$\begin{aligned} S_{f \cdot g} &= S_{f_g \cdot g} + S_{f_n \cdot g} \\ &= S_{f_g \cdot g}. \end{aligned} \quad (55)$$

The transfer function $\Phi(u, v)$ is derived from the cross-spectrum as:

$$\Phi(u, v) = S_{f \cdot g} / S_g. \quad (56)$$

Substituting Eq. (56) to Eq. (54), we obtain

$$F(u, v) = (S_{f \cdot g} / S_g) \cdot G(u, v) + F_n(u, v). \quad (57)$$

The raw spectrum of $S_{f \cdot g}$ and S_g are given by $S_{f \cdot g} = F(u, v) \cdot G(u, v)^*$, $S_g = G(u, v) \cdot G(u, v)^*$, where $*$ means the conjugate value. (58)

In the present study, smoothing of two-dimensional spectrum of $S_{f \cdot g}$ and S_g was performed by sampling mean method. On the other hand, smoothing of one-dimensional spectrum was executed by the convolution filter using Hanning window coefficients as:

$$[S_n] = 0.25 \cdot S_{n-1} + 0.5 \cdot S_n + 0.25 \cdot S_{n+1} \quad (59)$$

where n denotes wavenumber.

Using the smoothed spectrum obtained above,

we can derive the magneto-gravity response filter as:

$$[\Phi(u, v)] = [S_{f \cdot g}] / [S_g] \quad (60)$$

where bracket [] means smoothing operation.

The coherence between magnetism and gravity is also calculated in a conventional form as:

$$\text{Coh}(u, v) = ([S_{f \cdot g}])^2 / [S_g \cdot S_f]. \quad (61)$$

Using the magneto-gravity response filter defined in the above, we can extract magnetic anomaly correlative to gravity anomaly as follows:

$$\begin{aligned} f_g &= \iint F_g(u, v) e^{i(ux+vy)} du dv \\ &= \iint [S_{f \cdot g}] / [S_g] \cdot G(u, v) \cdot e^{i(ux+vy)} du dv. \end{aligned} \quad (62)$$

Then, the magnetic anomaly uncorrelative to gravity anomaly becomes:

$$f_n = f - f_g. \quad (63)$$

2.4.2 Numerical example

A numerical experiment is conducted using prismatic bodies which yield both magnetic and gravity anomalies in order to know the performance of magneto-gravity response filter for extracting magnetic field correlative with gravity field from a contaminated magnetic anomaly field. Fig.2.13(a) and , 2.13(b) show magnetic and gravity anomaly caused by the prism with magnetization of $D_r = -4^\circ, I_r = 38^\circ, J = 3.0 \text{ A/m}$ and density contrast $\rho = 0.3 \text{ g/cm}^3$. In Fig.2.13(c), is illustrated the composite magnetic anomaly which is the sum of the correlated magnetic anomaly shown in Fig.2.13(a) and uncorrelated magnetic field produced by a subprism having magnetization without density contrast. The magneto-gravity response filter was evaluated as an input-output system between the gravity anomaly shown in Fig.2.13(b) and the composite magnetic anomaly shown in Fig.2.13(c) in accordance with Eq. (60). Then,

the magnetic anomaly correlative with gravity field is calculated using Eq. (62). The magnetic anomaly thus obtained is illustrated in Fig.2.13(d). In comparison with Fig.2.13(a) some discrepancies are found in the pattern of Fig.2.13(d) in detailed part. The positive peak is somewhat suppressed in the extracted magnetic anomaly of Fig.2.13(d), but the features of Fig.2.13(d) generally represent a dipole pattern.

2.5 Response of gravity to topography

Similarly to sections 2.3 and 2.4, we can define a response function between topography and gravity field. Fourier transform of gravity field can be correlated with Fourier transform of topographic relief as shown in Eq. (27). By summing up the Fourier transform of topographic term, Eq. (27) is reduced to

$$G(u, v) = 2\pi G_c \rho \cdot \mathcal{K}(u, v) \quad (64)$$

where, $\mathcal{K}(u, v) = e^{-w^d \sum_{n=1}^d w^{n-1} / n!} \cdot H_n(u, v)$.

From Eq. (64) the density contrast ρ can be calculated by:

$$\rho = G(u, v) / \{2\pi G_c \cdot \mathcal{K}(u, v)\}. \quad (65)$$

When the topographic uplift has a uniform density contrast and is not compensated isostatically, the derived density ρ is to be constant against the wavelength of the gravity field. On the other hand, if isostatic compensation holds, the derived density contrast is to be reduced as the wavelength of gravity anomaly becomes longer.

Figure 6.4 shows apparent density variation against the wavelengths of the free-air gravity anomaly for the case of the Daito ridge. The obtained density means the density contrast against the surrounding water density of 1.03 g/cm^3 . This figure indicates that the density contrast of the Daito ridge is too small in the long-wavelength range. It is less than 1.0 g/cm^3 for the

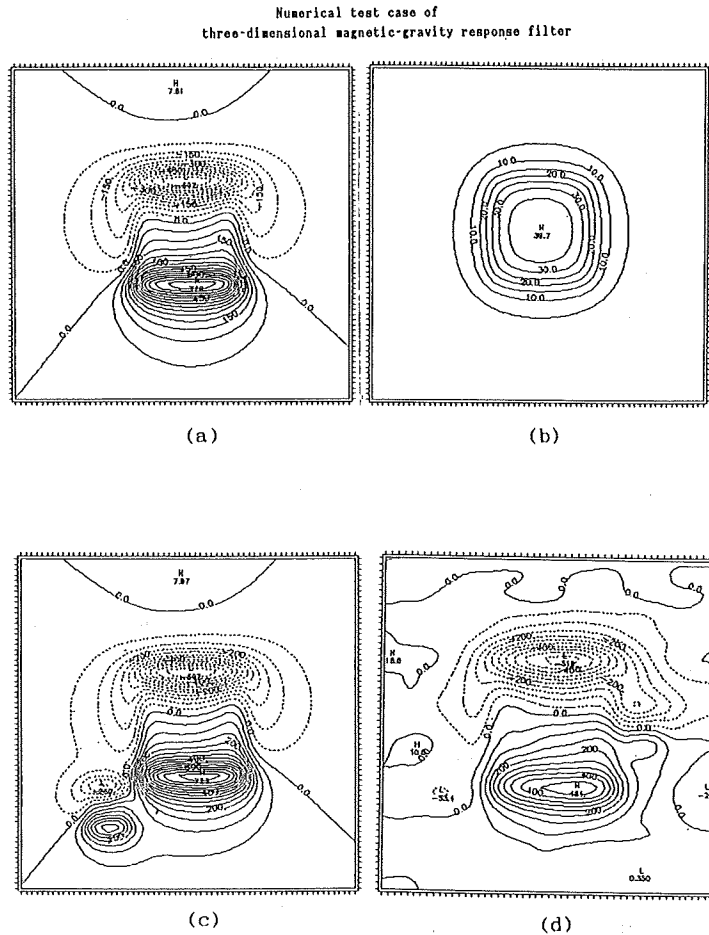


Fig.2.13 Numerical example of three-dimensional magneto-gravity response filter.

- (a): Magnetic anomaly caused by a prism body. Top and bottom is 2km and 7km below the observed plane, horizontal dimension is 20km×20km, magnetization intensity and direction are 3.0A/m, $D_r = -4^\circ$, $I_r = 38^\circ$, respectively.
- (b): Gravity anomaly caused by the prism body of (a). Density contrast is 0.3g/cm³. This gravity anomaly is used as the output gravity field for calculation of response filter.
- (c): Magnetic anomaly caused by another prism body without density contrast is added to (a), which is used as input magnetic anomaly data for calculation of response filter.
- (d): Output magnetic anomaly of magneto-gravity response filter for input field of (c).

wavelengths longer than about 80km. This fact may imply that the isostatic compensation holds to a considerable degree as depicted from the crustal model proposed by Segawa (1976).

2.6 Correlation analysis in the space domain

Using the inversion technique mentioned in the

fore-going section, magnetic anomaly can be converted to a magnetic basement relief and pseudo-gravity. These converted data offer useful information about the crustal structure, when compared with the raw topographic relief, free-air and Bouguer gravity anomalies. In Fig. 2.14 the correlation methods used in the present study

are summarized.

Calculation of correlation coefficients (cor) and amplitude ratio (r) between two-dimensional variables of topographic height (d_{ij}) and magnetic basement high (h_{ij}) is given by:

$$\text{cor} = \frac{\sum \sum (h_{ij} \cdot d_{ij})}{[\sum \sum h_{ij}^2 \cdot d_{ij}^2]^{1/2}} \quad (66)$$

$$r = \frac{\sum \sum (h_{ij}^2)}{\sum \sum h_{ij} \cdot d_{ij}}$$

where (ij) denote grid coordinate of two-dimensional variables (Grauch, 1987). In the above procedure, calculations are carried out at each grid point using a moving window which defines the range of calculation. The size of the window should be determined in accordance with the wavelengths of interest.

The correlation between magnetic basement and topography gives information of magnetization of the topographic uplift. When the topographic uplift has uniform magnetization, the positive correlation is expected between the derived magnetic basement and topography when the assumed direction of magnetization coincides with that of the uplift. The low correlation coefficients may occur when the uplift has non-uniform magnetization or the magnetization direction differs from the assumed direction of magnetization. We can also estimate the magnitude of magnetization from the amplitude ratio (r) as

$$J = J_0 \cdot r, \quad (67)$$

where J_0 denotes magnetization intensity used for calculation of magnetic basement. It may also be possible to determine magnetization direction by finding the magnetization direction giving the maximum correlation coefficients. Thus, the above correlation method is helpful for a rapid estimation of magnetization of topographic uplifts.

A correlation between pseudo-gravity and observed gravity field gives the ρ/J ratio of the causative body. As a free-air gravity anomaly mainly reflects topographic relief, the correlation between free-air anomaly and pseudo-gravity provides ρ/J ratio of the near surface structure (Hagiwara, 1980). On the other hand, the correlation between Bouguer gravity anomaly (assumed density = 2.67g/cc for Bouguer correction) and pseudo-gravity offers the ρ/J ratio of the deep-seated magnetic body with the density greater than 2.67g/cc. As already mentioned in section 2.5, it is generally conceived that the gravity anomaly with wavelengths longer than 160km is partly compensated isostatically (Hagiwara, 1979). However, the shallow source with a large horizontal dimension also creates the long-wavelength gravity anomaly. Taking the above

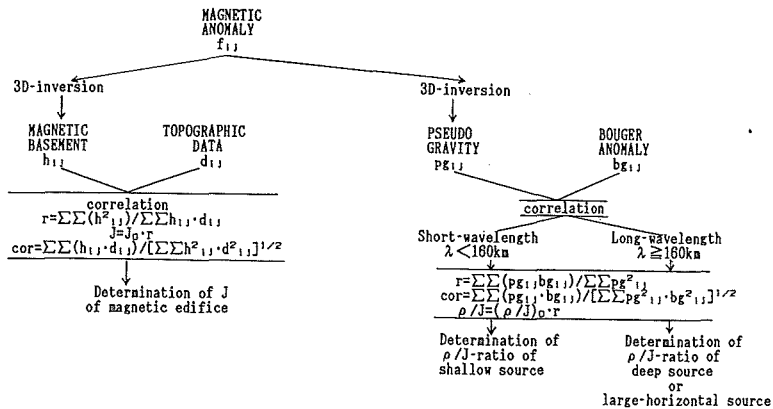


Fig.2.14 Flow chart of magnetic and gravity analysis in space domain.

mentioned matters into consideration, we may judge that the correlation in the wavelengths longer than 160km may reveal the ρ/J ratio at the Moho boundary or the relatively shallow source with a large lateral dimension. On the contrary, the correlation in the short wavelengths informs us of the ρ/J ratio of the shallow source in the crust.

CHAPTER III. CRUSTAL STRUCTURE OF KURILE AND HONSHU ARCS AS REVEALED FROM MAGNETIC AND GRAVITY FIELD ANALYSIS

3.1 Airborne magnetic survey by the Hydrographic Department of Japan (JHD)

The magnetic anomaly profiles analyzed in the present study were measured by a YS-11 aircraft as part of the 12th whole Japan magnetic survey program conducted by the Hydrographic Department of Japan (JHD) from Oct. 1984 to Nov. 1985 (JHD, 1988). The YS-11 employed for magnetic survey was capable of continuous flight as long as 1200 n.m. at a standard speed of 200 mile/h. The position of the aircraft was determined with a VLF Omega positioning system. Flight altitude was 12500ft except for the case of flight over Minami-Tori-sima (Marcus) island (6000ft.). A ring-core type flux-gate magnetometer was installed in the tail-stinger attached to the rear of the aircraft. Attitude of the aircraft was measured with an inertial system composed of three axial gyros. Resolution of the magnetometer was 1nT and that of the inertial system is 0.1° for pitching and rolling angles and 0.2° for heading angle (JHD, 1988). These measurements were combined with positions and clock signals and recorded on a cassette MT in a digital form every

second. The attitude angles were used for the conversion of the rectangular coordinate system fixed to the magnetic sensor to the absolute geographical coordinate system with x-axis directed north, y-axis east, and z-axis downward. The total intensity of magnetic field, which was calculated geometrically from the three axial components of the fluxgate magnetometer is free from attitude angles of the aircraft. So, the resultant accuracy of total intensity value is better than that of each component by a factor of one order. A proton precession magnetometer was also used to measure the total intensity field for the transection of the Izu-ogasawara Arc. These data as well as those by the fluxgate magnetometer are used in the present study.

3.2 Data processing of airborne magnetic survey data

3.2.1 Correction for aircraft's magnetization

Prior to the airborne magnetic survey, aircraft's magnetic field was measured in case of calibration flight in the eight directions of different azimuth with the interval of 45° , crossing an aeronautical beacon station at Cape Siono Misaki at the tip of the Kii Peninsula. For the case of the total intensity values measured by a proton precession magnetometer, an azimuth dependence shows the sinusoidal curve with the amplitude of about 40nT. On the other hand, the azimuth dependence of total intensity values measured by a fluxgate magnetometer are twice as large as that of the proton precession magnetometer (Ueda, 1990). This may be attributable to the difference of the sensor position in the tail-stinger. The azimuth dependence mentioned above was approximated by trigonometric functions to be used for the correc-

tion for the aircraft's magnetic field.

3.2.2 External field correction

As the external field variation caused by the ionosphere was relatively calm as indicated by *k*-index which is less or equal to 3 during the period of the magnetic surveys, an external field correction was executed based on hourly mean values on the ground at the magnetic observatory which is located close to the track lines. Variations of hourly means were approximated in the form of Fourier expansion series with respect to local time. The diurnal variation at the position of the aircraft was estimated by the above trigonometric approximation while taking into account the local time difference.

3.2.3 Calculation of magnetic anomaly

The WC-85 main field model derived by Quinn et al. (1986) was adopted as the reference magnetic field model for the calculation of magnetic anomalies. This model was derived based on the MAGSAT data collected from 1979 to 1980 and the Project MAGNET vector data acquired by NAVOCEANO during the period of 1980-1983. The WC-85 model, which was authorized by the International Hydrographic Office as the model for calculation of magnetic variation cited in the nautical chart for the epoch between 1985.0 and 1990.0, consists of spherical harmonics coefficients of degree and order 12. Truncating this model to degree 10 yields the US-UK model, whose weighted mean coefficients, together with those of the other candidate models, are adopted as DGRF1985. Langel and Estes (1982) reported that the degree and order 12 or 13 was necessary to represent the core field in terms of the spherical harmonics coefficients. According to this opinion, the author has adopted WC-85 model instead of DGRF1985 of degree and order 10.

3.3 Gravity anomaly data used in the present study

Regional gravity anomaly maps covering the Japanese islands have been compiled by several authors and organizations. Tomoda and Fujimoto (1982) compiled the Bouguer gravity anomaly map at the scale of 1/3,000,000. Although their map is now widely quoted, the contour lines with the interval of 20mgal is a little too rough for numerical analysis. Ganeko and Harada (1982) also produced 10' × 10' grid data file by the least-squares estimation technique. These grid data, which are available from JODC at present, were interpolated along the track lines of airborne magnetic surveys at 4km intervals for analytical use. The topographic profiles were also digitized from the bathymetric map (No. 6301, 6302) for calculation of terrain correction value. Thus, the Bouguer gravity anomaly profiles (assumed density is 2.67g/cm³) were made for the sea areas in the vicinity of Japan. As to the land area, Bouguer gravity anomaly map, published by the Geographical Survey Institute (GSI, 1985) with the scale of 1/2,000,000 was digitized along tracklines at 4km intervals. The above Bouguer gravity anomaly profiles were then merged and adopted for the synthetic magnetic and gravity field analysis.

3.4 General features of magnetic anomaly profiles over the Japanese Islands and their adjacent seas

Total intensity magnetic anomaly profiles are shown in Fig. 3.1. This figure shows characteristic features of magnetic anomalies originating from the continental crust of the Japanese Island Arcs. Several papers can be cited for the consid-

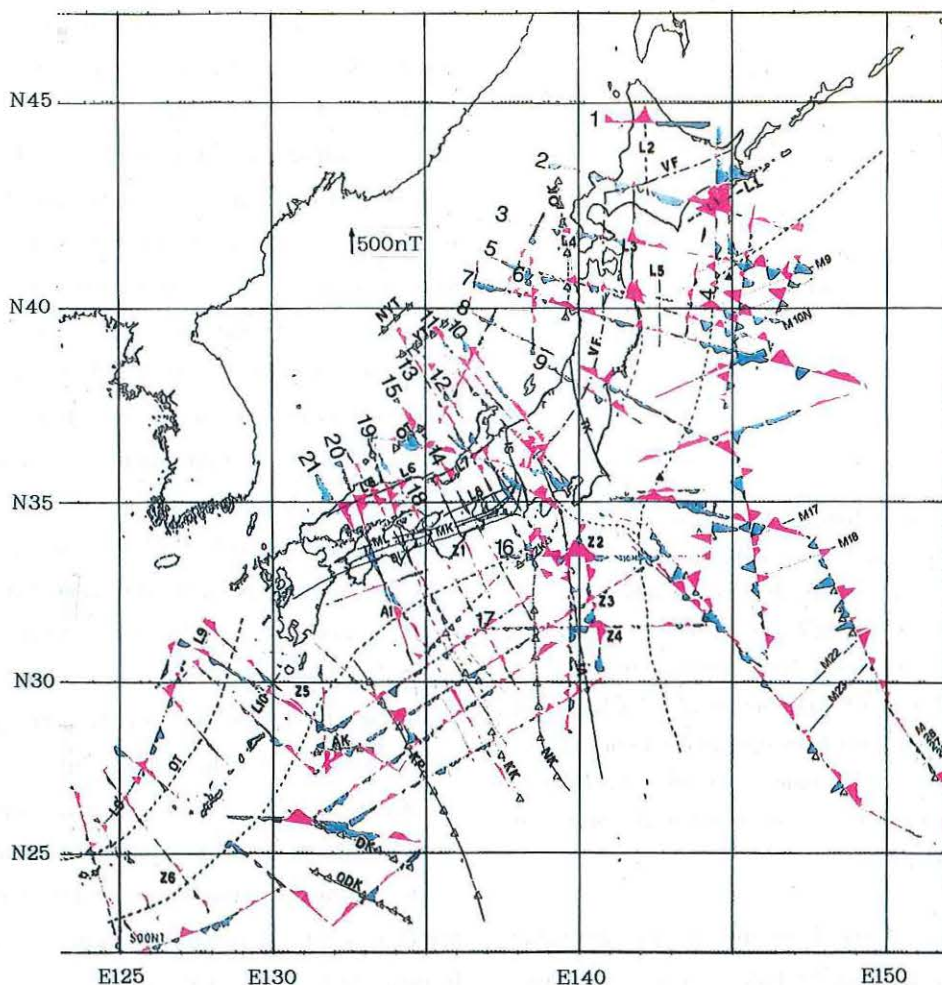


Fig.3.1 Total intensity magnetic anomaly profiles along track lines.

Numerals mean the identified number of profiles. Observed height is about 3800 meters above sea level. VF:volcanic front, OK:Okusiri ridge, NYY:Kitayamato bank, YT:Yamato bank, OT:Oki bank, AK: Amami plateau, DK:Daito ridge, ODK:Oki Daito ridge, KP:Kyusyu-Palau ridge, KK:Kinan seamount chain, NK:Nisi-Sitito ridge, ZK:Zenuis ridge, TK:Tanakura tectonic line, ML:Median tectonic line, MK:Mikabu tectonic line, BL:Butsuzo tectonic line, trench axis is shown by broken lines.

eration of magnetic anomalies in and around the Japanese Islands, as reported by Oshima et al. (1975), Segawa and Oshima (1975), Segawa and Furuta (1978), Ogawa and Suyama (1975), Kobayashi et al. (1979), Tanaka et al. (1984, 1986), Okubo et al. (1985), Isezaki and Miki (1979), Isezaki (1986), Ueda (1986), and Oshima (1987).

In reference to these articles and tectonic map

shown in Fig.3.2, the characteristic features of the magnetic anomalies are briefly summarized as follows.

On the northeast Japan and its adjacent seas, three prominent linear magnetic anomalies marked by L1, L2, L3 are found: L1 lies on the continental shelf and the slope in the south offing of Hokkaido, L2 corresponds to the intrusive

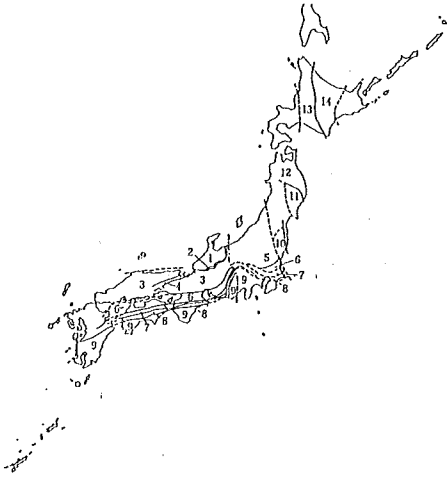


Fig. 3.2 Tectonic map of the Japanese Islands.

1:Hida belt, 2:Hida marginal belt, 3:Sangun, Mino and Tamba belts, 4:Maizuru belt, 5: Asio block, 6:Ryoke belt, 7:Sambagawa belt, 8:Chichibu belt, 9:Shimanto belt, 10: Abukuma belt, 11:Southern part of Kitagami block, 12:Northern part of Kitagami block, 13:Ishikari, Kamuikotan belts, 14:Hidaka, Tokoro belts (after Geological survey of Japan, 1982).

mafic bodies of the Kamuikotan metamorphic belt, and L3 to Sanriku-Isikari linear anomaly. Parallel to L3, two N-S trending anomalies are recognized as shown by L4 along the Okusiri ridge in the Japan Sea and L5 along the continental slope of northeast Honshu. Magnetic anomalies corresponding to volcanic front are less prominent in amplitude in contrast to those of L1, L2, L3. As to the origin of L1, L3, Segawa and Oshima (1975) ascribed these anomalies to basic rocks corresponding to the Mesozoic volcanic front. On the other hand, Okubo et al. (1985) ascribed L3 to granitic massives of magnetite series. In the inner region of southwest to central Honshu, prominent positive anomaly zones (L6, L7), with intermediate amplitude ($>300\text{nT}$) lie over San-in district (L6) and Hokuriku district

(L7). The anomaly zone L6 coincides well with the distribution of Cretaceous to Early Tertiary granitic massives of magnetite series. In the outer region of central to southwest Honshu, we see the broad negative anomaly zone (L8) trending parallel to the Median tectonic line. It is well known that the mafic rock outcrops along the Kurosegawa tectonic belt, but the associated magnetic anomaly is subtle. This fact implies that the Kurosegawa tectonic belt does not have significant underground magnetic structure.

As to the Izu-Ogasawara Arc, the peculiar magnetic anomalies (Z2, Z3, Z4) are recognized over the continental shelf and slope. On the other hand, magnetic anomaly of the Ryukyu Arc is generally featureless except for the positive anomalies (L9, L9') lying over the outer margin of the Tunghai shelf. These features also appear in the areal magnetic anomaly maps, which are to be described in detail in Chapters IV and V.

The magnetic anomalies over the ocean basin are also observed: prominent magnetic lineations trending in ENE-WSW direction in the northwestern Pacific Basin, small amplitude magnetic lineations in the Sikoku Basin, and obscured lineations trending NE-SW over the Yamato Basin. In the Philippine Basin, conspicuous magnetic anomalies are recognized over the Kyusyu-Palau ridge, the Amami plateau and the Daito ridge. The Oki ridge in the Yamato Basin also shows a remarkable magnetic anomaly of reversed pattern. It should be pointed out that the ridges having continental crust show more distinct magnetic anomalies than the surrounding oceanic crust.

3.5 Hokkaido and northeast Honsyu

The magnetic and gravity anomalies of the representative profiles in Fig.3.1 are analyzed with the method described in chapter II and their tectonic implications are discussed from geological and geophysical point of view.

3.5.1 Hokkaido and Tohoku region

3.5.1.1 Analysis of profile-1 (Kamuikotan belt)

The profile-1 transects the Tesio and Kitami massives in the northern part of Hokkaido from west to east. The geological unit of northern part of Hokkaido consists of several groups trending in N-S direction(Fig.3.3). The westernmost zone is a volcanic belt of Miocene age, and to the east there are Kabato massif of pre-Cretaceous volcanic zone, Isikari belt, Kamuikotan metamorphic belt and Hidaka metamorphic belt. A prominent positive anomaly amounting to 300 nT (a in Fig.3.4A) is seen over the Kamuikotan belt in association with mafic to ultramafic intru-

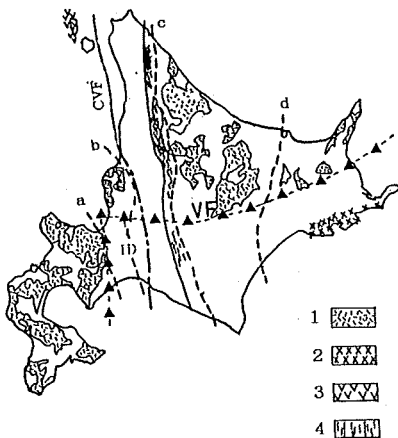


Fig.3.3 Geological map of Hokkaido, Japan.
 1:Miocene volcanic rocks, 2:Nemuro group in Late Cretaceous age, 3:Early Cretaceous volcanic rocks, 4:mafic rocks in the Kamuikotan belt, a,b,c,d: tectonic boundary, a-b: Ishikari depression zone.(modified from Fujii and Sogabe,1978)

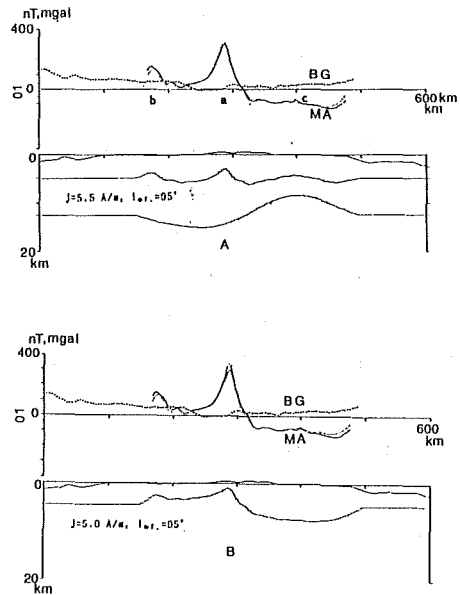


Fig.3.4 Magnetic basement model of profile-01.

Solid line is observed magnetic anomaly (MA), and broken line calculated one. Dotted line is Bouguer gravity anomaly(BG). Parameters for model A and B are as follows;

- A: Effective intensity of magnetization is 5.5 A/m, upper surface: $\lambda < 160\text{km}$, Lower boundary: $\lambda > 160\text{km}$.
- B: Effective intensity of magnetization is 5.0 A/m,

sive rocks. Another peak amounting to 150nT (b in Fig.3.4A) lies over extrusions of andesite and basaltic rocks of Miocene age, which are widely distributed in Teuri and Yagisiri islands. The negative bias of about -100nT (c in Fig.3.4A) is observed to the east of the Kamuikotan belt. In the lower part of Fig.3.4A and B, are shown the best-fit magnetic structures for this profile. In derivation of model A, magnetic anomalies of wavelengths shorter than 160km are ascribed to the upper boundary and those of wavelengths longer than 160km to the lower boundary of the magnetic layer. On the other hand, model B explains the magnetic anomalies by the upper

boundary of the magnetic layer only. The lower boundary of the magnetic layer is usually defined by either Curie point depth or Moho boundary if it is above Curie point isotherm. If model A should be true, the elevated Curie isotherm is expected to the east of Kamuikotan belt, but such features are not confirmed by geophysical sounding. According to model B, the upper surface of the magnetic basement is depressed toward east of the Kamuikotan belt. It is unreasonable to ascribe the depression to the thick sedimentary layer because of positive trend of the Bouguer gravity anomaly profile.

Recent study of tectonics of Hokkaido reveals that the eastern margin of the Kamuikotan belt was a subduction zone of the old oceanic plate coming from east in Early Cretaceous age (Kimura, 1985). In the course of subduction, the eastern part of Hokkaido which was part of the Okhotsk block collided against the southwestern part of Hokkaido of the northeast Japan block in the middle Miocene, which resulted in the formation of Hidaka massif. This hypothesis may lead us to ascribe the conspicuous difference of magnetic structure mentioned above to the different magnetic property of the respective blocks once having collided each other.

3.5.1-2 Analysis of Hokkaido-Kurile linear anomaly (profile-4, Fig. 3.5)

The outstanding feature of this profile is a large amplitude ($>400\text{nT}$) and widely spreading magnetic linear anomaly (a in Fig. 3.5) located in the south offing of Kusiro district, southeastern part of Hokkaido. Several names are given for this linear anomaly, such as Doto magnetic belt (Ogawa and Suyama, 1975), Tokati-Kurile linear magnetic anomaly (Oshima et al., 1975), the Hokkaido-Kurile linear anomaly (Segawa and

Furuta, 1978). Referring to Fig. 1 of Segawa and Furuta (1978), this anomaly is elongated in the ENE direction along the continental slope facing the Kurile trench. It should be pointed out that another anomaly b is located to the north of anomaly a. The latter anomaly b, accompanied by the Nemuro group formed by the igneous activity in the late Cretaceous time, is associated with a marked positive Bouguer gravity anomaly. Here, we name the former linear anomaly the Hokkaido-Kurile linear anomaly (HKLA) and the latter the Kusiro-Nemuro linear anomaly (KNLA). The magnetic anomaly over the Quaternary volcanic zone (c in Fig. 3.5) is small in amplitude in comparison with that of HKLA. The oceanic lineations (M7, M8) belonging to the Japanese lineation set are also recognized in the left side of the profile.

For calculating 2-D magneto-gravity response function, the regional trend of the Bouguer gravity anomaly is approximated by running mean method and removed from the original Bouguer gravity anomaly. Then, 2D-magneto-gravity response function is calculated for the range between A and B as marked in Fig. 3.5(a). The calculated effective inclination is plotted against the wavenumber as shown in Fig. 3.5(b). The effective inclination has a value about 35° in the wavelengths longer than 40km, and then approaches the present effective inclination at wavelengths around 25km. The coherence is good in the long-wavelength range and becomes poor in the short-wavelength zone, which reduces the reliability of the derived effective inclination values in the short-wavelength zone ($<20\text{km}$). As the azimuth of the profile points nearly to the north, the effective inclination may reveal the real inclination of a magnetized body. Although

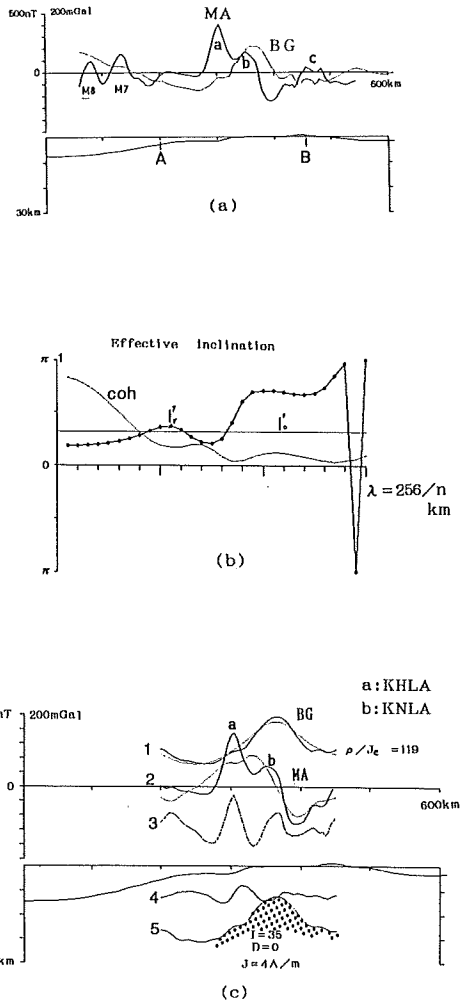


Fig.3.5 Magneto-gravity response analysis on profile-04.

- (a) Total intensity magnetic anomaly (solid) and trend-removed Bouguer gravity anomaly (dot) profiles. Data between A and B were adopted for analysis. a:Honsyu-Kuril linear anomaly, b:Kusiro-Nemuro linear anomaly, M7,M8: Oceanic magnetic lineations.
- (b) Effective inclination of magnetization vector (I_r') and that of magnetic field (I_0'). Coh is coherence between magnetic and gravity anomalies.
- (c) Magnetic basement model of profile-04 derived from response filter method. Dotted magnetic basement is from gravity-correlated magnetic anomalies (magnetic response), and overlapping basement relief is from residuals. Assumed magnetization is $D_r=0^\circ, I_r=35^\circ, J=4.0$ A/m. 1:observed Bouguer gravity (Solid) and pseudo-gravity (dot) calculated from magnetic response, 2: observed magnetic anomaly (solid) and magnetic response (dot), 3: residual magnetic anomaly, 4:magnetic basement for residual anomaly, 5:magnetic basement for gravity-correlated magnetic anomaly whose ρ/J_{eff} is 119 g/emu.

the derived effective inclination does not agree with that of the present field direction in the long-wavelength range in a strict sense of the word, but, they deny the equatorial origin of the magnetic body, which may be true with the oceanic crust showing the Japanese lineation sets in the offing of Hokkaido (Hilde et al., 1976).

The magnetic structure estimated by magneto-gravity response filter is shown in Fig.3.5(c). This result shows a close correlation between the KNLA and Bouguer gravity high and no appreciable correlation with the HKLA. The magnetic

basement relief for KNLA amounts to about 10 km and has the ρ/J_{eff} ratio (g/emu) of 119. If the density contrast is in the range between 0.4 and 0.5g/cm³, the resulting magnetization falls in the range between 3.3A/m and 4.2A/m. Taking this estimation into consideration, we may conceive the possible magnetic source for the KNLA to be basic rocks with high density contrast. On the other hand, the origin of the HKLA is to be ascribed to serpentinized materials with high-magnetization and low density contrast.

Ogawa and Suyama (1975) assume that the

HKLA is caused by the intrusive body of serpentized mafic rocks outcropping presumably in the Early Cretaceous age. As for KNLA, Oshima et al. (1975) ascribed it to the igneous rocks in the late Cretaceous to Oligocene age forming the Nemuro group. Their interpretations are suggestive, but they neglected the difference of magnetic structures for the HKLA and KNLA.

Concerning the origin of KNLA, following two interpretations may be possible. One attributes the source to the Conrad boundary, and the other to the detached oceanic crust itself. The former is based on the idea that the Conrad boundary is the most distinguishable density boundary within the crust, but, more sensitive seismic exploration may be necessary to confirm the plausibility. The latter may have arisen from the phenomenon of ridge descent inferred from the chronology of the Japanese lineation sets (Uyeda and Miyashiro, 1974). We think, however, that the derived inclination of magnetization seems to be in favour of the former interpretation.

The magnetic source of HKLA is thought to be serpentized materials as mentioned above. As for the origin of the serpentinite suites, there are two possibilities, one is serpentization of lower crust basic rocks caused by water supply from the subducting Pacific plate, and the other is the serpentized oceanic crust accreted to the continental crust. Taking the model derived (see to Fig. 3.5(c)) into consideration, which indicates a serpentized magnetic source overlapping the buried magnetic basement high within the lower crust, the former interpretation seems likely. However, we can not get a unique solution in this stage.

A cross-section of seismic hypocenter distribution along profile-4 shows three inactive zones, as

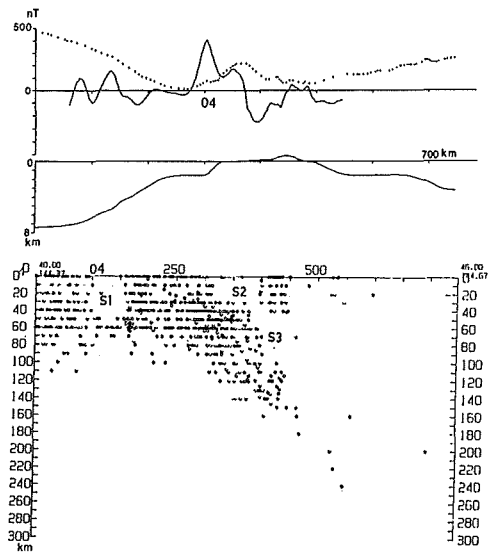


Fig. 3.6 Cross-section of hypocenters along profile-04.

S1, S2 and S3 indicates non-active seismic regions.

marked by S1, S2 and S3 (see Fig. 3.6). It appears that the zone S2 corresponds to magnetic basement high of KNLA and S3 to the aseismic mantle wedge. The above correspondence between the magnetic massif and the inactive seismic zone is also reported for the northeast Honsyu Arc, and the forearc region of the northern Izu-Ogasawara Arc (Oshima, 1987, Ueda, 1990).

3.5.1-3 Analysis of the Sanriku-Isikari linear anomaly (profile, 3, 6)

(1) Previous work

The Sanriku-Isikari linear anomaly (SILA) is one of the most conspicuous anomalies observed in the Japanese Islands (Oshima et al. 1975; Ogawa and Suyama, 1975; Segawa and Furuta, 1978). Some models have been proposed to explain the anomaly. Oshima et al. (1975) analyzed the west-east cross-section of SILA along N41° by a tabular body of 4km wide and 30km

thick with a top at a depth of 10km, which is magnetized in the dip angle of 125° (as measured from eastward horizontal axis) with magnetization 10.0A/m . In the northern extension of SILA, two test drillings were performed at Sorati (about 3.7km in depth) and Nanporo (about 4.3 km in depth) sites in Hokkaido (Petroleum Development Corporation Agency:PDCA, 1971 and 1973; Segawa and Furuta, 1978). Basement rocks obtained from Sorati and Nanporo sites are metabasalt and metadolerite, respectively. The magnetization intensity, vector sum of remanent and induced magnetization of these samples, is less than 3.5A/m . This value is considerably smaller than that of the Oshima's model. Based on the above information, Segawa and Furuta (1978) proposed another tabular model magnetized in the direction of $\text{Dec} = -45^\circ$, $\text{Inc} = 53^\circ$ with a magnetization intensity of 3.0A/m . The top and bottom of their tabular model are located at the depth of 5km and 15km with a width of 20km. The declination of magnetization vector of these models which is deflected westward is based on the fact that the Cretaceous granitic rocks collected from northeast Honsyu are magnetized in the $\text{N}45^\circ\text{W}$ direction (Kawai et al., 1971). On the contrary, Koënigsberger ratio (Q-ratio) of the drilled specimens ranges from 0.3 to 0.4, which is too small for the source body to keep the westward deflected magnetization vector.

Recent palaeomagnetic study about Tertiary rocks sampled at northeast Honsyu revealed that the mean direction of magnetization becomes $\text{Dec} = -41.2^\circ$, $\text{Inc} = 56.5^\circ$ with the samples whose age ranges from 21Ma to 32Ma (Otofuji et al., 1985). This result supports the counter-clockwise rotation of northeast Honsyu. As mentioned above, elucidation of magnetization of SILA is

an important subject related to tectonics of north-east Honsyu. In this section profile-3 and profile-6 crossing SILA are analyzed with the method described in the fore-going section.

(2) Results of analyses of profile-3

This profile is a transection from the Japan Sea to the western Pacific Ocean, crossing the Okusiri ridge and the Oshima peninsula in ESE direction. We can recognize four anomaly zones (a, b, c and d in Fig. 3.7) over the continental

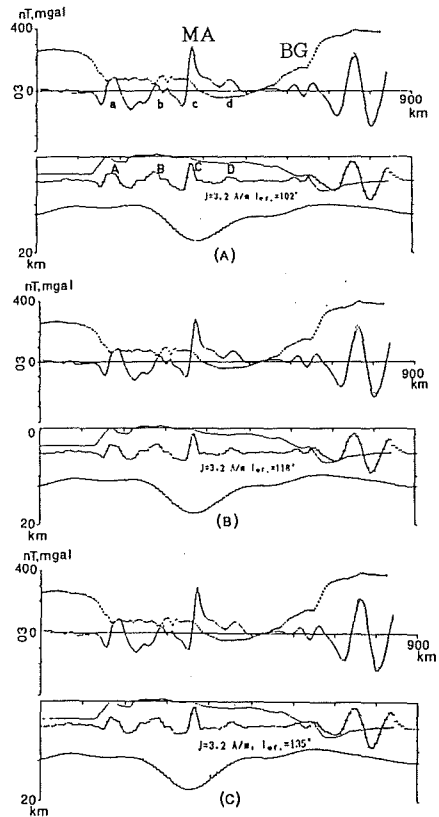


Fig. 3.7 Magnetic basement model of profile-03.

Solid lines are observed magnetic anomalies (MA), BG: Bouguer gravity anomaly. Effective magnetization intensity is 3.2 A/m , Azimuth of profile is 100° .

Directions of magnetization vector are as follows,

Model A: present field direction ($I_r' = 102^\circ$),

Model B: $I_r' = 118^\circ$,

Model C: $I_r' = 135^\circ$.

crust. Magnetic lineations caused by sea-floor spreading are recognized in the right end of the profile. Anomaly a corresponds to the Okusiri ridge, b to the Quaternary volcanic zone, c to SILA. Anomaly d runs in N-S direction parallel to SILA from the east offing of the Sanriku district to the south offing of the Erimo cape, Hokkaido. For the elucidation of magnetization of SILA, the magnetic structural models derived by Fourier expansion method are described at first, and then proceed to 2D-Magnetogravity response analysis.

[Magnetic structural model derived by Fourier expansion method]

Figure 3.7 shows the results of magnetic analyses for three different magnetization directions (model A, B and C), where a value of 3.2 A/m is assumed as an effective magnetization intensity. Model A is the result under the assumption that the magnetization direction coincides with the present field direction. As the skewness parameter of model A is relatively small (24°), the positions of four upheavals of the magnetic basement (A to D in model A) coincide with those of magnetic anomaly highs. The magnetic basement of the Quaternary volcanic zone shows a gentle slope, i.e. 100km in width and 3~4km in elevation, whereas that of SILA is an isolated structure, i.e. about 20km in width and 4~6km in elevation. Model B is derived under the assumption of westerly declination of the magnetization vector (Dec = -41° , Inc = 56°), whose effective inclination of magnetization vector becomes 118° . The magnetic basement high corresponding to SILA becomes more symmetric in shape in model B than in model A. This tendency is strengthened in model C, where the value of 135° is assumed for the effective inclination of magnetization vector.

The fact that the symmetry is enhanced as the effective inclination increases may support westerly deflected magnetization vector of the buried magnetized body, when the vertical tabular body is assumed as the source geometry of SILA as conducted by Oshima et al. (1975) and Segawa and Furuta (1978).

The lower boundary of the magnetic layer for these models is downward bent beneath SILA. These features imply the thickening of magnetic layer, which otherwise is likely to be interpreted by the upheaval of a magnetized lower crust. The model obtained here does not take into account the features of the Bouguer gravity anomaly, so the synthetic analysis of magnetic and gravity anomalies is to be described in the following section.

[2D-magneto-gravity response analysis]

The 2D-response function was calculated for

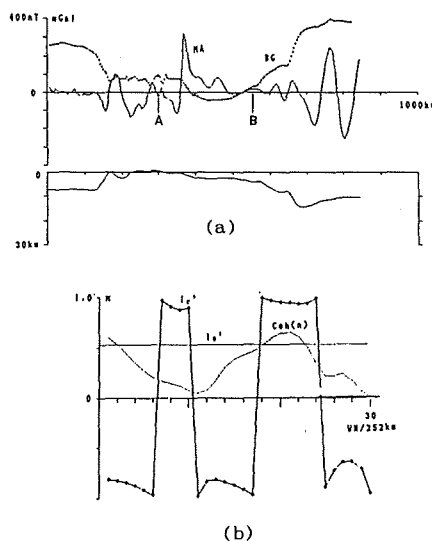


Fig.3.8 Magneto-gravity response analysis on profile-03.

- (a): Data between A and B were adopted for analysis. MA:magnetic anomaly, BG: Bouguer gravity anomaly.
 (b): Effective inclination of magnetization vector (I_e') and coherence (coh)

the magnetic and gravity anomalies between A and B shown in Fig.3.8(a), and the derived effective inclination is indicated in the lower part. Although the effective inclination of magnetic field is 95° in this profile, that of magnetization vector ranges from -150° to -170° in the long wavelength band ($\lambda > 60\text{km}$). This will indicate that the buried magnetized body responsible for SILA is magnetized in the westerly direction with small upward component. Figure 3.9 shows the comparison between the Bouguer gravity and pseudo-gravity profiles derived under the assumption of different effective inclination of I_r' ($a = -173^\circ$, $b = 113^\circ$, $c = 95^\circ$). Possible combinations of declination and inclination become $(-45^\circ, -5^\circ)$ for $I_r' = -173^\circ$, $(-41^\circ, 56^\circ)$ for $I_r' = 113^\circ$ and $(-8^\circ, 56^\circ$:present field direction) for $I_r' = 95^\circ$, although

the unique combination can not be determined. The second combination of the above is from the result of palaeo-magnetic measurement by Otofujii et al. (1988). The correlation coefficient for $I_r' = -173^\circ$ has the maximum value of 0.95 among the three cases, which is consistent with the result obtained by 2D-response function method. Now that the ρ/J_{eff} ratio for the optimum case has the value of 64, J_{eff} varies from 3.1A/m to 6.3A/m with the range of density contrast from 0.2g/cm^3 to 0.4g/cm^3 .

Figure 3.10 indicates the magnetic structure calculated by 2D-response filter method. This

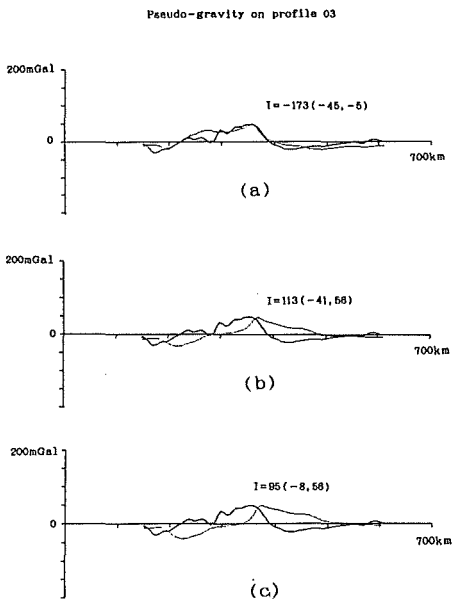


Fig.3.9 Pseudo-gravity analysis on profile-03.

The correlation coefficient between Bouguer gravity anomaly and pseudo-gravity becomes the highest value for model (a), which gives the values of $\text{corr.} = 0.95$ and $\rho/J_{\text{eff}} = 69$, respectively. Azimuth of profile is 90° .

(a): $I_r' = -173^\circ$, (b): $I_r' = 113^\circ$, (c) $I_r' = 95^\circ$.

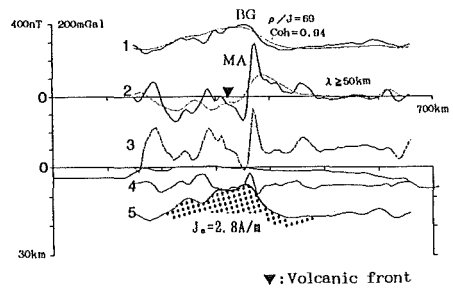


Fig.3.10 Magnetic basement model of profile-03 derived from magneto-gravity response filter.

Dotted magnetic basement is from gravity-correlated anomalies, and overlapping basement relief is from residuals. Effective magnetization intensity is 2.8 A/m. Calculation is conducted for the azimuth of 90° .

1:observed Bouguer gravity (Solid) and pseudo-gravity calculated from magnetic response, 2: observed magnetic anomaly (solid) and magnetic response for $\lambda \geq 50\text{km}$ (dot), 3: residual magnetic anomaly, 4:magnetic basement for residual ($J = 4.0\text{A/m}$, $D_r = -45^\circ, I_r = -5^\circ$), 5:magnetic basement for gravity-correlated magnetic anomaly (magnetic response) whose J_{eff} is 2.8A/m, $I_r' = -173^\circ$ ($J = 4.0\text{A/m}$, $D_r = -45^\circ, I_r = -5^\circ$) and ρ/J_{eff} becomes 69 g/emu.

structure shows the large-scale basement high (5 in Fig.3.10) producing the main features of the Bouguer gravity anomaly on which lies the magnetic basement relief of low density contrast (4 in Fig.3.10), corresponding to residual anomalies (3 in Fig.3.10). The assumed magnetization direction for the residual anomaly is not definitive, so another magnetization direction can be assigned for this overlapping body. The underlying magnetic body (5 in Fig.3.10) seems to extend to the lower crust.

(3) Results of analyses of profile-6

Profile-6 is a transection over northeast Honshu from the Japan Sea to the northwest Pacific basin. Four lineations denoted by a to d (see Fig.3.11) can be traced northward as in profile-3. The most prominent anomaly marked by c is SILA, which has a good correspondence to Bouguer gravity high. The magnetic structure

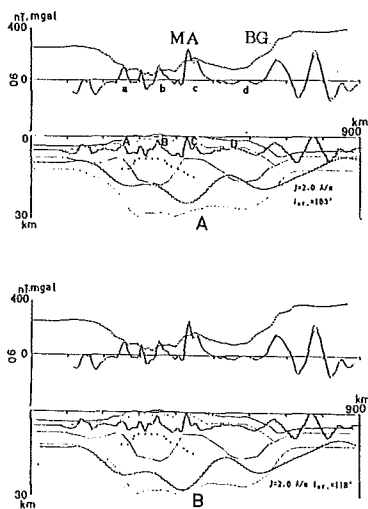


Fig.3.11 Magnetic basement model of profile-06.

MA:magnetic anomaly, BG:Bouguer gravity anomaly. Calculated parameters of models A and B are as follows;

model A: $I_r = 103^\circ$, $D_r = -8^\circ$, $I_r = 54^\circ$, $J_{eff} = 2.0 \text{ A/m}$, $AGL = 101^\circ$

model B: $I_r = 118^\circ$, $D_r = -41^\circ$, $I_r = 56^\circ$, $J_{eff} = 2.0 \text{ A/m}$, $AGL = 101^\circ$

derived by Fourier expansion method is shown in the lower part. The magnetic layer is assumed to be magnetized in the present field direction for model A and in the westerly magnetization direction ($Dec = -41^\circ$, $Inc = 56^\circ$) for model B with an effective magnetization intensity of 2.0 A/m . Four upheavals of magnetic basement are seen in correspondence to magnetic anomaly highs. The magnetic basement high for the Quaternary volcanic zone (B in model A) is about 100 km in width and about 5 km in elevation, whereas that of SILA is about 60 km in width with an elevation of about $6 \sim 8 \text{ km}$. Although no remarkable difference of magnetic basement is recognized between Model A and B due to small difference in effective inclination of the magnetization vector, it should be pointed out that the symmetry of western and eastern basement depths for SILA becomes better for the westerly magnetization model as is the case for profile-3. This features may imply that the short wavelength anomalies of SILA are ascribed to the westerly magnetization of the source. It should also be noted that the upheaval of magnetic basement of SILA coincides well with that of the lower crust inferred from seismic velocity structure (Yoshii and Asano, 1972). Thickening of effective magnetic layer beneath SILA can be interpreted by the upheaval of the magnetic lower crust which is in harmony with seismic velocity structure. In the following section, more convincing results are given by the 2D-magneto-gravity response analysis.

[2D-magneto-gravity response analysis]

Prior to the calculation of 2D-magneto-gravity response function, the regional trend of Bouguer gravity anomaly is removed using the method similar to that described in section 3.5.1-2. The

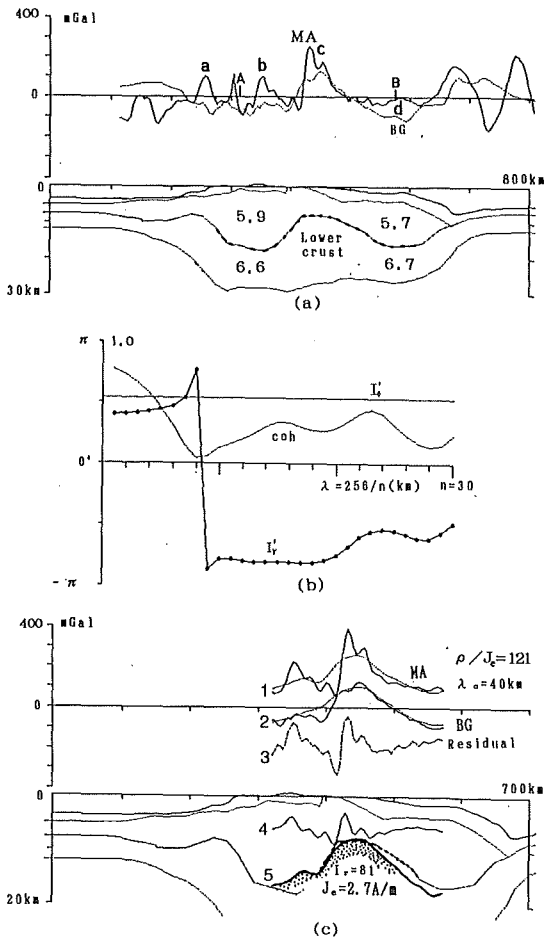


Fig.3.12 Magneto-gravity response analysis on profile-06.

- (a): Profiles of total intensity magnetic anomaly (MA) and Bouguer gravity anomaly (BG) along profile-06, Data between A and B are adopted for analysis. The seismic velocity structure is shown in the lower part (after Yoshii and Asano, 1972).
- (b): Effective inclination of magnetization vector and coherence (coh) calculated by response function.
- (c): Magnetic basement model derived from magneto-gravity response filter.

1: observed magnetic anomaly (solid) and magnetic response (dot), 2: observed Bouguer gravity anomaly (solid) and pseudo-gravity of response magnetic anomaly (dot), 3: residual, 4: magnetic basement for residual, 5: magnetic basement for gravity-correlated magnetic anomaly (magnetic response) whose ρ/J_{eff} is 121 and $J_{\text{eff}}=2.7\text{A/m}$, $I_r'=81^\circ$, respectively.

upper part of Fig.3.12 shows the reduced Bouguer gravity anomaly and the magnetic anomaly adopted for the analysis. The derived effective inclination of magnetization vector is shown in the middle part. This result indicates that effective inclination in the long-wavelength band ($\lambda > 45\text{km}$) is stable around the value of 80° and then changes to about -170° in the short wavelength band ($\lambda < 25\text{km}$). The above feature implies that the buried magnetic bodies responsible for SILA can be separated into two sources, one is the normally magnetized body located at depth with considerable horizontal dimension, and the other is the westerly magnetized body at shallow depth. The third part shows the magnetic basement model derived from 2D-magneto-

gravity response filter method. Dotted magnetic basement high (5 in Fig.3.12(c)) corresponds to a gravity-correlated magnetic anomaly, and the overlying structure (4 in Fig.3.12(c)) to a residual magnetic anomaly. It is noteworthy that the dotted magnetic basement high agrees well with the Conrad boundary estimated from seismic explosion investigation (Yoshii and Asano, 1972). The ρ/J_{eff} (g/emu) ratio of this basement high become 121, which is very close to the value obtained for KNLA of profile-4.

(4) Concluding remarks concerning magnetic structure of SILA

The magnetic and gravity field analysis of SILA reveals that the short wavelength anomaly of SILA is well explained by westerly deflected

magnetization with slight upward component. On the other hand, the long-wavelength component is to be ascribed to the upheaval of the magnetic lower crust. The lower crust beneath profile-6 is magnetized nearly in the normal field direction, but that of profile-3 is magnetized in the similar direction as that of short wavelength anomalies. If magnetic and gravity anomalies associated with SILA are originated from a common source, the effective inclination derived from profile-3 suggests that the magnetic body producing SILA was generated at the equatorial region in the southern hemisphere, and then emplaced to the continental crust of the palaeo-Asian continent along with subduction process of the oceanic crust. If the source of SILA appearing in profile-3 is different from that of the Bouguer gravity high, the effective inclination suggesting the westerly deflected magnetization with slight upward component may be unsubstantial.

The normal magnetization of the lower crust of profile-6, on the other hand, may be attributable to induced magnetization or viscous remanent magnetization acquired during Brunhes normal epoch. This is more convincing because of a good agreement between the derived model and the seismic velocity structure.

The magneto-gravity analysis of profile-6 suggests that the lower crust beneath northeast Honshu is magnetic. This aspect gives some information concerning rockmagnetism and petrochemistry of the deep-seated lower crust facing active subduction zone.

3.6 Central Honshu

3.6-1 Background

The magnetic anomalies denoted by L7 and L8 characterize magnetic features of central Hon-

shu. The positive anomaly zone (L7) is an ENE extension of L6 overlying San-in district as shown in Fig.3.1. The negative anomaly zone (L8) occurs over the land area from Tokai district to the inland part of the Kii peninsula. Fig. 3.13 shows the magnetic and Bouguer gravity anomalies along the profiles from 12 to 20. This figure illustrates the continuity of the negative magnetic anomaly zone (L8), which is particularly evident in profile-12 to profile-14. The Median tectonic line (denoted by \uparrow) is located within the coverage of this negative anomaly zone, but no significant local anomaly associated with the tectonic line is recognized.

3.6-2 Magnetic basement models and pseudo-gravity of profile 12 to 14.

Fig. 3.14 shows pseudo-gravity and derived magnetic basement structures of profile-12 to profile-14. According to this figure, the negative magnetic anomaly zone (L8) should be explained by the magnetic basement tilted down toward the inland area of central Honshu. It is controversial

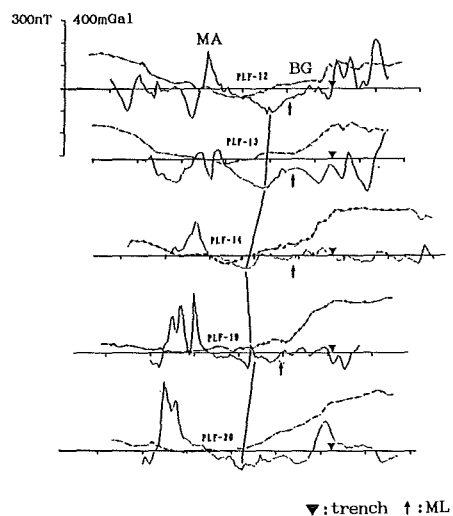


Fig.3.13 Total intensity magnetic anomaly and Bouguer gravity anomaly along profiles of 12 to 20. ▼:trench, \uparrow :Median tectonic line.

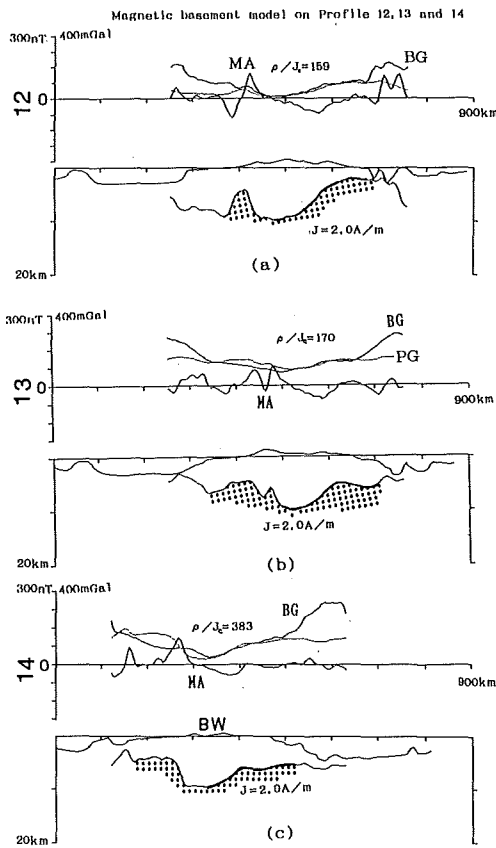


Fig.3.14 Magnetic basement models of profiles 12, 13 and 14.

The values of ρ/J_{eff} ratio derived are indicated on each profile. Effective magnetization intensity of the magnetic basement is assumed to be 2.0A/m and magnetization direction to be present field direction.

MA:magnetic anomaly, BG:Bouguer gravity anomaly, PG:Pseudo-gravity(dot), BW: Biwa lake.

- (a): $\rho/J_{eff}=159$ g/emu, (b): $\rho/J_{eff}=170$ g/emu,
- (c): $\rho/J_{eff}=383$ g/emu,

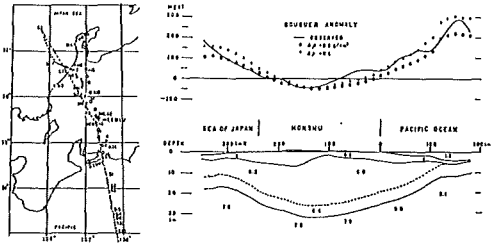
that the inclined magnetic basement corresponds to the real magnetic layer existing in the crust or merely a ghost reflecting magnetic anomaly of the subducting plate. Here, we examine the former possibility at first and then proceed to the latter case.

The correlation coefficients between Bouguer

gravity anomaly and pseudo-gravity becomes 0.99 for profile-12, 0.93 for profile-13 and 0.97 for profile-14 for the range of the negative magnetic anomaly zones. The best fitting ρ/J_{eff} (g/emu) ratio obtained from the above calculations are 159(profile-12), 170(profile-13) and 383(profile-14), respectively. These values may give the maximum estimates of the ρ/J ratio. The high correlation coefficients mentioned above imply that the magnetic basement plays the role of the density boundary producing the concave features of the Bouguer gravity anomaly.

The increasing trend of ρ/J_{eff} ratio, as seen for the above profiles from 12 to 14, can be explained in two ways, one is the increasing density contrast, the other is decreasing effective magnetization intensity. Now that the ρ/J_{eff} ratio increases with the decreasing amplitude of the negative magnetic anomaly(L8), the change of ρ/J_{eff} ratio may be attributable to decreasing trend of J_{eff} . If the density contrast is 0.3g/cm³, then the effective magnetization intensity becomes 1.89A/m, 1.76A/m and 0.78A/m for the corresponding ρ/J_{eff} ratios of 159, 170, and 383, respectively. If these magnetization intensity values were adopted in calculation of each magnetic basement, the depressions of the magnetic basements shown by thick lines in Fig.3.14 might become the similar scale among three models.

A seismic velocity structure beneath central part of Honsyu was investigated by Aoki et al. (1972) as shown in Fig.3.15. This structure is helpful for the interpretation of magnetic basement structure of profile 12,13. The general features of the upper surface of the velocity layer of 6.0-6.3km/s are analogous to that of the derived magnetic basement; the seismic surface is



Crustal structure beneath central part of Japan (Aoki et al., 1972).

Fig.3.15 Seismic velocity structure of central Honshu(Aoki et al., 1972)

relatively flat from the trench axis to the land area in about 100km from the coast and then gently tilts down toward the inland. This resemblance, though there remain some disagreements in the vertical size and relative position of the tilted surface in a strict sense, may imply that the inclined magnetic basement reflects the seismic velocity boundary within the crust. These features may become more apparent through the 2D-magneto-gravity response analysis mentioned in the following section.

As to the profile-14, the derived magnetic basement is depressed beneath the lake Biwa. These features are consistent with a seismic velocity structure obtained by Hurukawa.N.(1983), which suggests that the Conrad and Moho boundaries beneath the lake Biwa are depressed by the amount of several kms in comparison with the surrounding depths.

3.6-3 2D-magneto-gravity response analysis of profile-12

Prior to the calculation of 2D-response function, the regional trend of Bouguer gravity anomaly was removed to delineate gravity anomalies corresponding to density boundary within the crust. Fig. 3.16 shows the result of analysis of profile-12. The upper part indicates the effective inclinations of magnetization against the wave-

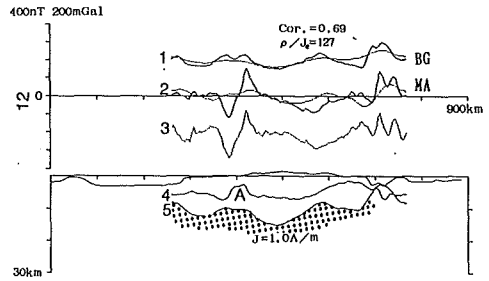
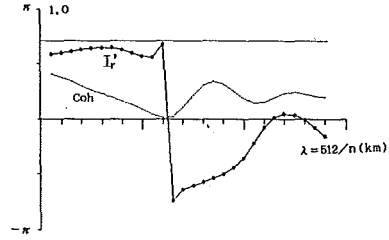


Fig.3.16 Magneto-gravity response analysis on profile-12.

(a): Effective inclination of magnetization vector (I_r') and coherence(Coh) calculated by response function.

(b): Magnetic basement model derived from magneto-gravity response filter.

1: observed Bouguer gravity(Solid) and pseudo-gravity calculated from magnetic response, 2: observed magnetic anomaly (solid) and magnetic response(dot), 3: residual magnetic anomaly, 4: magnetic basement for residuals, 5: magnetic basement for gravity-correlated magnetic anomaly, magnetization direction is present field direction and J_{eff} is 1.0A/m and ρ/J_{eff} is 127, corr=0.69.

length of the anomaly field. It is noticeable that the value of I_r' can be explained by the present field direction for the magnetic anomalies with wavelengths longer than 40km. This result manifests that the induced magnetization mainly contributes to the observed magnetic anomalies. In the lower part, is shown the magnetic basement model derived by 2D-response filter method. The

magnetic basement correlated to gravity field (5 in Fig.3.16(b)) is marked by dotted pattern and the magnetic basement corresponding to residual anomaly is indicated by solid line 4. The similarity of the gravity-correlated magnetic basement to the upper velocity layer (Fig.3.15) is much improved compared with the model shown in Fig.3.14(a). Besides, the ρ/J_{eff} ratio is reduced to 127 for this profile. The magnetic basement high denoted by A seems to be composed of granitic rock of magnetite series, because the Bouguer gravity anomaly over the magnetic basement high is not distinct.

3.6-4 Interpretation of negative magnetic anomaly zone (L8) by the subducting plate

In the former section, the negative magnetic anomaly zone was explained by the magnetic basement relief within the crust. Here, we consider another possibility which ascribes the negative magnetic anomaly to the subducting plate.

Fig. 3.17 indicates the negative peak position of the magnetic anomaly zone (Z8) by a dotted belt, together with the depth contour map of the subducting plate estimated from seismic hypocenters (Hagiwara, 1986). It is noteworthy

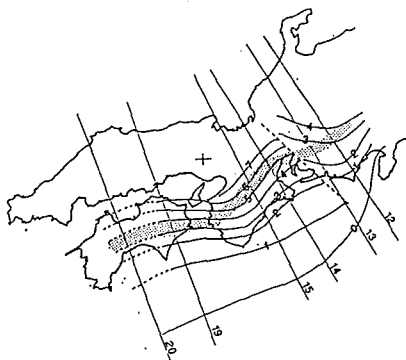


Fig.3.17 Depth to the upper surface of the subducting plate inferred from seismic hypocenters. Numerals on the contour line mean the depth in 10km unit (after Hagiwara, 1986).

that the negative peak position is almost parallel to the depth contours of the subducting plate. These features suggest that the negative magnetic anomaly zone is related to the subducting plate. To inspect this possibility, the author attempted to explain the negative magnetic anomaly zone by the forward modelling of the subducting plate. It is usually assumed that the Moho boundary is a magnetic boundary below which the structure is nonmagnetic (Wasilewski et al., 1979). So, the effective magnetic thickness of the subducting plate may be constrained by the Moho boundary. Taking the above condition into consideration, the magnetic layer of the subducting plate was approximated by two-dimensional polygons with thickness of 6 to 8km. In calculation of magnetic anomalies produced by the subducting plate, the value of magnetic susceptibility was adjusted so that the calculated anomaly fits to the observed one. The results are illustrated in Fig.3.18, from which it is seen that the agreement between observed and calculated magnetic anomalies is well as a whole, but a portion located at the tip of the subducting plate has to be neglected in the calculation except for profile-12 in order to have the calculated anomaly better fitted to the observed. Magnetic susceptibility required for the fitting amounts to 0.007cgs for the profile-12, -13 and it decreases to 0.003cgs for the profile-15, -19. These values are considerably larger than the mean susceptibility value (0.001cgs) of the basalt samples obtained by DSDP (Lowrie, 1973). This disagreement may be avoided if a larger thickness is assigned to the subducting plate model, but this will lead to the denial of the general conception that the Moho boundary is a magnetic boundary. It is also noteworthy that the region between profile-15 and

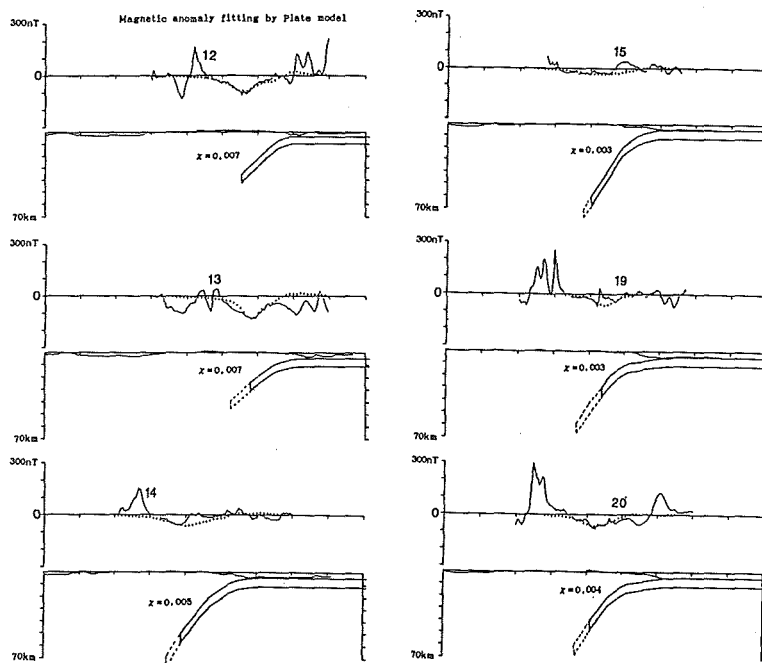


Fig. 3.18 Magnetic anomaly fitting by subducting plate model for profile 12 to 20. Estimated magnetic susceptibility (cgs) is shown in each profile.

Dotted part of the plate model should be neglected in order to fit the calculated anomaly to the observed one. $1.0 \text{ SI susceptibility} = 1/4\pi \text{ cgs}$.

-19, which is characterized by low susceptibility of the subducting plate, corresponds to north-western extension of the extinct spreading axis of the Sikoku Basin. High heat flow is also confirmed in the vicinity of the extinct spreading axis (Watanabe, 1972). These features suggest that the subducting plate near the extinct spreading axis is still hot, which reduces magnetic susceptibility of the subducting plate for profile-15 to 19. On the other hand, the high susceptibility for profile-12 and 13 may reflect the cold subducting plate with high magnetic susceptibility. The above interpretation, based on subducting plate model, however, seems to be unacceptable because of the unusually high susceptibility needed for simulating the observed anomalies.

3.6-5 concluding remarks

To explain the negative magnetic anomaly

zone, two alternative interpretations were proposed, one is ascribing the magnetic anomaly source to the magnetic boundary existing within the crust, the other to the effective magnetic layer of the subducting plate. The former interpretation seems to be consistent with a seismic velocity structure, but the latter needs unacceptably large susceptibility. Judging from these aspects, the former interpretation seems to be more plausible.

3.7 Southwest Honsyu

3.7-1 Background

Southwest Honsyu is characterized by a remarkable positive anomaly trending in the WSW-ENE direction. The magnetic zone (L6) extends as far as Hokuriku district as shown by L7 in Fig. 3.1. This anomaly is comparable to the

continental linear anomalies of HKLA and SILA in scale. Hereafter, we name this continental anomaly as southwest Honsyu linear anomaly (SWHLA) for convenience sake. The distribution of SWHLA agrees well with the outcrops of granitic rocks of magnetite series (Ishihara, 1979) of Late Cretaceous to Early Tertiary age. Here, we examine the possibility of ascribing SWHLA to granitic rocks of magnetite series. Palaeomagnetic measurement of igneous rocks provides important constraints for a magnetic inversion. In regard to this, palaeomagnetic investigation conducted by Otofujii et al. (1988) is instructive; they indicate that the mean direction of the remanent magnetization becomes $\text{Dec} = 66^\circ$, $\text{Inc} = 49^\circ$ for the Tertiary igneous rocks of southwest Honsyu. The easterly deflected magnetization direction is interpreted as the result of opening of the Japan Sea. Magnetic field analysis of SWHLA may be helpful for the inspection of the above palaeomagnetic result.

The outer region of southwest Japan can be divided into several tectonic belts which are arranged in parallel to the general trend of southwest Japan (see Fig. 3.2). The Kurosegawa tectonic belt, which is located geographically in the Chichibu belt is characterized by serpentinite suits holding land masses of remnant arc complex or microcontinent origin. For consideration of accretional tectonics of southwest Japan, it is an important subject to estimate the vertical and lateral extent of buried bodies of the Kurosegawa tectonic belt. The magnetic basement model presented here may be helpful for the above consideration.

3.7-2 Magnetic basement models of profile-19 to 21.

The magnetic and Bouguer gravity anomaly

together with the derived magnetic basements of profile-19 to profile-21 are shown in Fig. 3.19(a) to 3.19(c). In contrast to northeast Honsyu, the general features of the Bouguer gravity anomaly over southwest Honsyu is flat (GSI, 1985). These features are also apparent in the Bouguer gravity anomaly profile shown in Fig. 3.19. The small gravity amplitude corresponding to SWHLA suggests that the buried magnetic body producing SWHLA has no substantial density contrast. The correlation analysis between the observed Bouguer gravity and pseudo-gravity shows that the best-fit ρ/J_{eff} (g/emu) ratio becomes 50 to 60 for profiles-20 and 21. These low ρ/J_{eff} ratios reflect the small density contrast and the large effective magnetization intensity of the causative magnetic body. This fact is in favour of granitic rocks of magnetite series as the source body of SWHLA. Referring to Ishihara (1979), granitic rock of magnetite series should have magnetic susceptibility larger than 50×10^{-6} emu/g, but in the majority of cases, the value is less than 1×10^{-3} emu/g. For the susceptibility values varying from 1.0×10^{-4} to 1.0×10^{-3} emu/g, the expected induced magnetization falls in the range from 0.1 A/m to 1.3 A/m under the ambient magnetic field of 47500 nT. The thickness of the derived magnetic basement of profile-19 amounts to 10 km under the assumed magnetization intensity of 2.0 A/m (see Fig. 3.19(a)), which is considerably large value for the granitic rock of magnetite series. The magnetic basement models of profile-20 and 21, which were calculated under the assumed magnetization intensity of 3.0 A/m, also show a similar scale of the magnetic body responsible for SWHLA (model A in Fig. 3.19(b), 3.19(c)). The vertical size of the causative magnetic body might become larger, if the small-

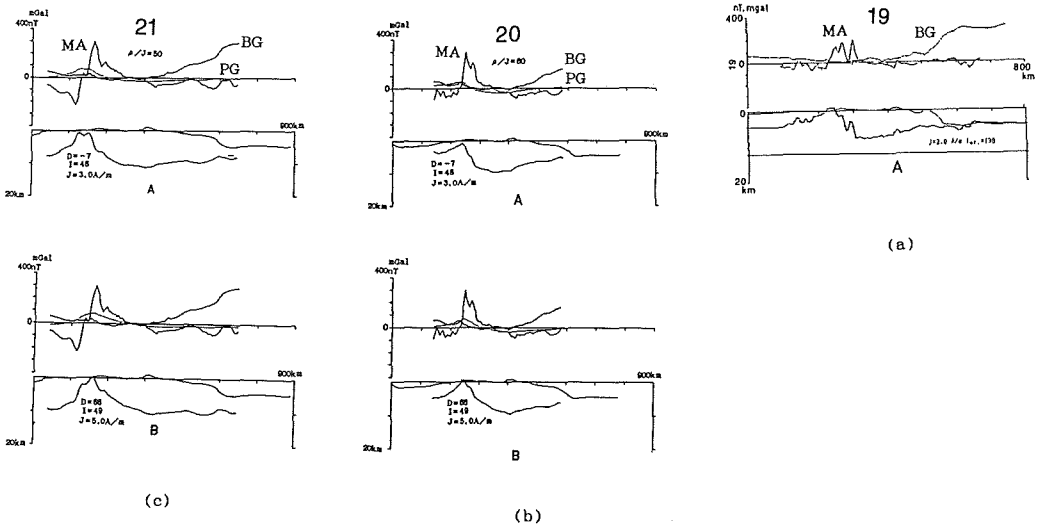


Fig.3.19 Magnetic basement models of profiles 19 to 21.

Magnetization direction of the models are as follows, Model A: present field direction, model B: easterly deflected direction of $D_r=66^\circ$, $I_r=49^\circ$ as derived from palaeomagnetic measurements. The derived ρ/J_{eff} ratio and assumed magnetization intensity are shown in the figure. MA:magnetic anomaly, BG:Bouguer gravity anomaly, PG:Pseudo-gravity.

(a): for profile-19, (b): for profile-20, (c): for profile-21.

ler magnetization intensity were assumed in magnetic inversion. On the other hand, steep thermal gradient observed in the inner region of southwest Honsyu (Watanabe,1972) may constrain the magnetic source at relatively shallow depth. The models obtained above reveal that the huge granitic body is required to explain the observed magnetic anomaly by the granitic body of magnetite series. These buried magnetic bodies, however, have not been confirmed by seismic exploration.

In the above discussion, the source body is assumed to be magnetized in the present field direction. The palaeomagnetic measurement of Tertiary igneous rocks in southwest Honsyu, however, reveals that the mean direction of the remanent magnetization becomes $Dec = 66^\circ$, $Inc = 49^\circ$. The models B in Figs 3.19(b), 3.19(c) are magnetic basement models incorporating the

above palaeomagnetic measurements. As the easterly deflected magnetization vector aligns sub-parallel to the strike of SWHLA, the effective magnetization intensity becomes less than that of normal magnetization vector. Besides, the effective inclination changes from 130° to 94° in accordance with variation of magnetization direction from present field direction to easterly deflected magnetization direction. The above features result in the large magnetization intensity appearing in easterly magnetization model (Fig.3.19(b), 3.19(c)) in contrast to the present field model; i.e. the magnetization intensity of $5.0A/m$ is needed for easterly deflected magnetization model in place of $3.0A/m$ for the normal magnetization model.

Such a large magnetization intensity required for the easterly deflected magnetization model exceeds the acceptable value for the granitic

rocks of magnetite series. To avoid such contradiction, we should ascribe the observed magnetic anomaly to the induced magnetization and/or viscous remanent magnetization instead of thermal remanent magnetization. Viscous remanent magnetization may be likely to conquer the results of the palaeomagnetic measurements showing the easterly deflected magnetization vector. The viscous remanent magnetization generally tends to increase under the steep thermal gradient at depth (shimizu,1960). This fact may support the viscous remanent magnetization for the origin of SWHLA.

3.8 Discussions and concluding remarks of chapter III

Two-dimensional analysis gives the effective intensity and inclination of magnetization vector as shown in Fig.2.1. Several combinations of declination and inclination can produce the same effective inclination, so generally, the magnetization intensity can not be determined uniquely from two-dimensional analysis. However, when the declination and inclination, producing the calculated effective inclination, are given, the intensity of magnetization can be determined from the effective magnetization intensity. As seen in Fig.2.1, the effective magnetization intensity becomes smaller than the original magnetization intensity depending on the azimuth of profile. In Table 3.1 is shown the relationship between 3D-magnetization parameters and 2D-ones for each profile. From the ratio of J_{eff}/J we can calculate the original magnetization intensity from the effective one for the given magnetization direction. The derived magnetization parameters are summarized in Table 3.2, which were deduced from the relation shown in Table 3.1.

The magnetic and gravity field analysis of the Kurile and northeast Honsyu Arcs reveals the magnetic basement high corresponding to upheaval of the density boundary within the crust. Especially, the magnetic basement high of northeast Honsyu(profile-06) agrees with the upheaved conrad boundary derived from the seismic velocity structure. Referring to the effective magnetization intensities estimated from the derived ρ/J_{eff} ratios for the density contrasts of $0.3g/cm^3$, the magnetization intensity of the lower crust becomes $2.5A/m$ for the Kurile Arc and $3.0A/m$ for the northeast Honsyu Arc. In addition, it also becomes apparent that the magnetic bodies of low ρ/J_{eff} ratio plays the important role to the observed magnetic anomaly. No remarkable gravity anomaly is recognized over the KHLA in the offing of southeast Hokkaido. This may imply

Table 3.1 Relation between 3D and 2D magnetization parameters for each profile.

No.	AGL	D.	I.	I _e '	J _e /J	F nT	χ cgs	J = χF emu/cm ³ (10 ⁻³)
01	89°	-9°	58°	95°	0.85	50,000	1	0.50
02	106°	-9°	57°	106°	0.86	49,500	1	0.50
03*	90°	-8°	56°	95°	0.83	48,500	1	0.49
	90°	-41°	56°	113°	0.91			
	90°	-45°	-5°	-173°	0.71			
04	1°	-8°	56°	56°	0.99	48,500	1	0.49
06	101°	-8°	56°	102°	0.85	48,000	1	0.48
	101°	-41°	56°	118°	0.94			
07	105°	-8°	53°	106°	0.83	47,500	1	0.48
12	147°	-7°	49°	128°	0.96	46,000	1	0.46
13	149°	-7°	49°	128°	0.96	46,000	1	0.46
14	150°	-7°	49°	129°	0.97	46,500	1	0.47
15	154°	-7°	48°	130°	0.98	46,500	1	0.47
16	90°	-6°	46°	95°	0.72	445,000	1	0.45
19	161°	-7°	49°	130°	0.99	47,500	1	0.48
	161°	66°	49°	94°	0.78			
20	160°	-7°	48°	131°	0.99	47,500	1	0.48
	160°	66°	49°	94°	0.78			

AGL:Azimuth of profile, F:total intensity magnetic field
 J_e:effective magnetization intensity
 susceptibility(cgs)·4π=susceptibility(SI), 10⁻³·emu/cm³=A/m
 θ: This azimuth is orthogonal to the magnetic lineation. Azimuth of flight line is 100°.

J_e:effective magnetization intensity,

F:total intensity of magnetic field,

χ :magnetic susceptibility, @:1cgs=1/4πSI,

#:1emu/cm³=10³A/m.

Table 3.2 ρ/J ratio and magnetization of the crust of Kurile and Honsyu Arcs.

Assumed boundary		ρ/J_{eff} (g/emu)	ρ (g/cm ³)	J_{eff} (emu/cm ³) 10 ⁻³	J (emu/cm ³) 10 ⁻³	χ (cgs) 10 ⁻³
Outer region of Kurile Arc (04)	Conrad?	119	0.2 0.3	1.7 2.5	1.7 2.5	3.5 5.2
	Conrad?	69*	0.2 0.3	2.9 4.3	3.5 5.3	---
Outer region of NE Honsyu (03)	Conrad	121	0.2 0.3	1.7 2.5	2.0 3.0	4.2 6.3
	Upper crust?	≤ 159	0.2 0.3	≥ 1.3 1.9	≥ 1.3 2.0	≥ 2.8 4.2
Outer region of central Honsyu ¹ (12)		127*	0.2 0.3	1.6 2.4	1.6 2.4	3.5 5.3
		≤ 170	0.2 0.3	≥ 1.2 1.8	≥ 1.2 1.8	≥ 2.6 3.9
(13)		≤ 383	0.2 0.3	≥ 0.5 0.8	≥ 0.5 0.8	≥ 1.2 1.7
	Upper crust	≤ 50	0.1	≥ 2.0	≥ 2.0	≥ 4.2
Inner region of SW Honsyu ²						

note: susceptibility(cgs) $\cdot 4\pi$ = susceptibility(SI), 10^{-3} emu/cm³ = A/m

*: result by magnetic-gravity response analysis

0: magnetization direction (D, = -45, I, = -5) is to be explained by remanent magnetization.

1: Derived ρ/J_{eff} ratios of central Honsyu may become less than the derived values, when the depressed Moho boundary were taken into account.

2: The derived ρ/J_{eff} ratio of southwest Honsyu gives the maximum value as shown by featureless Bouguer gravity anomaly.

that serpentinite suites of low density contrast lies beneath KHLA. Such a magnetic structure is significant in the consideration of the process of serpentinization occurring in the forearc region. As to northeast Honsyu, the magnetic bodies of low density contrast overlaps the magnetic basement high corresponding to the upheaval of the lower crust. Referring to Ishihara(1979), the above overlapping body seems to be granitic rocks of magnetite series. On the other hand, the results of analyses in central Honsyu reveal that the magnetic boundary corresponds to the upper surface of the layer with the velocity of 6.0 to 6.3 km/s seismically obtained. However, this conclusion is still of debate because of scarcity of evidence available, so more extensive and detailed explorations are required to derive a definite conclusion.

The large amplitude anomaly occurring in San-in district, southwest Honsyu may be

ascribed to an enhanced susceptibility of granitic rocks of magnetite series. Besides, the viscous remanent magnetization in favour of normal magnetization may also be responsible for the origin of the observed large amplitude anomaly. The depth of the buried magnetic bodies seems more or less 10km, but the corresponding seismic structure has not been confirmed yet. The derived ρ/J_{eff} (g/emu) ratio of SWHLA become 50 to 60, which may reflect low density contrast of the causative body.

The derived magnetic basement models for the outer region of southwest Japan shows no conspicuous magnetic basement high corresponding to the Mikabu and Kurosegawa tectonic zones. These features suggest that the tectonic belts are not accompanied with magnetic bodies comparable to the Kamuikotan belt which is associated with conspicuous magnetic basement high as seen in Fig.3.4. As mentioned above, forearc regions of the Kurile and northeast Honsyu Arcs are characterized by the magnetic lower crust. In contrast to this, forearc region of southwest Japan is featureless in magnetic structure.

Wasilewski and Mayhew(1982) measured the magnetic property of the crustal xenoliths from two locations in Japan with different tectonic settings in regard to hydration and temperature gradient in the lower crust. According to their measurements, Hornblend gabbros and amphibolites recovered from the Ichinomegata crater in the northeast Honsyu Arc is highly magnetic with Curie point near 550°C. They ascribed the high magnetization of these xenoliths to hydrous and relatively low-temperature melting above the descending Pacific plate. The above oxidation condition produces titanomagnetites rich in magnetite content with a large magnetiza-

tion intensity and high Curie point. The hydrous condition of the crust beneath the forearc region of Northeast Honsyu, Kurile, and Izu-Ogasawara Arcs may also be attributable to dehydration of serpentine on the subducting slab (Tatsumi, 1989).

On the other hand, the pyroxene gabbros and granulites from Oki-Dogo island in the neighbourhood of southwest Honsyu contains abundant ilmenite and titanomagnetite with the composition like ulvospinel having low Curie point as 300° C. These magnetic minerals are produced under anhydrous condition with high heat flows. Takahashi (1978) ascribed the above reducing environment in the lower crust to the subduction of the Philippine plate in the state of hot and dry condition. Although the information available of rock-magnetism of xenolith samples is restricted, the above condition inferred from xenolith samples is suggestive for the understanding of the contrasting magnetic property of the lower crust between northeast Honsyu and southwest Japan.

Central Honsyu seems to be in intermediate state in regard to the magnetic property of the crust as inferred from the magnetic layer having density contrast within the crust (see Figs. 3.14, 3.16). The upper crust of central Honsyu (profile-12) has the ρ/J_{eff} ratio of 127 beneath the northeastern part, whereas it increases toward southwest as shown by the ρ/J_{eff} (g/emu) ratio of 383 for the profile-14 crossing the Kii peninsula. This trend seems to be caused by the decreasing trend of magnetization intensity of the causative magnetic layer in the crust. The lateral variation of magnetization intensity of the upper crust may also be correlated to hydrous and thermal conditions within the crust; i.e., the relatively high oxidation condition may be prevailing beneath

the northeastern part of central Honsyu, where the relatively colder and older Philippine Sea plate has been subducting. In contrast to this the relatively hotter and younger Philippine Sea plate has been subducting beneath the southwestern part of central Honsyu, which may make the crust in relatively reducing environment. The different oxygen fugacity ($f\text{-O}_2$)-temperature conditions in equilibrium state in the crust, resulting from the subducting slab of different state, may be responsible for the different magnetization contrast beneath the outer region of central Honsyu.

The conspicuous positive anomaly over the inner region of southwest Honsyu may be explained by granitic rocks of magnetite series. However, the large magnetization intensity for granitic rocks may suggest that the magnetic susceptibility and/or viscous remanent magnetization of the source body has been enhanced. Judging from the xenolith samples from Oki-Dogo island, which are rich in ilmenite and titanomagnetite with composition close to ulvospinel, reducing environment (hot and dry condition) seems to be prevailing in the crust of southwest Honsyu. On the contrary, there exist granitic rocks of magnetite series as mentioned before. The above contradiction may arise from the different equilibrium condition in the Late Cretaceous age under which the granitic massives of magnetite series in the inner region of southwest Honsyu were formed.

CHAPTER IV. CRUSTAL STRUCTURE OF THE IZU-OGASAWARA (BONIN) ARC AS REVEALED FROM MAGNETIC AND GRAVITY FIELD ANALYSIS

4.1 Data description

The geophysical data used for this study are based on the sea-bottom surveys conducted by JHD. The track lines and cruise files are shown in Fig.4.1 and Table 4.1, respectively. These data are now supplied on request from JODC in MGD77 format (Hittleman et al., 1981). The

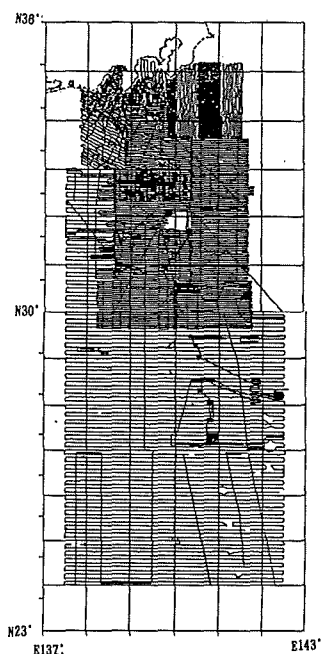


Fig.4.1 Track lines of sea-bottom survey data on the Izu-Ogasawara (Bonin) Arc. The dense track lines were measured by S/V Shoyo and rough ones by S/V Takuyo of JHD. The data file names are listed in Table 4.1, which were released from JODC in MGD77 format.

Table 4.1 MGD77 data file names used for mapping the geophysical data of the Izu-Ogasawara Arc.

At the scale of 1/200,000	At the scale of 1/500,000
HN6801, HN7402, HN7404, HS7502	HT8501, HT851124, HT860111
HN7601, HS7604, HS7802, HS8005	HT881004, HT881101, HT881201
Vicinity of Izu-islands 1983	HT881202, HT891801, HT891802
South of Hatizyo part-1 1983	HT881101
South of Hatizyo part-2 1984	
Vicinity of Sumisu 1984	
Vicinity of Tori-sima 1985	
Vicinity of Tori-sima 1986	
East of Hatizyo 1987	
East of Sumisu 1988	

dense track lines in Fig.4.1 are about 2 nautical miles(n.m.) in spacings and relatively rough track lines are about 5 n.m.. The former were surveyed by the S/V Shoyo of JHD as part of the Basic Map of the Sea Project at the scale of 1/200,000 and the latter by the S/V Takuyo of JHD as part of continental shelf survey at the scale of 1/500,000 for the establishment of 200 n.m. economic marine zone. The survey items are composed of depth sounding, seismic profiling, and magnetic and gravity measurements. Depth sounding was conducted by a single beam echosounder installed on the S/V Shoyo or a sea-beam system on the S/V Takuyo. In preparation for digital mesh depth data, an ETOPO5 depth file of 5'×5' mesh offered from NGDC(National Geophysical Data Center) of NOAA were also employed to cover the unsurveyed area.

The proton precession magnetometer was towed about 250m to 300m behind the vessel to avoid the ship's magnetic field. The diurnal dis-

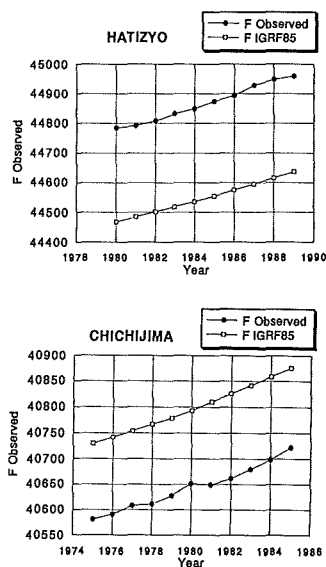


Fig.4.2 Secular variation of total intensity magnetic field at Hatizyo and Chichijima(Titi-sima) islands.

turbing field was removed based on the magnetic data observed at the adjoining stations in Hatizyo or Titi-sima islands. The IGRF1985 model was adopted for calculation of magnetic anomaly, because this model incorporates well approximated secular variations (see Fig.4.2).

The gravity field was measured by the surface ship gravimeter of TSSG before the fiscal year of 1983 and then of KSS-30 made by Bodenserwerk. Free-air gravity anomaly was deduced by subtracting the normal gravity value from the observed one.

The above survey data are compiled into a MGD77 format and then released to users through JODC. To prepare the grid data for analytical use, these data sets were projected on a x-y coordinate on the basis of Mercator projection whose origin and reference latitude are listed in Table 4.2. The grid data were then calculated by the iteration method using the 2nd degree polynomial fitting. The magnetic and gravity field in the vicinity of the Myozinsyo reef and other islands were interpolated from the surrounding data, so the contour lines over these land areas are not exact.

Table 4.2 Projection parameters for X-Y conversion of the MGD77 data of the Izu-Ogasawara Arc.

1. Northern part of the arc
Origin: N28°, E137°
Reference latitude: N32°
Projection: Mercator
Azimuth of Y-axis: 0°
2. Southern part of the arc
Origin: N24°, E139°
Reference latitude: N26°
Projection: Mercator
Azimuth of Y-axis: 0°

Terrain effect of gravity field (TE) was calculated by Parker's inversion method described in Chapter II using digital depth data. The target area was divided into several subareas which were overlapped at the margin each other. The Bouguer gravity anomaly (BG) at grid points is given by $BG = FG - TE + 68.75 \cdot D$ (mgal) for the assumed density of 2.67g/cm^3 , where FG is a free-air gravity, and D is a grid-mean depth within the subarea in km unit. The calculated Bouguer gravity anomalies for the contiguous areas were then connected continuously by calculating the distance-depending weighted mean for the overlapping area.

Thus the obtained grid data were expressed as the contour maps of bathymetry, free-air and Bouguer gravity anomaly and the total intensity magnetic anomaly, covering the northern and southern part of the Izu-Ogasawara Arcs (Fig.4.3 to 4.6). Although there are some inconsistency at the adjoining zones due to different reference latitude of contraction and numerical errors of terrain effect, the general features can be observed continuously between the northern and southern parts. Explanations of abbreviations shown in these maps are given in Table 4.3.

4.2 Geological settings

Bathymetry of the Izu-Ogasawara Arc is shown in Fig.4.3 and the representative topographic names and abbreviations are listed in Table 4.3.

The Izu-Ogasawara Arc is characterized by N-S trending ridges named the Nisi-Sitito ridge, the Sitito-Iozima ridge, and the Ogasawara ridge from west to east in parallel to the Izu-Ogasawara trench. The Sitito-Iozima ridge corresponds to the Quaternary volcanic front. The configuration and geological features are quite

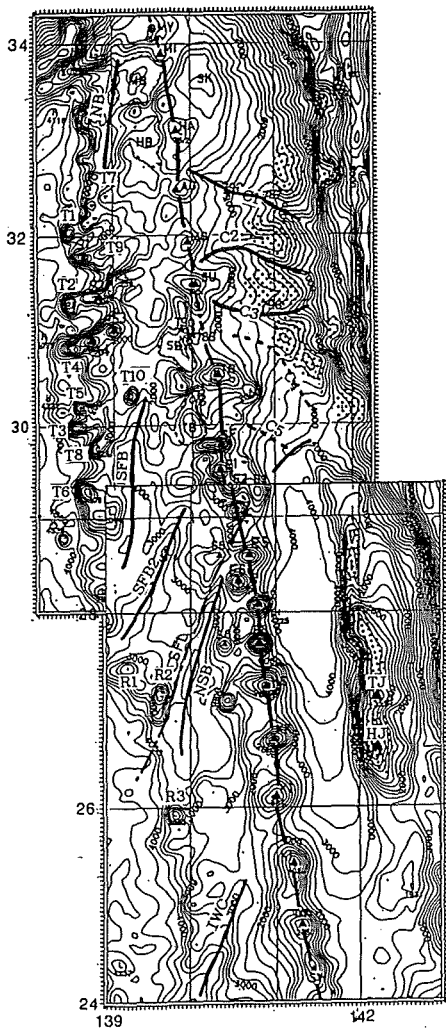


Fig. 4.3 Bathymetry of the Izu-Ogasawara Arc. Contour interval is 250m.

SFL: Sofugan tectonic line, C1 to C5: submarine canyons, IWC: Ito submarine canyon, SFB: Sohu trough, NB: Nisi-Sitito trough, MB: Mikura depression, HB: Hatizyo depression, SB: Sumisu depression, TB: Torisima depression (Tamaki and Miyazaki, 1984). Other abbreviations are listed in Table 4.3. Dotted areas indicate the topographic rises in the forearc region of the arc. The sites of ODP Leg126 cruise are indicated by the site numbers with ★ mark (Fujioka et al., 1989). A colour image map is shown in annex-1(a).

Table 4.3 Topographic names of the Izu-Ogasawara (Bonin) Arc.

Abbr.	name	position	
		Lat	Lon
MY	Miyake Sima	34° 05'	139° 31'
MI	Mikura Sima	33 52	139 35
HA	Hatizyo Sima	33 07	139 48
AG	Aoga Sima	32 28	139 45
MG	Myozin Syo	31 55	140 00
SU	Sumisu Sima	31 30	140 05
TR	Tori Sima	30 32	140 22
SF	Sohu Gan	29 47	140 21
E1	Nitiyo SMT	29 28	140 21
E2	Getuyo SMT	29 18	140 28
E3	Oomati SMT	29 12	140 50
E4	Kayo SMT	29 02	140 32
E5	Suiyo SMT	28 35	140 45
E6	Mokuyo SMT	28 20	140 35
E7	Kinyo SMT	28 05	140 47
E8	Doyo SMT	27 40	140 52
S6	Sawa SMT	27 39	140 28
NS	Nisino Sima	27 14	140 58
KK	Kaikata SMT	26 42	141 30
KT	Kaitoku SMT	26 05	141 00
KI	Kita-Io Sima	25 24	141 18
IW	Io Sima	24 46	141 19
SW	Minami-Io Sima	24 12	141 28
S1	Kanbun SMT	31° 45'	138° 40'
S2	Tenwa SMT	31 22	138 43
S3	Genroku SMT	30 58	138 57
S4	Houei SMT	30 52	138 39
T1	Nisi Syoou SMT	32 03	138 22
T2	Nisi Teikyo SMT	31 18	138 21
T3	Kanei SMT	29 57	138 24
T4	Seitoku SMT	30 47	138 21
T5	Kanpo SMT	30 10	138 36
T6	Anei SMT	29 17	138 40
T7	Seiho SMT	32 20	138 45
T8	Meiwa SMT	29 43	138 40
T9	Hanzi SMT	31 52	138 57
T10	Houeki SMT	30 18	139 16
R1	Nisi Tenpo SMT	27 15	139 22
R2	Tenpo SMT	27 09	139 36
R3	Nisi Kaitoku SMT	25 56	139 49
TJ	Titi Sima	27 03	142 09
HJ	Haha Sima	26 38	142 12
C1	Aogasima submarine canyon		
C2	Myozin submarine canyon		
C3	Sumisu submarine canyon		
C4	Torisima submarine canyon		
MB	Mikura Basin		
HB	Hatizyo Basin		
SB	Minami Sumisu Basin		
TB	Tori Sima Basin		

different between the northern part and the southern part of the arc which may be bordered by the Sofugan tectonic line as noted by Yuasa and Murakami (1985). The inner region (the region to the west of volcanic front) of the northern part is characterized by the en-echelon arrangement of the ridges in the west, the rifting zone such as Mikura, Hatizyo, Sumisu and Torisima depressions in the east and in between the province of

troughs and knolls. On the other hand, the outer region (forearc region) is characterized by acoustic basement highs and sediment filled basin structure; inner arc highs such as the Sinkurose bank the Sumisu spur etc. in the west and then followed trenchward by forearc basins and outer forearc highs on the continental slope break. The diapiric seamounts are also recognized in the landward trench slope break east of Aoga-sima island from which numerous serpentinite melanges were recovered (Maekawa et al., 1989). The submarine canyons are also well developed in the forearc region.

The southern part of the Izu-Ogasawara Arc consists of zonal arrangements of the Sitito-Iozima ridge, the Ogasawara trough and the Ogasawara ridge from west to east. In contrast to northern part of the Izu-Ogasawara arc, an en-echelon arrangement of the Nisi-Sitito ridge becomes vague. In addition, the discrete features of the seamounts of the Sitito-Iozima ridge become more apparent.

As to the chronology of the basement rocks of the Izu-Ogasawara Arc, no rocks older than Eocene age have ever been recovered. The rock samples from the forearc region show the wide range of age from 6.0 Ma to the value around 40 Ma. The dredged volcanic rocks from the Sinkurose bank shows the K-Ar age of 6.0 MaBP (Yuasa and Murakami, 1985). This samples were subject to weathering in considerable degree, so the above dating may mean the minimum age. On the other hand, DSDP drilling holes (leg 126, 792) on the continental slope east of Aoga-sima island revealed the Mg-rich andesite overlain by the sediments of turbidite facies of late Oligocene age (Fujioka et al., 1989). In the southern arc, the boninites and dacite samples recovered from

Titi-sima island have the age of 26 to 41 MaBP (Kaneoka et al., 1970; Tsunakawa, 1983). Besides, Nummulites recovered from Haha-sima island in the southern part of the Ogasawara ridge favours the Eocene time as the ridge formation.

In contrast to forearc region, few dated rocks are available for the Nisi-Sitito ridge. The basaltic rocks dredged from a seamount (D368) 100km west of Sumisu island gives a unique K-Ar age of 2.2 MaBP (Yuasa and Murakami, 1985).

The rock chemistry of the Sitito-Iozima ridge reveals the along-arc variation (Yuasa and Nohara, 1992); i.e. the northern part (Osima to Sohugan) of the arc is characterized by low alkaline tholeiite and the southern part (Nisinosima to Minami-Io-sima) by high alkaline tholeiite. The Quaternary volcanic islands of Osima, Miyake, Mikura, Hatizyo are accompanied by basaltic stratovolcanoes. The other volcanoes, Sumisu-sima, Tori-sima, Sohugan also outcropped the basaltic rocks. On the other hand, acidic rocks such as dacitic and rhyolitic rocks were dredged from submarine calderas of Kurose hole, Daini-daisan Aogasima knolls, Myozin knoll, Sumisu-sima, Daisan-Sumisu knoll in the northern arc. These acidic rocks are rich in TiO_2 , FeO relative to the average value of Japanese granitoids (Yuasa and Nohara, 1992). The acidic to andesitic rocks were also sampled from the inner forearc high of Omurodasi, Sinkurose bank, and DSDP hole 792, 793 (Fujioka et al., 1989).

As to the volcanic chains in the southern Izu-Ogasawara Arc, three segments are proposed by Yuasa and Nohara (1992) in terms of alkali content. The first group consists of Oomati, Sawa and Sitiyo seamounts located in the Nisinosima

trough, the second: Nisino-sima to Kita-Io-sima and the third: Io-sima to Minami-Io-sima. The first group is further divided into three groups, younger group (Getsuyo, Kayo, Kinyo, Doyo), older group (Nitiyo, Omati, Sawa) and intermediate one (Suiyo, Mokuyo) in terms of topographic, magnetic and seismic features. The first group outcropped mainly andesite rocks, whereas intermediate-group and the Doyo seamount outcropped basaltic rocks. From the Ogasawara ridge loading the Ogasawara islands, boninites and Mg-rich andesites were recovered as mentioned before.

4.3 Characteristic features of magnetic and gravity anomalies

4.3.1 Gravity anomaly

To extract the gravity anomalies corresponding to shallow sources in the crust, the high-pass filtered anomaly ($\lambda_c=160\text{km}$) was calculated based on the Bouguer gravity anomaly map (Fig. 4.5) as shown in Fig. 4.8. Free-air gravity anomaly map (Fig. 4.4) indicates conspicuous gravity anomalies associated with the Ogasawara ridge, whose amplitude amounts to 360mgal. The positive gravity anomaly seems to extend northward in good accordance with the outer forearc high. The negative free-air gravity anomaly lying over the Ogasawara trough can also be traced up to $N32^\circ15'$ as the concave pattern corresponding to the forearc basin. The above features are also recognized in the Bouguer gravity anomaly map (Fig. 4.5). The complicated free-air gravity anomaly of the Nisi-Sitito ridge becomes featureless in the Bouguer gravity anomaly, which suggests that the mean density of the ridge agrees well with the assumed density of 2.67g/cm^3 . The Bouguer gravity anomalies associated with

Quaternary volcanoes also become subdued in comparison with the free-air gravity anomalies, but some oval patterns remain over seamounts in the southern part, which are especially apparent at Kaitoku seamount and Kita-Io-sima island. These features are clearly shown in the high-pass filtered Bouguer gravity anomaly map (Fig. 4.8). This fact suggests that the mean density of the southern seamounts (from Nisino-sima to Minami-Io-sima) is larger than the assumed density (2.67g/cm^3) reflecting the basaltic composition of the edifices or the buried basements. The back-arc depressions of the northern arc (Hatizyo, Sumisu, Torisima basins) seem to be accompanied with relative gravity highs as shown in the short-wavelength Bouguer gravity anomaly map (Fig. 4.8), which may manifest intrusive basic bodies of large density. In the northern arc, low Bouguer gravity anomaly zone (140 to 150 mgal) occurs to the west of the Quaternary volcanic front. The above low Bouguer gravity anomaly zone becomes obscured to the south of the boundary shown by the steep gravity gradient zone running in WSW from the vicinity of Torisima island (G-G' in Fig. 4.5). As the general trend of Bouguer gravity low is due to the crustal thickening, afore-mentioned features suggest that the crustal thickness of the inner arc decreases abruptly at the above gravity boundary.

In contrast to the northern arc, the southern arc has the low Bouguer anomaly zone over the Ogasawara trough to the east of the volcanic front (forearc region). The minimum of Bouguer gravity anomaly which is less than 100mgal occurs over the southern part of the Ogasawara trough. The amount of gravity depression exceeds 100mgal relative to the surrounding val-

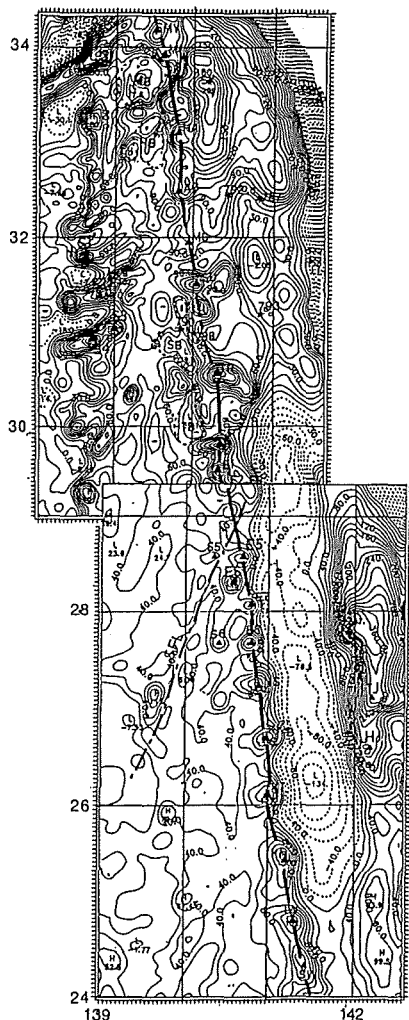


Fig.4.4 Free-air gravity anomaly of the Izu-Ogasawara Arc.

Contour interval is 10mgal in the northern part and 20mgal in the southern part respectively. Quaternary volcanic front is shown by thick lines. A colour image map is shown in annex-1(c).

ues, which may not be attributable to the sedimentary layer of negative density contrast only. To elucidate the cause of such a low Bouguer gravity value, seismic velocity structure beneath this zone should be investigated.

The Nisinosima trough, which is bounded to the north by the Sofugan tectonic line, is char-

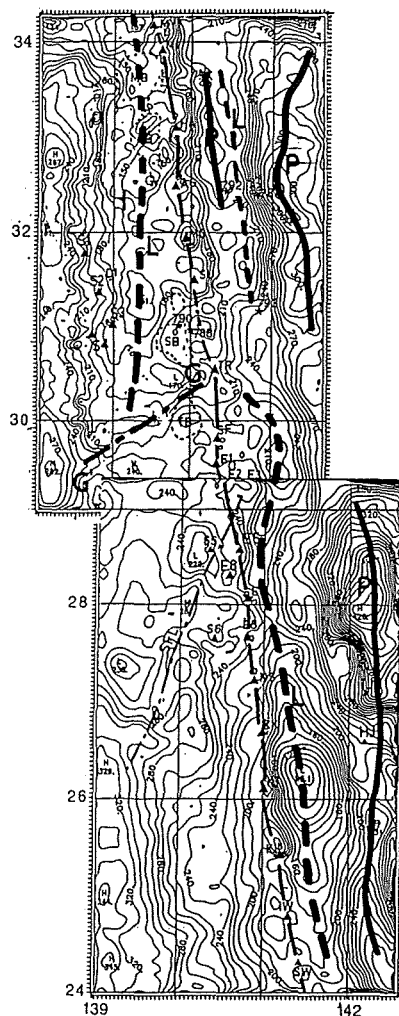


Fig.4.5 Bouguer gravity anomaly of the Izu-Ogasawara Arc.

Contour interval is 10mgal. Positive belts are shown by the thick lines(P) and negative ones by dotted lines(L). G-G' is the sharp gravity gradient separating the northern and southern arcs. A colour image map is shown in annex-1(d).

acterized by the relative Bouguer gravity high amounting to 30 to 40mgal. These features imply the thinning of the crust, which may be consistent with the rifting origin proposed by Yuasa (1992). The extraordinarily large Bouguer gravity amounting to 400mgal in amplitude, occurring over the Ogasawara ridge, may be simulated by

the upheaval of the Moho boundary, but some amount of them may be ascribed to the ridge itself as noted from the associated positive short-wavelength Bouguer anomaly (Fig.4.8).

4.3.2 Magnetic anomaly

The forearc region of the northern part of the Izu-Ogasawara Arc are characterized by the intermediate amplitude ($>300\text{nT}$) and long-wavelength magnetic anomalies (1 to 5 in

Fig.4.6). These anomalies may correspond to igneous rocks of Eocene to Oligocene age as mentioned in the foregoing section. Some of them are associated with the low Bouguer gravity anomalies, which may be resulting from skewness effect of remanent magnetization or low density contrast of the buried magnetic source. The positive anomalies (6 to 9 in Fig.4.6) occur over the continental slope break in good correspondence with the positive Bouguer gravity highs as shown in Fig.4.8. The conspicuous anomalies are observed over the Quaternary volcanoes reflecting the basaltic to andesitic bodies. Marked anomalies with amplitude larger than 400nT are recognized in the west of the Sinkurose bank, south of Hatizyo island, near of Aogasima island and in the vicinity of Sohugan island (10 to 13 in Fig.4.6). Some volcanoes are not accompanied by appreciable anomaly (SU, TO, E1, E2 in Fig 4.6). These features may reflect the differences in petrochemical composition of these volcanoes.

Yamazaki et al. (1991) proposed that the Sitiyo volcanoes (Nitiyo to Doyo seamounts) can be classified into four groups according to the associated topography, seismic profiling and magnetic anomaly patterns. According to their classification, seamounts E5, E6 belong to the old volcanic group as inferred from magnetic anomaly pattern suggesting the easterly deflected magnetization, which are disclosed for the circum Philippine islands older than Oligocene age (Haston and Fuller, 1991). The easterly deflected anomaly pattern of these seamounts is also confirmed by the present magnetic anomaly map; the negative peak to the east and positive one to the west of the edifices (E5, E6). However, it is also possible to ascribe the clockwise deflected

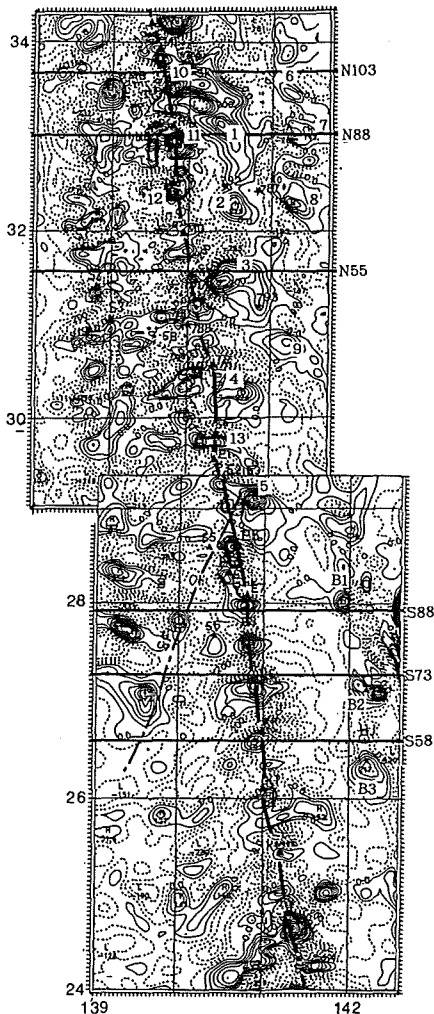


Fig.4.6 Total intensity magnetic anomaly of the Izu-Ogasawara Arc.

Contour interval is 50nT . Identified numbers of cross-sections are shown, which are referred to in chapter IV. A colour image map is shown in annex-1(b).

anomaly pattern to the nonuniform magnetization of the seamount instead of easterly deflected magnetization of the edifice. The fresh igneous rock samples recovered from these seamounts suggest the recent volcanic activities, which may favour the latter interpretation. Besides, the older seamounts of Sawa and Nitiyo also show the magnetic anomaly pattern of normal magnetization. These features may pose a question to the clockwise rotation of these seamounts.

The other seamounts from E7 to KK are characterized by the dipole magnetic anomaly patterns with large amplitude, suggesting the normal magnetization of the uplifts. On the contrary, the magnetic anomaly patterns of seamounts from KT to SW are somewhat different from the dipole pattern of normal magnetization; i.e. slightly westward-deflected pattern of KT, the enhanced negative peak of KI, the E-W elongated magnetic anomaly far apart from the edifices of SW. These features may be ascribed to the underlying magnetic bodies or to non-uniform magnetization with in the volcanic edifices as well as to unusual magnetization direction.

The magnetic anomalies over the Nisi-Sitito ridge show typical dipole anomaly, negative to the north, positive to the south. These features suggest that the volcanic edifices were magnetized in the normal field direction. On the contrary, the dating samples dredged from D368 (N31°30.3', E139°01.4') indicates the igneous activity probably in the Matsuyama reverse epoch (2.2Ma by Yuasa and Murakami, 1985). Although few dated samples are available for the Nisi-sitiro ridge, the normal magnetization pattern indicates that the ridge formation occurred in the present N-S arrangement or after the clock-wise rotation of the entire Izu-Ogasawara

Arc.

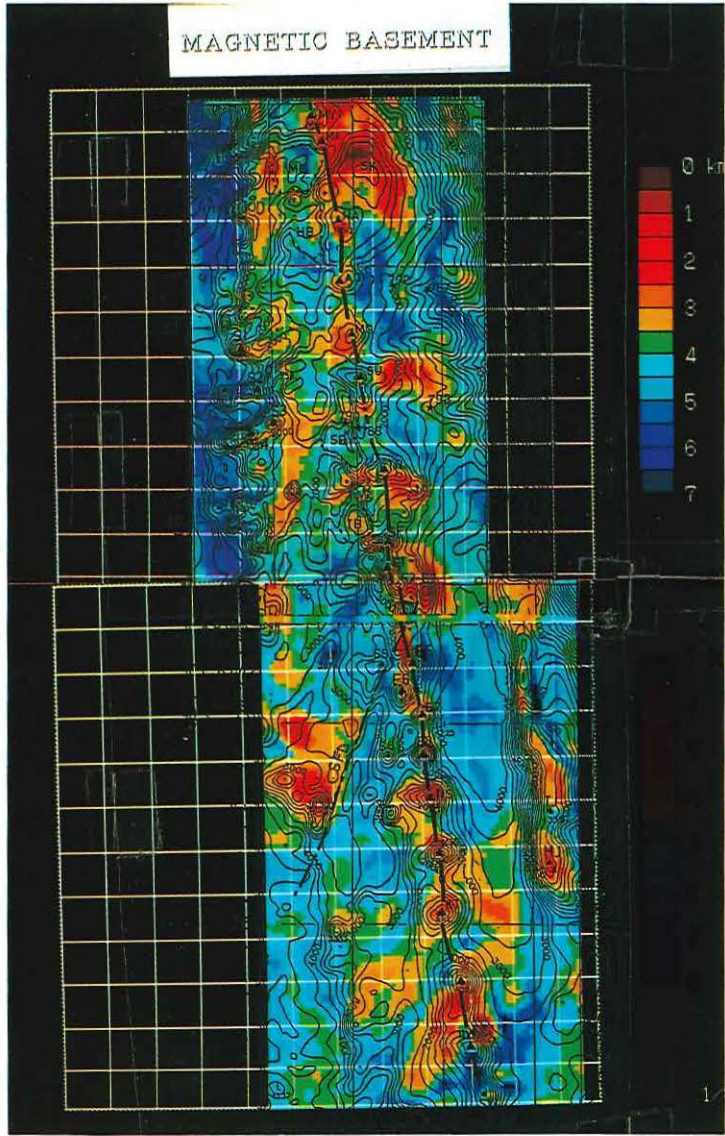
Appreciable magnetic anomalies are seen over the back arc depression zones (denoted by HB, SB, and TB). Especially linear anomalies trending N-S are distinguishable over the Hatizyo and Sumisu depressions. These anomalies are thought to be originated from intrusive igneous rocks due to on-going rifting process. The hydrothermal activity discovered in the Sumisu depression also favours the above interpretation.

The Ogasawara ridge is characterized by isolated anomalies with a significant amplitude. These features suggest that the Ogasawara ridge is a composite of several magnetic blocks. The anomaly B1, B2 (in Fig. 4.6) show paired anomalies; negative peak to the east and positive one to the west. This pattern indicates the eastward magnetization direction resulting from clockwise rotation of the ridge. However, the above features become obscured with the anomaly B3, which shows the normal magnetization of the causative body.

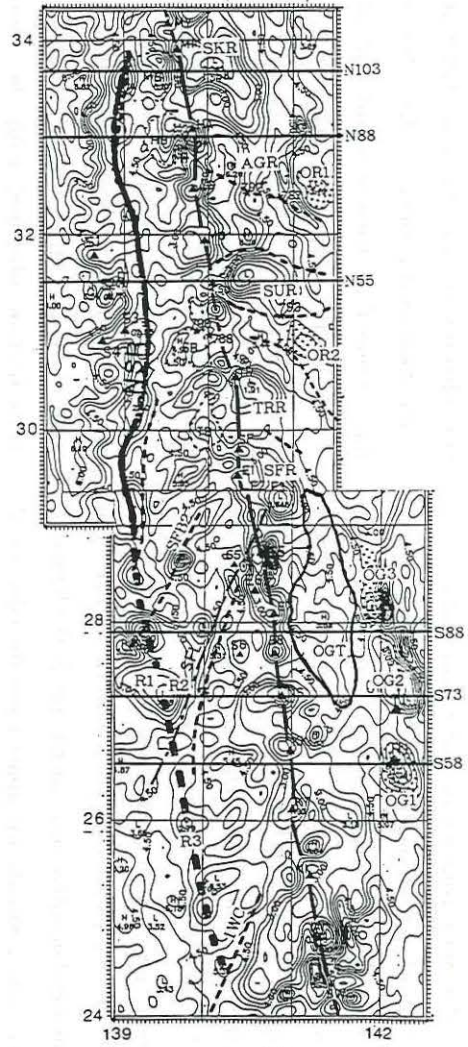
4.4 Characteristics of the crustal structure

4.4.1 General view of magnetic basement structure

The magnetic basement model was calculated by iteration method described in Chapter II under the assumption that the magnetic basement is polarized in the present field direction (normal magnetization) with magnetization intensity of 5.0A/m. The reference depth of the magnetic basement was postulated to be 4.0km below sea level in the above calculation. Figure 4.7 shows the calculated result, on which topographic lineaments are superimposed. Remarkable magnetic basement highs (SKR, AGR, SUR, TRR, SFR) occur beneath the continental shelf to slope of the



(b)



(a)

Fig.4.7 Magnetic basement model of the Izu-Ogasawara Arc.

Assumed magnetization intensity is 5.0A/m and the magnetization direction is the present field direction. The reference depth is 4km below sea level. Contour interval is 500m. Identified numbers of cross-sections are shown, which are referred to in chapter IV.

- (a): Basement depth contour map. Hatched areas show the magnetic basement highs in the outer forearc region relative to topographic rises. NSR: magnetic basement high corresponding to the Nisi-Sitito ridge, SKR, AGR, SUR, TRR, and SFR show the magnetic basement blocks in the forearc region, OGT: Ogasawara Trough.
- (b): Colour image map showing relief of magnetic basement. Topographic contour lines are superimposed on the coloured basement map.

northern arc in good correspondence with magnetic anomalies. The basement high marked by SFR is Oomati seamount. These basement highs seem to extend to the present volcanoes; SUR to Sumisu island, TRR to Tori-sima island, SFR to Sohugan island. The submarine canyons or topographic depression zones in the forearc region seem to segment the above basement blocks, which may suggest the structural origin of these topographic depressions. On the continental slope break, several magnetic basement highs are recognized in good correspondence with topographic uplifts (OR1, OR2).

The magnetic basement relief of the Nisi-Sitito ridge shows close resemblance with topographic one. These features imply that the Nisi-Sitito ridge is mainly composed of igneous rocks of considerable magnetization intensity polarized in the present field direction. The N-S trending uplift of the magnetic basement high also becomes apparent (NSR). This uplifted zone can be traced southward across the Sofugan tectonic line (SFL), although the features become subtle to the south of SFL.

The Quaternary volcanoes are also accompanied by discrete magnetic basement highs. However, considerable variation of the bulk magnetization, the product of magnetization intensity by volume, can be recognized. These variations seem to have resulted from the difference of the basic magma production rate and/or duration of the volcanic activity. It is also noted that the bulk magnetization of the seamounts belonging to the southern arc (here, E5 to IW) is significantly larger than those of the northern arc.

The local magnetic basement highs are recognized beneath the back-arc depression zones (HB,

TB). On the contrary, Mikura basin is characterized by the depressed basement structure.

We see a good correspondence between the magnetic basement high (OG1) and the topographic uplift loading Haha-sima island of the Ogasawara ridge. These features suggest the normal magnetization of the ridge. The other basement highs (OG2, OG3), which also show similarity with topographic highs, however, are accompanied with basement depressions to the east. The latter may manifest the easterly deflected magnetization or non-uniform magnetization of the buried magnetic body.

We see the close correlation between the faults or topographic depressions and magnetic basement structure. The Sofugan tectonic line (SFL), an estimated fault with a sharp cliff on the north, seems to be accompanied with vertical displacement of the magnetic basement. Other topographic depressions such as IWC (Io submarine canyon), SFB2 (depression to the south of the Sohu trough) also show good correspondence with magnetic basement low. It seems unreasonable to ascribe the above features to the topographic effect only, instead, the structural origin of these depressions is necessary. The trend of these faults/depressions coincides with that of the minor ridge arrangement of the Parece-Vela Basin. This suggests that these topographic features accompanied by magnetic basement depressions are reactivated vestiges of tectonically weak zones, resulting from the tectonic stress caused by the collision of the Ogasawara Plateau against the southern Izu-Ogasawara Arc.

The Sofugan tectonic line (SFL) seems to have appeared after the formation of the Nisi-Sitito ridge, because it intersects the magnetic basement of Tenpo (R2) seamount, which is located

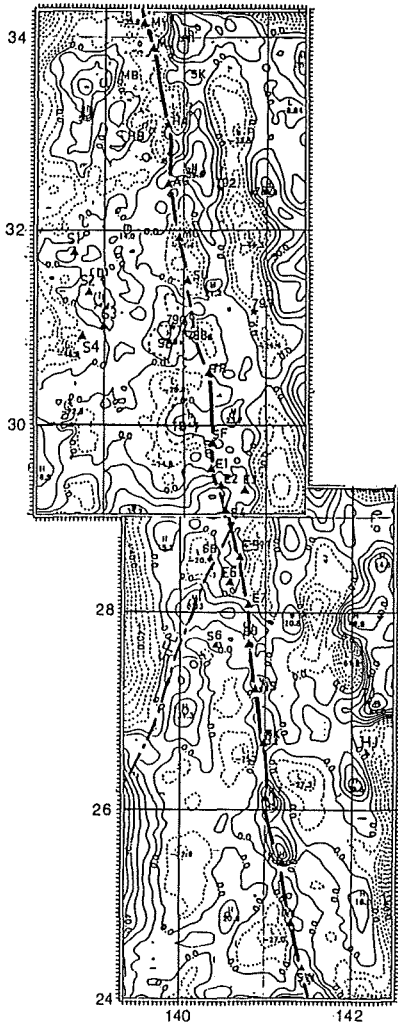


Fig.4.8 Short-wavelength (high pass-filtered) Bouguer gravity anomaly. Cut of wavelength is 160km. Contour interval is 10mgal.

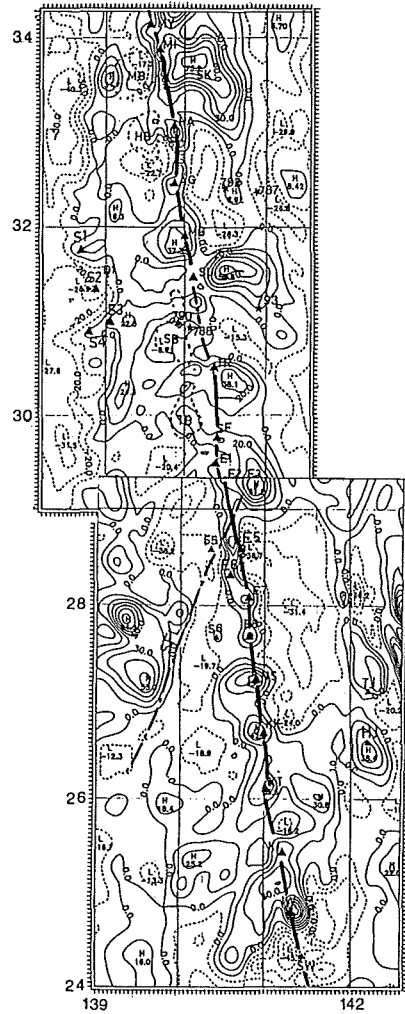


Fig.4.9 Pseudo-gravity of the Izu-Ogasawara Arc. The assumed ρ/J ratio is 100 g/emu. Contour interval is 10mgal.

on the southern extension of the Nisi-Sitito ridge.

4.4.2 Cross-sectional view of magnetic basement and other geophysical data

(1) Northern part of the Izu-Ogasawara Arc

In order to clarify the characteristics of magnetic basement, a pseudo-gravity was calculated and compared with the short-wavelength gravity anomaly. Fig. 4.9 shows the pseudo-gravity calculated under the assumption of normal magnet-

ization with ρ/J (g/emu) of 100. In Fig. 4.10, several cross-sections of the magnetic basement and other geophysical data are shown.

The section-N103 transects the ridge eastward from the Mikura basin to the Sinkurose bank. The amplitude of the short-wavelength Bouguer gravity anomaly over the Sinkurose bank is very small relative to that of pseudo-gravity; i.e. about one third of the latter. These features reveal that the magnetic basement high corre-

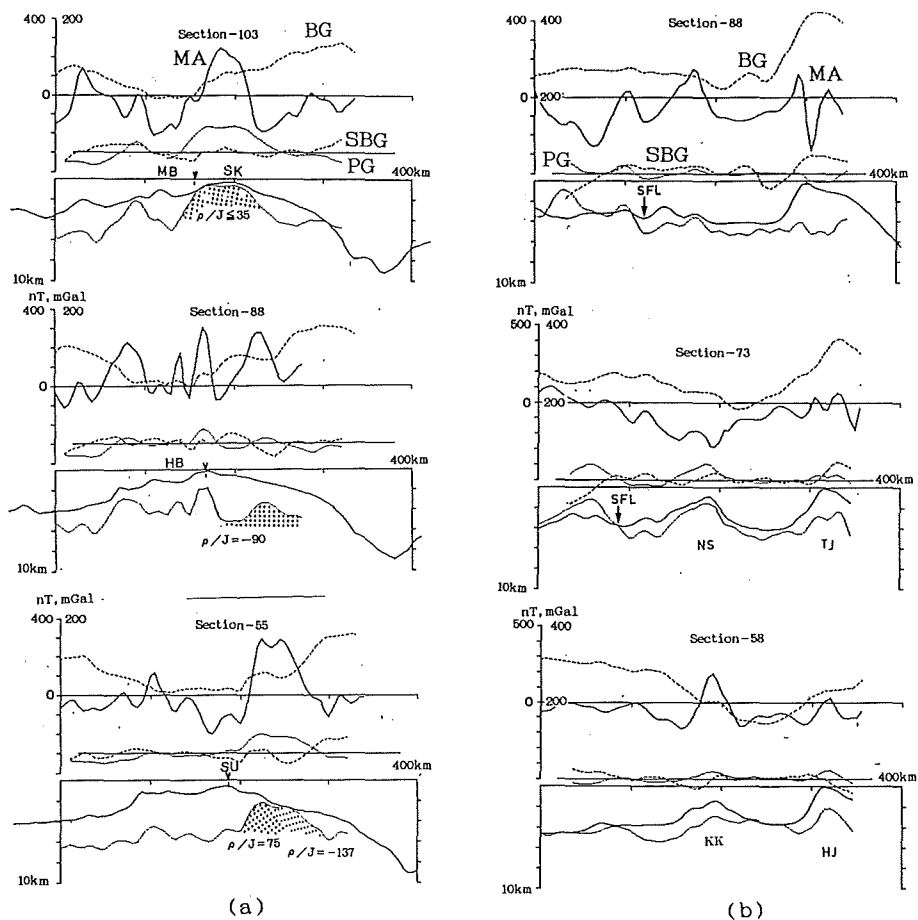


Fig.4.10 Cross-sections of magnetic basement model and the related geophysical data.

The positions of cross-section are shown in Figs 4.6 and 4.7.

upper: magnetic(MA, solid) and Bouguer gravity anomaly(BG, dot) profiles, middle: short wavelength Bouguer gravity anomaly(SBG, broken) and pseudo-gravity anomaly(PG, dot), lower: bathymetry(solid) and derived magnetic basement relief(dot).

(a): northern part of the arc, section N103, N88, N55 (b): southern part of the arc, section S84, S73, S58

sponding to the Sinkurose bank has a small ρ/J ratio which is less than 35.

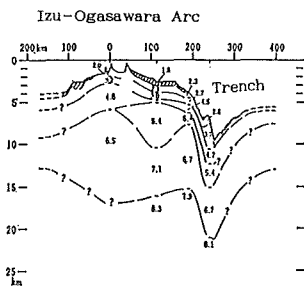
In section-N88, we see a reciprocal pattern between Bouguer and pseudo-gravity anomaly in the forearc side, where the best-fitted ρ/J ratio becomes -90 . This pattern may be attributable to two cases, one is reversed magnetization of the basement, the other is the buoyant magnetic source of negative density contrast. When the latter holds true, the negative density contrast

should be -0.27g/cm^3 for $J=3\text{A/m}$, and -0.45g/cm^3 for $J=5.0\text{A/m}$, respectively.

The section-N55 also transects the forearc magnetic anomaly in the east of Sumisu-sima island. It is found that the features of short-wavelength Bouguer gravity anomaly can not be simulated by the pseudo-gravity anomaly calculated under the assumption of uniform magnetization. From the inspection of this section, the forearc magnetic basement high seems to be

divided into the inner and outer parts with different density contrast or magnetization direction. Bimodal peaks of the magnetic basement high may correspond to two parts with different ρ/J ratio. The ρ/J ratio of the inner basement high is 75 and that of the outer part is -137 . The inner part above mentioned may correspond to the inner forearc high and the outer part to the granitic to andesitic body with negative density contrast against the surrounding crust. In Fig. 4.11 is illustrated the crustal structure along the parallel of $N32^\circ$ obtained by Hotta (1970). This figure shows the thick intermediate velocity layer of 5.4 km/sec beneath the forearc region. If the seismic velocity structure represents the general structure of the northern arc, the forearc magnetic basement highs are to be correlated to this velocity layer. Then, the negative density contrast of the forearc magnetic basement may be explained by the depressed lower boundary of 5.4 km/sec layer. Fig. 4.11 also shows the upheaved Conrad boundary beneath the landward trench slope. The convex features are in good correspondence with the outer magnetic basement highs.

To elucidate the cause of mis-fitting between the short-wavelength Bouguer gravity anomaly and Pseudo-gravity anomaly for the forearc



section-S58, but it becomes obscured for the Titisima and the northern Titisima blocks(OG2, OG3), as revealed by section-S73 and -S88. This is probably due to the clockwise deflected magnetization direction of Titisima and northern Titisima blocks as inferred from palaeomagnetic data of the igneous rock samples recovered from Titi-sima island (Haston and Fuller, 1991).

4.4.3 Evaluation of magnetization of the seamounts

(1) Northern part of the Izu-Ogasawara Arc

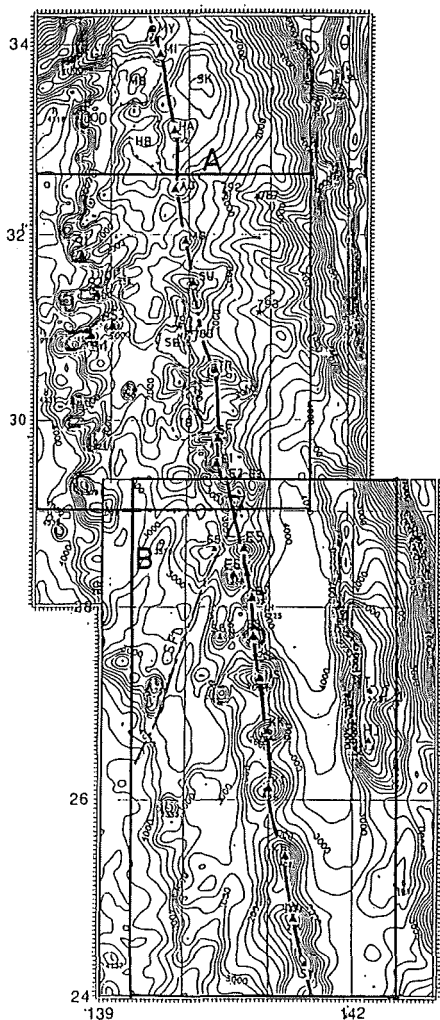


Fig. 4.12 Target areas(A, B) of the correlation analysis between topography and magnetic basement of the Izu-Ogasawara Arc.

A correlation analysis between topography and magnetic basement was executed for the area A shown in Fig.4.12 in order to evaluate the magnetization of the uplifts. The distribution of the derived correlation coefficient is shown in Fig.4.13. This figure shows three high correlation zones trending in along-arc direction. The widely spreading high correlation zones occur over the Nisi-Sitito ridge(A), which justifies the normal magnetization assumption of these topographic uplifts. The others are recognized in the forearc region(B,C). The inner zone(B) corresponds to the topographic rise on the inner forearc high, the outer zone(C) to the topographic uplifts on the continental slope break. The back-arc depression zones are generally characterized by the negative coefficient zone.

The estimated magnetization intensities of topographic uplifts are summarized in Table 4.4. In this table, the calculated density obtained by Ishihara(1985) as well as dredged samples are

Correlation

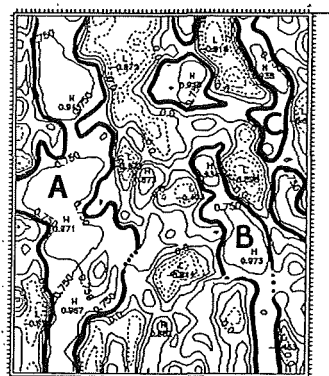


Fig. 4.13 Correlation coefficients between the topography and the magnetic basement model. Target area is the northern part of the Izu-Ogasawara Arc marked by A in Fig. 4.12. A:high correlation coefficient zone(corr. > 0.5) on the Nisi-Sitito ridge, B and C: high correlation zones on the forearc region of the arc.

shown. The correlation coefficients for the seamounts of the Nisi-Sitito ridge are high relative to those for Quaternary volcanic edifices. This is partly due to poor elevation data on land area. The magnetization intensity of the seamounts on the Nisi-Sitito ridge shows widely spreading values from 3.8A/m(T1) to 9.8A/m(T10). The magnetization intensity of seamount S2(8.9A/m) is consistent with basaltic rocks dredged from this seamount. On the other hand, seamount S4 indicates relatively low magnetization intensity(4.2A/m) inspite of the dredged basaltic samples, but this value is consistent with the derived small density(2.55g/cm³), suggesting the porous composition with relatively weak magnetization intensity. The averaged magnet-

ization intensity of the seamounts lying on the Nisi-Sitito ridge is indicative of the andesitic composition of intermediate magnetization intensity. The derived magnetization intensity tends to increase toward east; 3.9A/m(T4) increases to 4.2A/m(S4), further to 6.3A/m(S3), and 4.7A/m(T8) increases to 9.8A/m(T10) etc.. The magnetization intensities of the Quaternary volcanic islands tend to some extent to be larger than that of the Nisi-Sitito ridge. This increasing trend may reflect a different crustal anatexis or crystal fractionation process, but further petrographical study of volcanic rocks of the Nisi-Sitito ridge is required for the elucidation of this trend.

(2) Southern part of the Izu-Ogasawara Arc

A correlation analysis of the southern part was conducted for the area B shown in Fig.4.12. The correlation coefficient and the derived magnetization intensity are shown in Fig.4.14 and Table 4.4. Fig.4.14 shows several high correlation zones such as B1, B2, A1, A2, C1, C2 and C3. The zone A1 corresponds to the Quaternary volcanic front between Mokuyo seamount(E6) and Kaikata seamount(KK), which justifies the normal magnetization assumption of these topographic uplifts. Some uplifts along the volcanic chain indicate low correlation coefficients; E5 in Sitiyo seamounts, KI, IW and SW in the southern part of the chain. These low coefficients may arise from unusual magnetization direction and/or non-uniform magnetization resulting from demagnetization effect due to high geothermal gradient (Oshima et al., 1985) and compositional variation within the edifice. The derived magnetization values with high correlation coefficients seem to be consistent with dredged basaltic/andesitic samples as shown in Table 4.4.

Table 4.4 Magnetization intensity of the seamounts of the Izu-Ogasawara Arc derived from correlation analysis between magnetic basement model and topography.
N: northern arc, S: southern arc

Area	Abbr.	J A/m	Corr.	ρ^* g/cm ³	Dredged* samples
N	VF	AG	*	0.47	2.72
N	VF	SU	14.0	0.51	2.64
N	VF	TR	*	0.54	BA, AN
N	VF	SF	7.2	0.74	BA
N	VF	E1	8.4	0.62	AN
N	VF	E2	7.8	0.71	AN
N	VF	E3	*	0.45	AN
S	VF	E4	8.5	0.66	2.70
S	VF	E5	*	-0.00	3.18
S	VF	E6	15.9	0.71	2.98
S	VF	E7	6.4	0.93	2.74
S	VF	E8	6.3	0.93	2.71
S	VF	S6	7.4	0.83	2.65
S	VF	NS	7.2	0.96	AN
S	VF	KK	10.2	0.67	BA, AN
S	VF	KT	7.5	0.96	BA
S	VF	KI	17.1	0.59	AN, DA, BA
S	VF	IW	*	0.40	TR
S	VF	SW	*	0.27	TR, BA
N	NSR	S1	4.5	0.95	2.74
N	NSR	S2	8.9	0.69	2.71
N	NSR	S3	6.3	0.88	2.59
N	NSR	S4	4.2	0.94	2.55
N	NSR	T1	3.8	0.88	
N	NSR	T2	3.7	0.52	
N	NSR	T3	6.1	0.65	
N	NSR	T4	3.9	0.91	
N	NSR	T5	5.5	0.88	
N	NSR	T6	5.3	0.82	
N	NSR	T7	5.9	0.32	
N	NSR	T8	4.7	0.96	
N	NSR	T9	7.0	0.79	
N	NSR	T10	9.8	0.72	
S	NSR	R1	8.8	0.83	
S	NSR	R2	11.5	0.68	
S	NSR	R3	4.6	0.89	
S	OGS	TJ	9.4	0.52	BO, AN
S	OGS	IJJ	6.6	0.88	AN

The magnetic basement model shown in Fig.4.7 was used for the estimation of bulk magnetization per unit square. The assumption that the magnetization is normal seems to hold true for the volcanic frontal area as mentioned in section 4.4.3, although there still remains uncertainty for the magnetic bodies in the forearc area. We defined the cross-arc variation as the X-dependent variation orthogonal to the extension of the arc, and along-arc as Y-dependent one parallel to the extension of the arc.

Fig. 4.15 shows the cross-arc variation of the bulk magnetization per unit km^2 (hereafter referred to BMR). From this figure, we can recognize that the forearc region of the northern arc is characterized by high BMR value. In addition, another peak corresponding to the Nisi-Sitito ridge is also recognizable in Fig.4.15a. The latter peak is suppressed in comparison with that of volcanic front due to the oblique trend of the

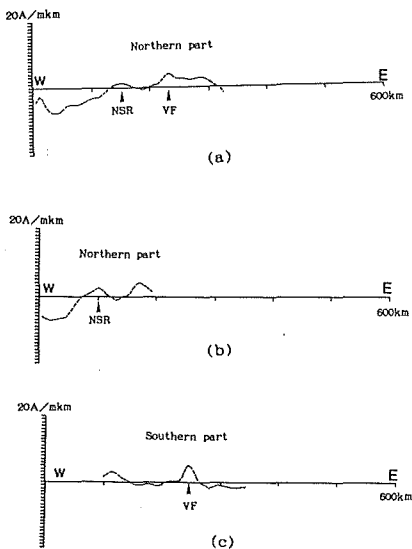


Fig.4.15 Cross-arc variation of the bulk magnetization of the Izu-Ogasawara Arc. Unit of bulk magnetization per unit km^2 is $\text{A/m}\cdot\text{km}$.
(a) and (b): northern arc, (c):southern arc.

Nisi-Sitito ridge against the volcanic front of the reference line. Figure 4.15c also shows the BMR for the southern arc. Two peaks corresponding to the present volcanic chain and the Nisi-Sitito ridge occur. The former peak is somewhat larger than the latter.

In Fig. 4.16, three along-arc variations are indicated. These values represent the mean value within 20km width in E-W direction along the volcanic front (Fig.4.16a,c) and the Nisi-Sitito ridge (Fig.4.16b). These figures show the clustered pattern of BMR, which may arise from along-arc segmentation of the igneous activity. The

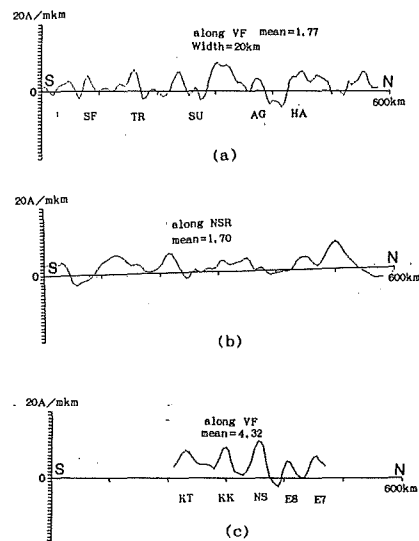


Fig.4.16 Along-arc variation of the bulk magnetization of the Izu-Ogasawara Arc. Unit of bulk magnetization per unit km^2 is $\text{A/m}\cdot\text{km}$. Calculated values represent the means for the 20km width orthogonal to the volcanic front. Total means become $1.77\text{ A/m}\cdot\text{km}$ for the volcanic zone of the northern arc, $1.70\text{ A/m}\cdot\text{km}$ for the Nisi-Sitito ridge, and $4.32\text{ A/m}\cdot\text{km}$ for the southern arc respectively.

- (a): volcanic zone of the northern arc,
- (b): Nisi-Sitito ridge,
- (c): volcanic zone of the southern arc.

mean value of along-arc BMR of the Quaternary volcanic front in the north of Sohugan island is very close to that of the Nisi-Sitito ridge; the former is 1.77 and the latter is 1.70, respectively. The above similarity may manifest that the Nisi-Sitito ridge was an old volcanic front having nearly the same production rate of magnetic materials as the present volcanic one of the northern arc. On the other hand, along-arc variation of BMR between Kinyo(E7) and Kaitoku(KT) seamounts is considerably enhanced relative to that of the northern volcanic chain as seen in Fig.4.16(c). The mean value of along-arc BMR of the southern volcanic chain becomes 4.32, which is about 2.3 times that of the northern volcanic chain. These features suggest that the production rate or duration of volcanic activity producing magnetic materials is much larger in the southern volcanic front than in the northern volcanic one.

Table 4.5 Bulk magnetization of the representative magnetic sources of the Izu-Ogasawara, Arc.

Name	Bulk magnetization (A/m·km ³)
Aoga Sima	3004
Sumisu Sima	3636
Tori Sima	6589
Sofu Gan	3994
Sinkurose bank	83410
Sumisu Spur	26938
Torisima Spur	16081
Oomati SMT	30999
Kayo SMT	3320
Suiyo SMT	6032
Mokuyo SMT	3736
Kinyo SMT	4184
Nisino Sima	14877
Kaikata SMT	10092
Kaitoku SMT	11746
Kita Ito Sima	16895
Ito Sima	21223

In Table 4.5, are shown the bulk magnetizations estimated for the respective magnetic blocks. These values are ambiguous depending on the uncertainty of the extent estimation of each block, but they may be true as the order estimation. The magnetic basement in the fore-arc region has remarkably large bulk magnetization relative to those of Quaternary volcanoes by the amount of one or more than the northern volcanic edifices.

Summarizing the above mentioned aspects, we get conclusions as follows;

- (1) the extraordinarily strong igneous activity is expected to have occurred in order to explain the bulk magnetization of the forearc region of the northern arc,
- (2) the igneous activity forming the Nisi-Sitito ridge is similar to the Quaternary igneous activity along the northern volcanic front in terms of the bulk-magnetization.
- (3) The bulk magnetization of the southern Quaternary volcanic edifices to the south of Nisino-sima seamount is much larger than that of the northern volcanic chain.

4.5 Estimation of ρ/J ratio at the Moho boundary

To evaluate the ρ/J (g/emu) ratio at the Moho boundary, correlation analysis was conducted between the long-wavelength Bouguer gravity anomaly and the long-wavelength pseudo-gravity. The long-wavelength Bouguer gravity anomaly was calculated by subtracting the short-wavelength anomaly (Fig.4.8) from the Bouguer gravity anomaly (Fig.4.5). In Figure 4.17 is indicated the long-wavelength Bouguer gravity anomaly of the Izu-Ogasawara Arc thus obtained.

(1) Northern part of the Izu-Ogasawara Arc

The distribution of the derived correlation coefficient and ρ/J ratio are shown in Fig. 4.18 for the northern part of the Izu-Ogasawara Arc. The reversely correlated zone with high magnitude of correlation coefficient larger than 0.6 is shown by dotted areas in Fig. 4.18(a). From this figure we can recognize the reversely correlated zone in the western part of this map (A), where the Moho boundary is elevated toward the Sikoku Basin. The corresponding ρ/J ratio varies in the range from -100 to -300 . This may indicate that the

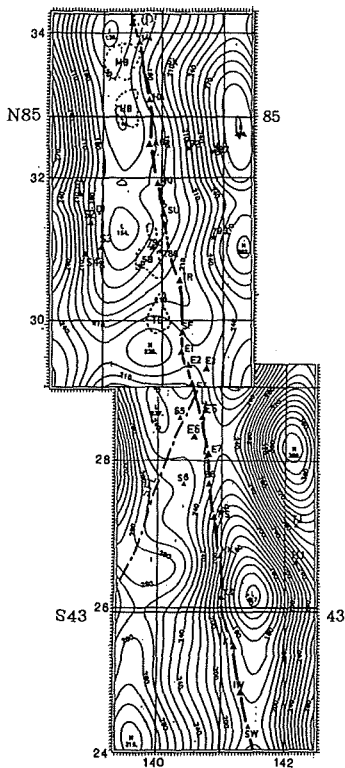


Fig. 4.17 Long-wavelength Bouguer gravity anomaly of the Izu-Ogasawara Arc. The short-wavelength Bouguer gravity anomaly is subtracted from the Bouguer gravity anomaly. Contour interval is 10mgal. Positions of cross-sections N85 (northern arc) and S43 (southern arc), which are analyzed by response function method, are indicated.

magnetic property of the lower crust near Moho boundary is of heterogeneity in the lateral direction. On the contrary, the other reversely correlated zones (B in Fig. 4.18(a)) has the ρ/J ratio in a narrow range from -75 to -150 .

In Fig. 4.19a are shown the results of two-dimensional analysis based on the response filter method. The section-N85 transects the magnetic anomaly zone to the south of Hatizyo islands. The derived ρ/J_{eff} ratio at the Moho boundary become -82 , which falls within the range of zone B. A similar result is also shown for the aeromagnetic profile transecting the northern part of the arc (Fig. 4.19(b)). From the results mentioned above, the followings may be concluded; the lower crust of the northern arc is magnetic, and the edge effect of the Moho boundary is

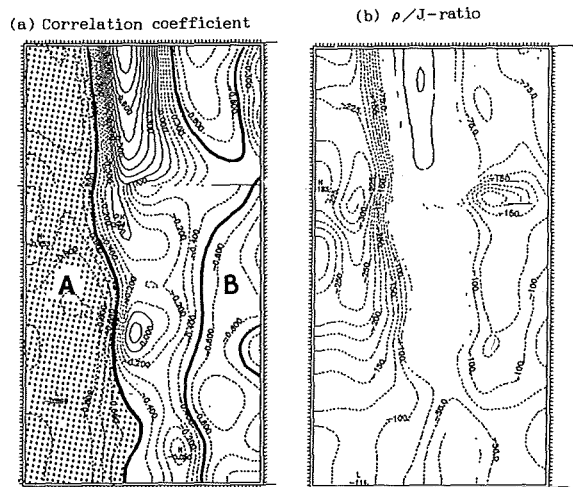


Fig. 4.18 Correlation coefficients (left) and the estimated ρ/J ratio (right) at the Moho boundary for the northern part of the Izu-Ogasawara Arc.

A: reverse correlation zone in the western margin of the arc, which may imply the edge effect by the upheaval of the Moho boundary,
B: reverse correlation zone in the forearc region.

observed for the western margin of the ridge, where the Moho boundary is upheaved toward the Sikoku Basin, resulting in the thinning of the crust.

(2) Southern part of the Izu-Ogasawara Arc

The results of correlation analyses of the southern part of the Izu-Ogasawara Arc are indicated in Fig.4.20. This result shows the negative correlation zone in the south and the positive correlation

zone in the north. The correlation is generally poor in comparison with that of the northern Arc, as seen from the fact that the high correlation zones are restricted. This may reflect the weak magnetization contrast and/or higher thermal condition at the Moho boundary. The reversely correlated zone corresponds to the western and eastern slope of the concave-shaped Bouguer gravity anomaly, whose central zone shows the minimum Bouguer gravity value of 120 mgal (Fig. 4.17). These features can be interpreted by the vertical configuration of the Moho and the Curie isotherm; the Moho boundary is depressed below the Curie isotherm beneath the zone of the minimum Bouguer gravity anomaly which may imply the existence of the thick continental crust beneath there, on the other hand, the Moho is elevated above the Curie isotherm in the both sides of this minimum. The ρ/J ratio corresponding to the high correlation coefficient zone

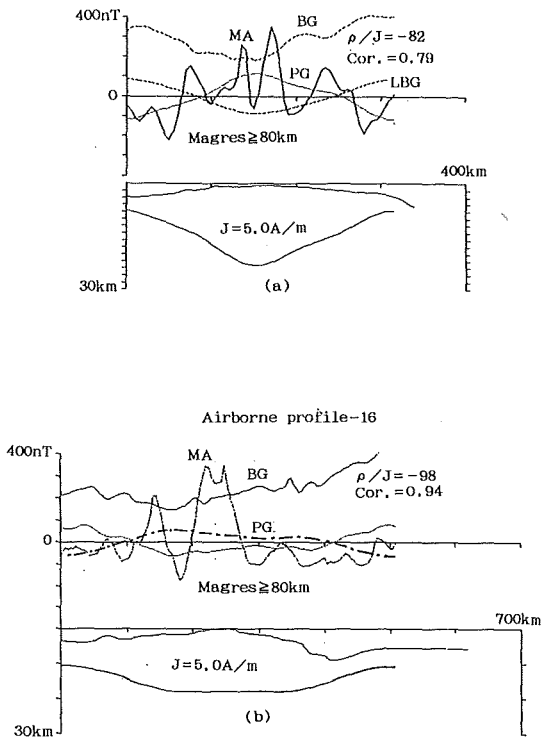


Fig.4.19 Two-dimensional magneto-gravity response analysis on section-N85 and an airborne magnetic profile-16 shown in Fig.3.3.

MA:magnetic anomaly, BG:Bouguer gravity anomaly, LBG:long-wavelength Bouguer gravity anomaly, PG:pseudo-gravity of magnetic response. Cor.:correlation coefficient between the long-wavelength Bouguer gravity anomaly and pseudo-gravity one.

- (a): result on cross-section N85 in Fig.4.17.
- (b): result on aeromagnetic profile-16.

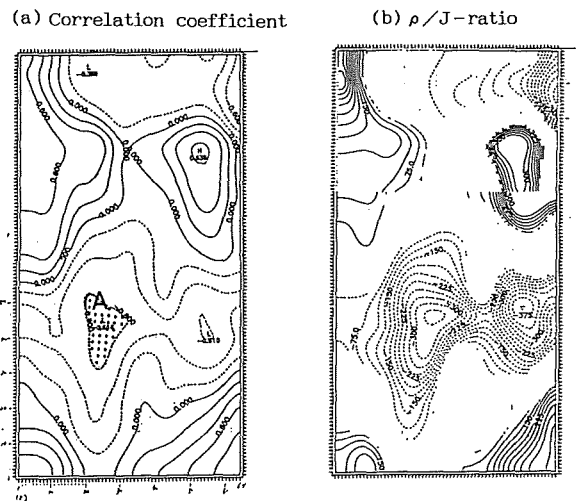


Fig.4.20 Correlation coefficients(left) and the estimated ρ/J ratio(right) at the Moho boundary for the southern part of the Izu-Ogasawara Arc. The reversely correlated zone is restricted within the small zone(A) beneath the southern Ogasawara Trough.

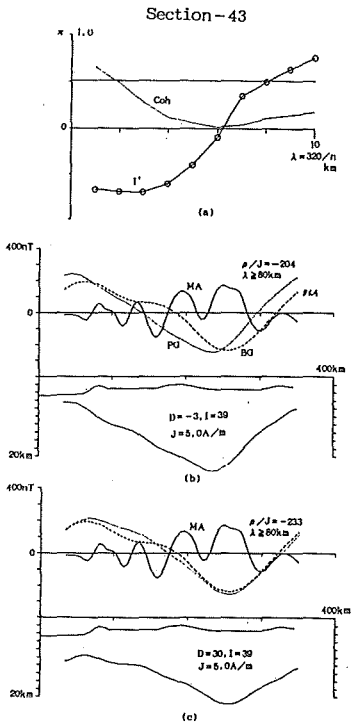


Fig.4.21 Two-dimensional magneto-gravity response analysis on section-S43 of the southern arc. Location of the profile is shown in Fig.4.17.

- (a): coherence (coh) and effective inclination (I_r) of magnetization vector against the wavelength of the magnetic anomalies.
- (b): magnetic lower boundary derived from response filter method under the present field assumption of $D_r = -3^\circ$, $I_r = 39^\circ$.
- (c): magnetic lower boundary derived from response filter method under the assumed magnetization direction of $D_r = 30^\circ$, $I_r = 39^\circ$.

ranges from -300 to -375 , which is relatively large in magnitude in comparison with the values in the northern arc. The positively correlated-zone observed in the northwestern part of the figure seems to be caused by the long-wavelength magnetic anomalies originating from the seamounts or buried bodies as seen in the pseudo-gravity map shown in Fig.4.9.

The two-dimensional response analysis was

also conducted along the section-S43, transecting the minimum Bouguer anomaly zone, to estimate the ρ/J ratio of the Moho boundary. The results of analysis are shown in Fig.4.21. The effective inclination in the wavelength longer than 80 km are shifted to the negative value by the amount of about 180° , against the present field direction, which may imply the magnetic response of the Moho boundary. The pseudo-gravity for wavelengths longer than 80 km was calculated and compared with the Bouguer gravity anomaly as shown in the lower part. The best-fit ρ/J ratio and the correlation coefficient becomes -233 and 0.99 , respectively, for the magnetization direction of $D_r = 30^\circ$, $I_r = 39^\circ$ (Fig.4.21(c)). When the present field direction is assumed for the magnetization direction, the correlation coefficient decreases to -0.61 . However, even in the latter case, the similar ρ/J ratio of -204 was obtained (Fig.4.21(b)).

From the above considerations for estimation of the ρ/J ratio at the Moho boundary of the Izu-Ogasawara Arc, followings are summarized.

First, the lower crust in the northern Izu-Ogasawara Arc seems to be more magnetic than that of the southern arc, as inferred from wider coverage of high correlation zone. Second, it is likely that the edge effect due to uprising of the Moho boundary seems to occur in the western margin of the northern part of the Izu-Ogasawara Arc. Third, the ρ/J ratio estimated for the Moho boundary is almost within the range from -100 to -250 in the northern arc. On the other hand, its absolute values are enhanced to the value from -225 to -375 in the southern arc, reflecting probably a small magnetization contrast at the Moho boundary.

4.6 Discussions and concluding remarks of chapter IV

From the present study of magnetic and gravity anomalies of the Izu-Ogasawara arc, following features have become apparent.

(1) The magnetic anomalies of the Nisi-Sitito ridge can be almost explained by the normal magnetization of the topographic uplifts. A good correspondence between the magnetic basement relief and the topographic features are recognized in the forearc region of the northern arc, especially for the depression of submarine canyons and for the rise at the continental slope break. These features may imply the structural origin of the characteristic topography.

(2) The N-S trending magnetic basement high of the Nisi-Sitito ridge is thought to be an old volcanic front as active as the present Quaternary volcanic front of the northern arc.

(3) The forearc region of the northern Izu-Ogasawara Arc is characterized by the segmented magnetic massives with relatively low ρ/J ratio. These magnetic massives have the extraordinary bulk magnetization which is larger than that of the present volcanic edifices by the amount of one order. Oomati seamount in the ESE of Getuyo seamount, and the Tenpo and Nisi-Tenpo seamounts facing the Sikoku Basin can also be grouped into the magnetic massif of low ρ/J ratio.

(4) The bulk magnetization of the Quaternary volcanic front in the southern arc from Kinyo to Kaitoku seamount is significantly larger than that of the northern volcanic front north of Sohugan island by a factor of about 2.3. To explain the above contrasting features, the following causes are likely; ① the volcanic front of the

southern arc has been confined at the same zone for a long period if compared relatively to that of the northern arc. The presence of the old volcanic groups overlapping the Quaternary volcanic edifices of the southern arc, as noted by Yuasa and Nohara (1992), may be consistent with this idea, ② the crustal thickness of the southern arc beneath the volcanic front is thinner than that of the northern arc, which resulted in highly efficient magma ascent (Ueda, 1986, Yuasa, 1992). ③ the petrochemical composition of magma is rich in basic composition in the southern volcanic front compared with that in the northern arc. This may be related to the depth of magma source and the crustal thickness causing the crustal anatexis, ④ the magma production rate itself is larger in the southern arc than in the northern arc.

The collision of the Ogasawara plateau and the steep inclination of the subducting slab are also characteristic features of the southern arc. These phenomena seem to be related to the contrasting features of bulk magnetization between the northern and southern arc, however construction of the concrete hypothesis on this subject is beyond the scope of this study.

(5) The Ogasawara ridge is composed of several magnetic blocks; the Haha-sima block loading Haha-sima island shows normal magnetization, besides the Muko-sima block loading the Muko-sima islands also favours normal magnetization. On the other hand, the Titi-sima block loading Titi-sima island shows clockwise deflected magnetization. These differences may pose a question on the entire clockwise rotation of the Izu-Ogasawara Arc. Palaeo-magnetic measurement of the deep-seated magnetic body of Haha-sima island may be necessary to elucidate the

above contradiction.

(6) In the northern arc, the low Bouguer gravity anomaly ranging from 150mgal to 180mgal is seen in the backarc side, whereas such a low Bouguer gravity anomaly zone is not seen in the backarc side of the southern arc. The steep gravity gradient zone extending in WSW direction from the Torisima basin may be the gravity boundary separating the northern part from the southern part of the Izu-Ogasawara Arc.

(7) It is likely that the undulation of Moho boundary is reflected as long-wavelength magnetic anomalies. As a whole, the lower crust of the northern arc is more magnetic than that of the southern arc. The ρ/J ratio of the Moho boundary in the southern arc is large relative to the northern arc. This may be ascribed to relatively small magnetization intensity of the lower crust, if the density contrast at the Moho boundary is constant.

Concerning the origin of the Nisi-Sitito ridge, several ideas have been proposed. Among them, the well-known idea is to ascribe the origin to fissure eruptions, which is caused by the collision of the Izu-Ogasawara Arc against the Honsyu Arc, i.e., the N-S compressive stress brings about the conjugate faults, which is situated obliquely making an angle of 45° from the N-S direction, then fissure eruptions occurred along these faults (Kaizuka, 1984). This idea is attractive, but it requires high thermal activity in the northern arc to explain the concurrent igneous activity in wide zone. Besides, it seems to be unreasonable to ascribe the edifices of the Nisi-Sitito ridge south of the Sofugan tectonic line to the fissure eruptions. So, the author, alternatively, would like to ascribe the origin to combination of the above faulting and the trenchward

movement of volcanic front due to retreat of the trench or gradual increase of the descending angle of the slab. This idea may explain en-echelon arrangement in the northern arc and the edifices of the southern arc recognized in the southern extension of the Nisi-Sitito ridge.

The present study proposes that the geomorphological characteristics of the Nisi-Sitito ridge was formed in the N-S arrangement of the northern arc, as revealed from the normal magnetization of the topographic uplifts. Such normally magnetized seamounts in the Nisi-Sitito ridge can be traced further southward as noted from Nisi-kaitoku seamount (R3) located at $N25^\circ55', E139^\circ45'$ belonging to the southern arc (see Table 4.4). These aspects seem to suggest a fundamental tectonic framework of the Izu-Ogasawara Arc.

Yuasa and Nohara (1992) described the contrasting features between the northern and southern Izu-Ogasawara Arc from the view points of petrological, geophysical and geomorphological aspects, and ascribed them to the different crustal thickness resulting from the southward Pacific plate subduction beneath the Philippine Sea plate before 42Ma (Seno and Maruyama, 1984). Yuasa (1992) also pointed out that the Nisinosima trough was a rifting zone creating the Parece-Vela Basin and that the Sofugan tectonic line was the western edge of this rifting zone. However, as mentioned before, the time when the Sofugan tectonic line appeared is assumed to be after the formation of the Nisi-Sitito ridge, which has normal magnetization favouring the N-S configuration of the arc. These features have forced the author to suggest that the Sofugan tectonic line, the remnant of the spreading axis of the Parece-Vela Basin, is a vertical fault reactivated by the collision of the Marcus-wake Pacific seamount

chains, which align in the ESE direction as seen from the Ogasawara plateau.

The narrow width of the volcanic front of the southern arc may be related to the steep inclination of the subducting plate, i.e. the lateral width of the magma sources on the Wadachi-Benioff zone becomes narrow in the case of a large dip angle. The large dip angle of the subducting plate is caused by the decoupling between the subducting slab and the overlying plate. As for the southern part of the Izu-Ogasawara Arc, the large dip angle has been ascribed to the last phase of the subducting cycle (Kanamori, 1977). However, such phenomena may also be caused by the low viscosity and high temperature condition of the surrounding mantle as suggested by Shiono et al. (1980). The low resistance against the subducting slab resulting from fluidous mantle materials may lead to the steep inclination of the subducting plate in the southern arc. Besides, the successive subduction/collision of the Pacific seamount chain against the southern Izu-Ogasawara Arc may have also caused the enhancement of frictional heat source, maintaining the high temperature condition of the surrounding mantle. This decoupling process may result in a relatively thin crustal layer in the southern arc. The collision must have caused the large undulation of the Moho boundary in the southern arc; i.e. the Ogasawara ridge corresponds to the upheaval of the Moho boundary.

It is likely that the Nisi-Sitito ridge continues to the West Mariana ridge as shown in the bathymetric map No.6302(JHD). The West Mariana ridge was also old volcanic chains in the late Pliocene age (Karig, 1971). The rock samples dredged from the Nisi-Sitito ridge also show the recent Pliocene age. This agreement may imply

that the volcanic activity or rifting phenomena in the northern arc occurred simultaneously with the rifting of the West Mariana ridge in the Pliocene age. The en-echelon arrangement of the Nisi-Sitito ridge may be ascribed the trenchward movement of volcanic front and conjugate faults arrangement. In the southern arc, the collision of the Ogasawara plateau prevents the retreat of the trench, producing a nodal point of the arc-trench system. The steep inclination of the subducting plate may have also confined the volcanic zone within a narrow range, which may have brought about a considerably large volume of volcanic edifices in the southern arc. This interpretation, however, is still speculative and further evidence about the chronological and palaeomagnetic data are necessary for verification.

CHAPTER V. CRUSTAL STRUCTURE OF THE RYUKYU ARC AND ITS ADJACENT SEAS AREAS AS REVEALED FROM MAGNETIC AND GRAVITY FIELD ANALYSIS

5.1 Data description

The geophysical data used for this study are based on the sea-bottom surveys conducted by JHD. The track lines and cruise files are shown in Fig.5.1 and Table 5.1. These data files were supplied from JODC in MGD77 format. The dense track lines in Fig.5.1 are with the spacings of about 2 n.m. and the relatively rough track lines are about 5 to 10 n.m.. The former were surveyed by S/V Shoyo and the latter by S/V Takuyo. The survey items, survey methods, and data reduction method are generally the same as those described in data description of the Izu-Ogasawara Arc.

As to the external field correction for the

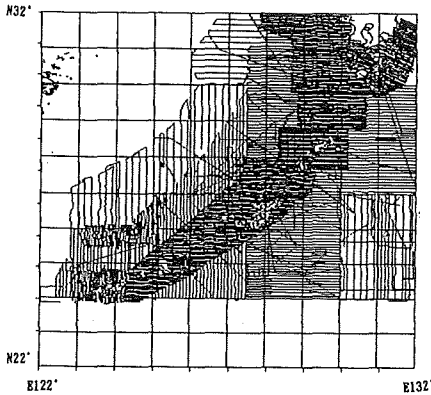


Fig.5.1 Track lines of sea-bottom survey data on the Ryukyu Arc and its adjacent seas (Nansei Syoto). The dense track lines were measured by S/V Shoyo and rough ones by S/V Takuyo of JHD. The data file names for the area are listed in Table 5.1, which were released from JODC in MGD77 format.

Table 5.1 MGD77 data file names used for mapping the geophysical data of the Ryukyu Arc and its adjacent seas(Nansei-Syoto).

At the scale of 1/200,000
 HS7303, HS7403, HS7405, HS7501
 HS7602, HS7603, HS7905, HS8003
 HS8102, HS8202, HS8203

At the scale of 1/500,000
 HT8301, HT8401, HT8402, HT8403
 HT8502, HT8510, HT8605, HT861016
 HT861102, HT8612, HT8701, HT871110
 HT880521

magnetic survey data, diurnal variation field observed at the adjoining station at Kanoya in the southern Kyusyu or a temporal observation point at Okinawa-sima island were used. The IGRF1985 model was also adopted for calculation of magnetic anomaly on the ground of well approximated secular variation model as seen in Fig.5.2.

The MGD77 data files released from JODC were projected on a x-y coordinate on the basis of

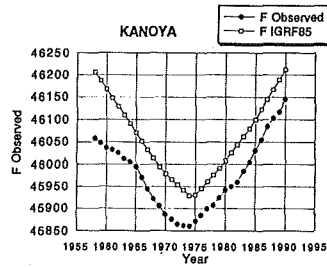


Fig.5.2 Secular variation of total intensity magnetic field at Kanoya

Table 5.2 Projection parameters for X-Y conversion of the MGD77 data of the Ryukyu Arc and its adjacent seas(Nansei-Syoto).

Area SW01
 Origin: N24.15°, E123.25°
 Reference latitude: N25.5°
 Projection: Mercator
 Azimuth of Y-axis: 0°

Area SW02
 Origin: N27°, E124°
 Reference Latitude: N26.5°
 Projection: Mercator
 Azimuth of Y-axis: 44°

Area SW03
 Origin: N29.5°, E125.5°
 Reference Latitude: N29°
 Projection: Mercator
 Azimuth of Y-axis: 42°

Mercator projection whose origin and reference latitude are listed in Table 5.2. The 5km×5km grid data were then calculated for analytical use by the same method mentioned in section 4.1.

Using the grid data thus obtained, are compiled the maps of bathymetry, free-air and Bouguer gravity anomalies and total intensity magnetic anomaly as shown in Figs.5.3 to 5.6. There are some inconsistency at the adjoining zones because of a different reference latitude for contraction and numerical errors of terrain effect, but general features can be traced continuously among

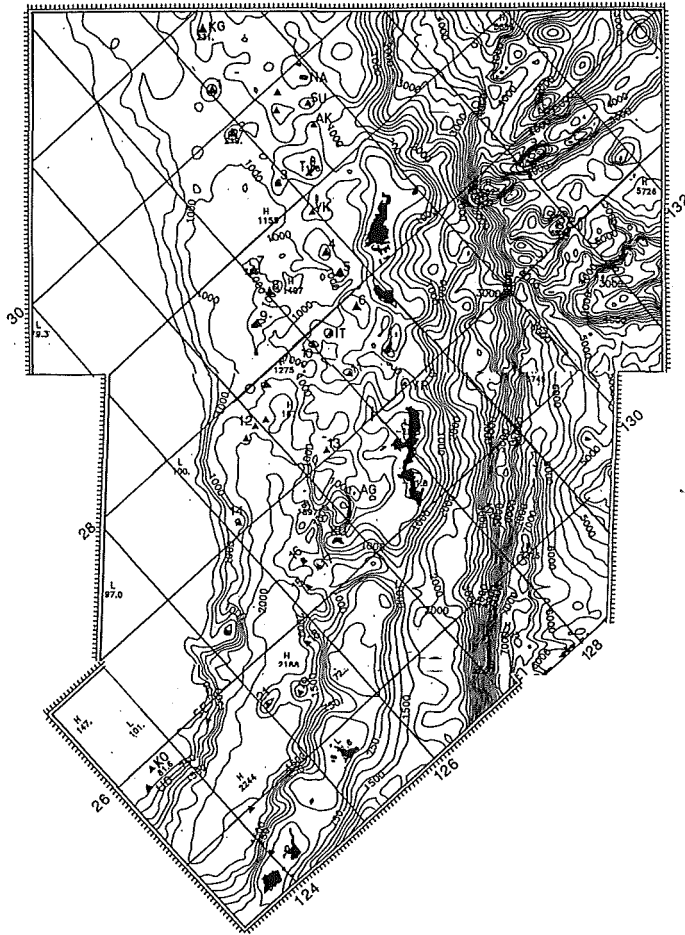


Fig.5.3 Bathymetry of the Ryukyu Arc and its adjacent seas(Nansei-Syoto). Contour interval is 250m. The meaning of abbreviations and numerals are listed in Table 5.3. Colour image map is shown in annex—2(a).

three areas of SW01, SW02, and SW03, respectively.

5.2 Geological settings

The area of investigation covers the southwestern region of the Tunghai shelf and eastwards, the Okinawa Trough, the Ryukyu Arc, the Ryukyu trench (Nanseisyoto trench) and the western part of the Philippine Basin. Bathymetric map is shown in Fig.5.3 and the representative topographic names are listed in Table 5.3. In Fig.5.7, are shown the general features of structural zones of the east China Sea and the Ryukyu

arc and trench system compiled by Kizaki (1986). Fig.5.8 indicates the general distribution of the topographic uplifts of the Ryukyu Arc. The Fukien Ryeognam belt corresponding to the Mesozoic metamorphic-plutonic massif is composed mainly of granitic rocks. Two subterranean basement ridges comprise the outer margin of the Tunghai shelf. One is the Goto ridge extending to the Goto islands and the other is the Senkaku ridge loading the Senkaku islands. These ridges are also called as the Taiwan-Shinji Folded Zone (Wageman et al., 1970) or the Goto-Senkaku Folded Belt (Aiba and Sekiya, 1979).

Table 5.3 Topographic names of the Ryukyu Arc and its adjacent seas.

Abbr.	name	position	
		Lat	Lon
1	Mekura Sone	30° 21'	129° 08'
2	Oki Gazya	29 53	128 50
3	Yokogan Sone	29 16	128 51
4	Daiiti Amami Tai	28 28	128 44
5	Daini Amami Tai	28 12	128 40
6	Tokuno Sima Tai	27 50	128 39
7	Kita Ense Kaikyu	28 50	128 05
8	Ense Kaikyu	28 33	128 02
9	Minami Ense Kaikyu	28 21	127 47
10	IO Torisima Tai	27 52	128 00
11	Igyo Sone	27 29	128 06
12	Iheya Kaikyu-gun	27 35	127 02
13	Izena Tai	27 04	127 12
14	Ise Kaikyu	27 05	126 07
15	Daigo Kume Kaikyu	26 12	126 11
16	Daiiti Kume Kaikyu	26 25	126 18
17	Daisan Kume Kaikyu	26 17	126 24
18	Daisan Miyako Kaikyu	25 50	125 45
19	Daiiti Miyako Kaikyu	25 30	125 22
20	Hokuto-Sekibi Tai	26 22	125 13
21	Miyako Kaizan	25 37	125 06
22	Isigaki Kaikyu	24 58	124 11
KG	Kusagaki Sima	30 49	129 27
NA	Nakano Sima	29 51	129 52
GD	Gazya Sima	29 52	129 33
SU	Suwanose Sima	29 38	129 43
GS	Gonno Sone	29 46	129 25
AK	Akuseki Sima	29 28	129 36
TS	Takara Sima	29 08	129 12
YK	Yokoate Sima	28 48	129 00
IT	Io Tori Sima	27 52	128 14
AG	Aguni Sima	26 34	127 13
KU	Kume Sima	26 20	126 46
SE	Sekibi Syo	25 52	124 32
KO	Kobi Syo	25 53	123 41
UO	Uoturi Sima	25 43	123 28

The seismic velocity structure obtained by Ludwig et al. (1973) shows the uprising features of 5.2 to 5.5km/s velocity layer beneath the eastern margin of the Tunghai shelf, which implies the existence of granitic body composing the basement of the Goto ridge. These ridges are assumed to have been rifted in the Middle Miocene to Pliocene age as inferred from igneous rocks of this age outcropping in the Goto and the Senkaku islands. These basement ridges dammed up sedimentary materials inside the ridge forming large sedimentary basins such as the Goto, Tunghai and Senkaku basins.

The Okinawa Trough is a back-arc basin of the Ryukyu arc-trench system. Hydrothermal activities, discovered at the Izena marine hole and Iheya knolls in the central part of the trough,

demonstrated high thermal activity characteristic of the back-arc basin. However, the development of back-arc basin is still in immature stage as revealed by the underlying thick continental crust (Murauchi et al., 1968; Ludwig et al., 1973). Recent detailed seabottom survey disclosed several grabens in en-echelon arrangement in the southern part of the Okinawa Trough (Yonakuni, Yayeyama, Miyako grabens). The small igneous knolls were also recognized at the central axis of the Yaeyama graben north of Isigaki island (Oshima et al., 1988). These aspects may indicate that the extensional stress field is prevailing in this area.

The Ryukyu Arc are separated into three zones by the topographic depressions of the Tokara channel and the Kerama Gap (the Miyako depression) as; the north, central, and south Ryukyu (Konishi, 1965). Moreover, the bathymetric map edited by JHD (1991) shows the other depression zones named the Yoron basin and the Okinoerabu basin in the central Ryukyu. These depressions may also segment the Ryukyu Arc as shown by the characteristic features of the corresponding magnetic anomaly mentioned in section 5.4. According to geomorphological and geological characteristics, the north to central Ryukyu Arcs can be divided into four along-arc zones from west to east as; the palaeo-Ryukyu volcanic belt (Pliocene to Pleistocene volcanic chain and some cases in Miocene), the Ryukyu volcanic belt (the Tokara volcanic chains: Quaternary volcanic-front), the Ryukyu islands (the Ryukyu geanticline) and the Tertiary sedimentary basin (Hatae, 1955). The zonal topographic depression named the Amami Trough is recognized between the Tokara volcanic chains and the Ryukyu islands. On the other hand, such a zonation

becomes vague in the south Ryukyu. Instead of Miocene volcanism in the north to central Ryukyu, the south Ryukyu shows Eocene volcanism as revealed from pyroclastic rocks and andesite flows with green tuff phases in Eocene age (Kizaki, 1978). Io-Tori-sima island was thought to be the southern end of the Quaternary volcanic front, but the topographic features shown in Fig. 5.8 suggest that the volcanic edifices extend further southwestward as the uplifts of the West Ryukyu knolls (Kato, 1982; Ueda, 1986). The Ryukyu geanticline corresponds to the non-volcanic Ryukyu islands from Amami to Okinawa-sima islands. The trend of Shimanto Super group is bent by about 60 degrees at the western coast of Kyusyu and then extends southward. Konishi (1965) identified the pre-Miocene basement complex occurring in the geanticline with those of the Shimanto Super group. Konishi (1965) and Kizaki (1986) also reviewed the tectonic contrast between the north-central Ryukyu and the south Ryukyu and assumed the topographic depressions of the Tokara channel and the Kerama Gap to be the left-lateral strike slip faults activated by the southeastward shift of the proto-Ryukyu islands in the Middle Miocene age.

A significant difference is also recognized in the configuration of forearc region between the north-central Ryukyu and the south Ryukyu. The deep sea terrace are well developed in the outer region offing of Miyako island. These features gradually extinct in the offing of Okinawa-sima island. The trench is also well developed in the offing of the south Ryukyu, where the trench becomes the deepest. On the other hand, the trench becomes vague in the offing of north-central Ryukyu due to uplifts of the Daito ridge and the Amami plateau. In other words, the

Daito ridge and the Amami plateau have collided against the north-central Ryukyu Arcs, which has resulted in the obscured trench configuration. The rapid uprising of Kikai-sima island to east of Amami-osima island may also be ascribed to this collision.

5.3 Characteristic features of gravity anomalies

Free-air gravity anomaly map of the Ryukyu Arc and its adjacent seas is shown in Fig. 5.4 and Bouguer gravity anomaly map for the assumed density of 2.67g/cm^3 in Fig. 5.5. The Bouguer gravity anomaly in the Philippine Basin amounting to about 360 mgal steeply decreases toward the eastern zone of the Ryukyu islands, where relatively low anomaly ranging from -8mgal to 30mgal is seen, then it increases over the the Okinawa Trough.

The eastern margin of the Tunghai shelf is characterized by positive free-air gravity anomaly ranging from 40 to 60 mgal. In accordance with this trend, relatively high Bouguer gravity anomaly amounting 30mgal are observed over the eastern margin of the Tunghai shelf (H1). Free-air gravity anomaly over the Okinawa Trough is generally flat and in the range between 0mgal and 20 mgal, which manifests that the isostatic compensation is developed. On the contrary, the Bouguer gravity anomaly has the maximum value amounting to 180mgal (H2) in the southern part of the Okinawa Trough and then it gradually decreases northeastward to about 90mgal in accordance with the shallowing of depth. The high Bouguer gravity anomaly over the southern Okinawa Trough may imply the upheaval of the Moho boundary as pointed out by Segawa (1976). It is also noteworthy that Miyako seamount is accompanied by relatively high Bouguer gravity

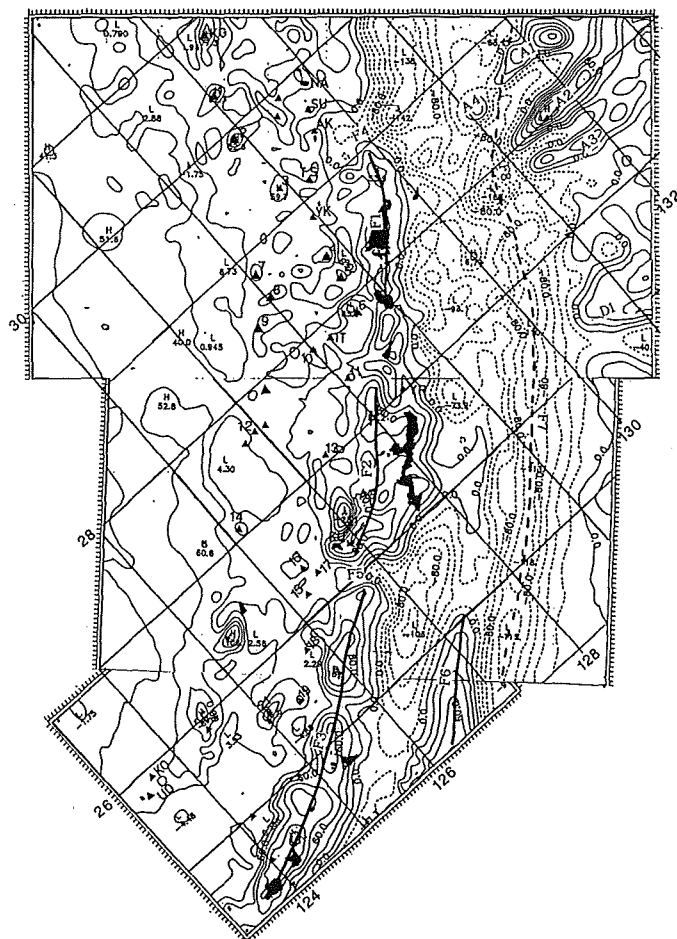


Fig.5.4 Free-air gravity anomaly of the Ryukyu Arc and its adjacent seas. Contour interval is 20mgal. F1, F2,F3:high anomaly zones corresponding to pre-Miocene complex, F4,F5: negative anomaly zones corresponding to the Tokara channel and the Kerama Gap, other abbreviations such as F6,F7,F8, A1, A2,A3, and A4 also show the characteristics of the free-air gravity anomaly. Colour image map is shown in annex-2(c).

anomaly of about 30mgal. This may imply that the seamount is underlain or composed of high density materials. In the northern part of the Okinawa Trough, two positive Bouguer gravity anomaly zones trending in NNE-SSW direction are recognized (H3, H4). The zone labeled by H3 is a continuation from the Kusagaki islands, where granitic rocks of Miocene age intrude the Palaeogene formation. The low Bouguer gravity anomaly zone (L3) is seen in good coincidence with the Amami Trough east of the Quaternary

volcanoes.

The Kume-sima and Aguni-sima islands are characterized by high Bouguer gravity anomaly (H5). This anomaly seems to extend in NE direction as far as west offing of Okinawa-sima island. The positive free-air anomaly overlies the geanticline of the Ryukyu islands (F1,F2,F3), but such convex features are compensated by the terrain effect as seen in the associated Bouguer anomaly pattern. The depressed gravity anomaly corresponding to the Tokara channel and the

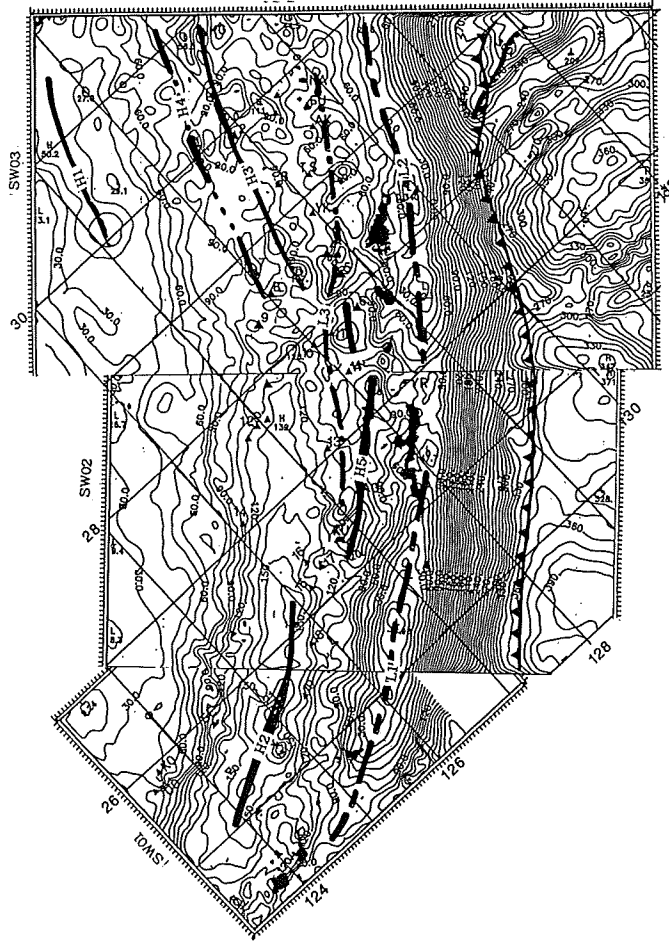
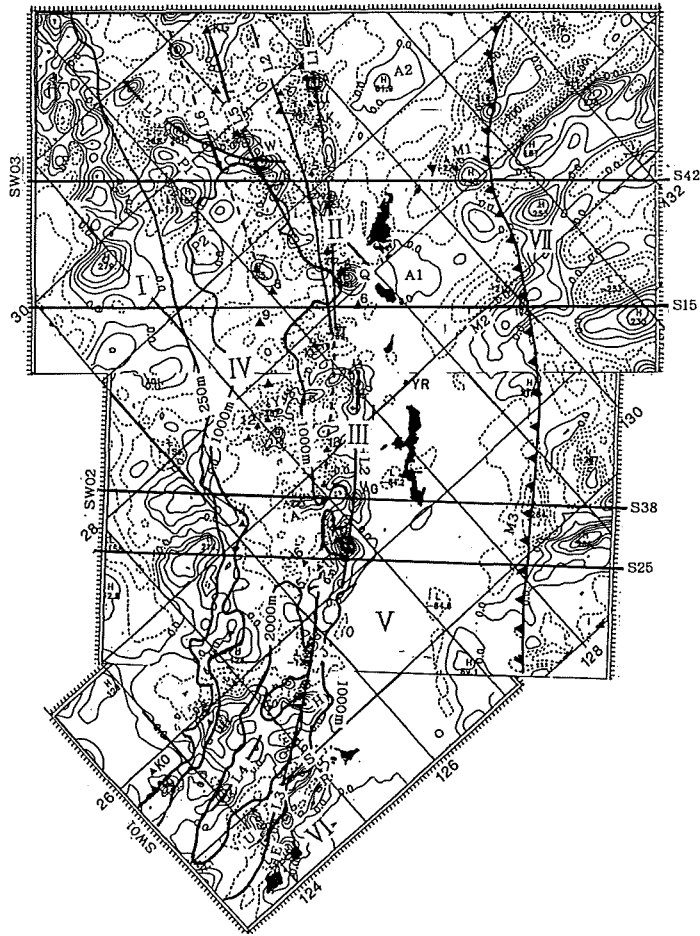


Fig. 5.5 Bouguer gravity anomaly of the Ryukyu Arc and its adjacent seas. Contour interval is 10mgal. H1 to H5: high Bouguer gravity anomaly zones, L1,L2,L3:low Bouguer gravity anomaly zones. Colour image map is shown in annex-2(b).

Kerama Gap (F4,F5) are seen in the free-air anomaly. The corresponding Bouguer anomalies also show concave features on the Kerama Gap, which may imply that the topographic depression of the Kerama Gap is due to structural origin. The positive free-air anomaly zone (F6) is recognized in the trenchward side of Miyako island, which may correspond to the forearc high damming up the sedimentary materials. The low Bouguer anomaly zones (L1,L2) run in parallel to the Ryukyu islands to the southeast of the geanticline. This low gravity zone may be

ascribed to the thick sedimentary layer of the Shimagiri formation. The negative free-air anomaly ranging from -115mgal to -113mgal occurs along the Ryukyu Trench (Nanseisyo Trench) offing of Okinawa-sima and Miyako islands. The topographic features of the northeastern part of the Ryukyu Trench become vague due to uplifts of the Daito ridge and the Amami plateau which have collided against the arc, but the negative free-air anomaly zone (F7) enables us to trace the axis northeastward as labeled by F8. The Bouguer anomaly also depicts the trench



ical/topographical characteristics of the region concerned, as follows, I: the long-wavelength and intermediate amplitude anomaly over the Tunghai shelf break. This zone also includes the short wavelength anomalies over the Senkaku islands. II: magnetic anomalies corresponding to volcanic edifices of the Tokara volcanic chain in the north and the West Ryukyu knolls in the south, III: Palaeo-Ryukyu volcanic zone of Miocene to Pliocene of age, IV: the Okinawa Trough, V: magnetic smooth zone corresponding to the geanticline of the Ryukyu islands and the Tertiary sedimentary basin of Shimagiri formation, VI: south Ryukyu to the south of the Kerama Gap, VII: a region from the continental slope to the Philippine Basin including the Daito ridge and the Amami plateau.

The characteristics and correspondence to geological/topographical features with each zone are described in the following section incorporating the derived magnetic basement model.

5.4.2 Magnetic basement model of the Ryukyu Arc and its adjacent seas

Magnetic basement models for the area of SW01, SW02 and SW03 were calculated on the assumption of the normal magnetization with magnetization intensity of 3.0A/m. The reference depth of the basement is postulated at 4.0km below sea level. The magnetic basement models are then combined in a single map with the same scale. The magnetic basement contour map obtained is shown in Fig.5.9a and colour image map in 5.9b. The magnetic basement model is helpful to correlate the magnetic anomaly to corresponding structures, which enable us to consider the tectonic implication of magnetic zonation in a more convincing way. In the following, descriptions are given as to the magnetic

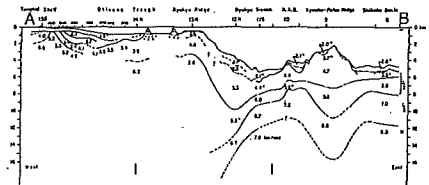
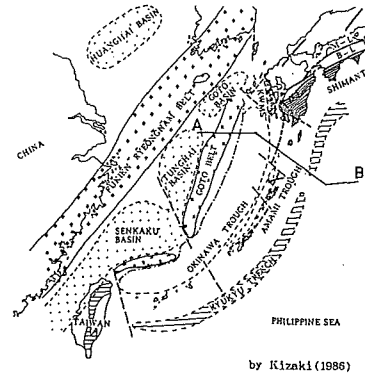


Fig.5.7 Tectonic map of the East China Sea and Ryukyu arc-trench system (after Kizaki, 1986).

Seismic velocity structure obtained by Ludwig et al. (1973) is shown in the lower part for the cross-section A-B.

anomaly zones classified in this section in order.

I: This magnetic anomaly zone is characterized by the patched pattern of the long-wavelength and intermediate amplitude anomalies over the Tunghai shelf break. These anomalies may correspond to the acidic intrusive rocks of Neogene age. The long-wavelength positive anomalies are intersected by the NW trending negative anomalies, some of which seem to extend in SE direction across the Okinawa Trough. The magnetic anomaly around the Senkaku islands is relatively flat except for the positive anomaly south of the Sekibi reef. The basaltic rocks were dredged from the Kobi reef, but no appreciable magnetic anomaly was recognized nearby.

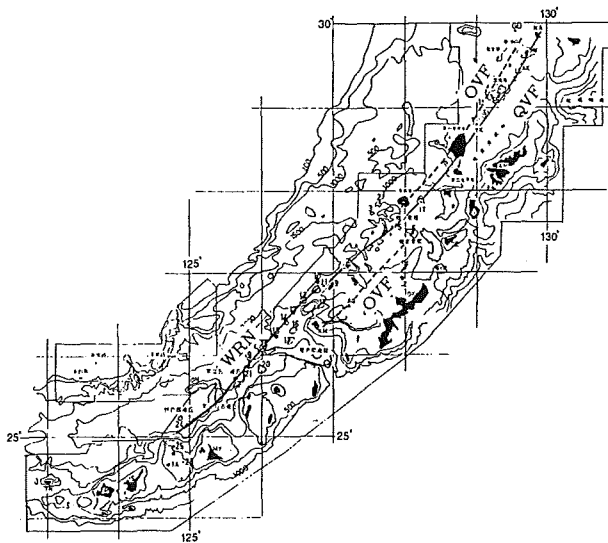


Fig.5.8 Topography in the vicinity of Nansei Syoto (Ryukyu Islands). Sources are from the bathymetric chart of the adjacent seas of Japan No.6302. Solid line means Quaternary volcanic front and broken lines Paleo-volcanic belt. The topographic uplifts of the West Ryukyu knolls are arranged on the western margin of the insular shelf from northwest offing of Okinawa-sima island to the north offing of Miyako island. WRN: West Ryukyu knolls, OVF: Paleo-volcanic front, QVF:Quaternary volcanic front, IG: Igyo sone, IT:Io-tori sima. (modified from Ueda(1986))

The magnetic basement around the Tunghai shelf shows segmented basement highs as denoted by B1 to B6 (in Fig.5.9a). Segmented blocks of B3 to B6 are consistent with the magnetic basement model derived by Okuma et al.(1991). Among them, the southern basement high loading the Sekibi reef seems to have been shifted southward relative to the other blocks. Besides, the segmented structures of the magnetic basement is well developed in the southern part of the Ryukyu Arc, where the outline of each magnetic basement block shows the jigsaw fitting pattern.

II : This zone corresponds to the volcanic zone extending from the Tokara volcanic chain to the West Ryukyu knolls. Three cross-arc segments are recognizable in the magnetic anomaly pattern, i.e. the northern zone (L1) north of Io-Tori-sima (N27°51', E128°13'), the central zone

between the south of Io-Tori-sima and the Kerama Gap, and the southern zone (L3) south of the Kerama Gap, respectively. The morphological boundary of the Tokara channel is featureless in the magnetic anomaly pattern. In place of above features, the depression zone between the Yoron basin and the north of Igyosone bank, which is located to the south of Io-Tori-sima island, may correspond to the conspicuous magnetic boundary segmenting the arc. In the western extension of this depression zone is there the Iheya knolls, characterized by high thermal activity. Such being the case, we name this depression zone the Yoron depression zone for convenience' sake. In the norther zone, north of Io-Tori-sima, the short-wavelength and intermediate amplitude anomalies prevail along Quaternary volcanic edifices. In the southern zone (south Ryukyu), conspicuous dipole anomalies are recognized in

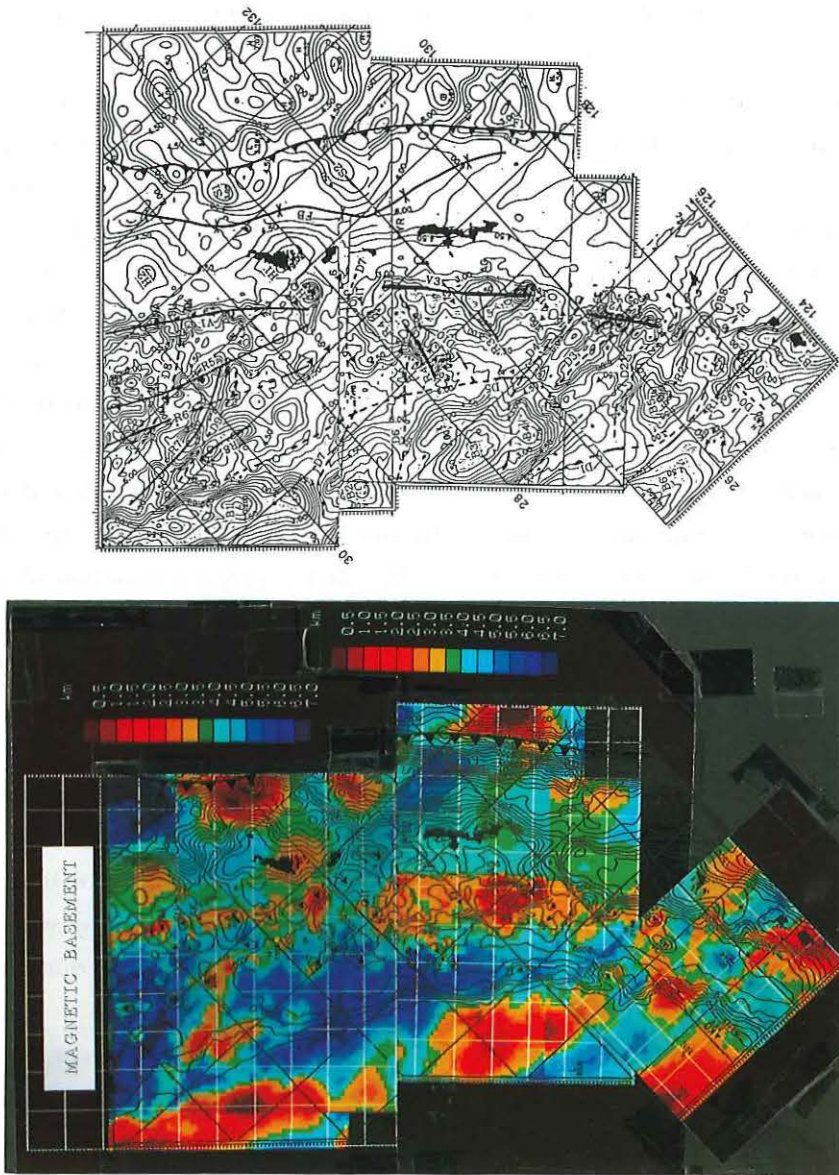


Fig. 5.9 Magnetic basement model of the Ryukyu Arc and its adjacent seas. Contour interval is 500m. Assumed magnetization intensity is 3.0A/m and the magnetization direction is the present field direction. The reference depth is 4km below sea level.

- (a): Contoured basement depth map.
 B1 to B6:magnetic basement blocks beneath the Tunghai shelf, V1:Quaternary volcanic zone of Tokara islands, V2:West Ryukyu knolls in south Ryukyu, V3:Miocene volcanic zone in central Ryukyu. R1 to R8:magnetic basement highs, D0 to D9:magnetic basement lows, FB:magnetic basement low in the forearc region. Trench axis is shown by the sequence of solid triangles.
- (b): Colour image map showing the magnetic basement relief. Topographic contour lines are superimposed on the coloured basement map.
 TS:eastern margin of the Tunghai shelf, VF:Quaternary volcanic front, 1:Nakano sima, 2:Gazya sima, 3:Yokoate sima, 4:Io-tori sima, 5:Igyo sone, 6:Iheya knolls, 7:Miyako Smt., 8:Uoturi sima, 9:Kume sima, K:Kusagaki sima. The Okinawa Trough deeper than 2000m depth is shown by a dot-line contour.

good correspondence with the West Ryukyu knolls in the southeastern margin of the Okinawa Trough. The central zone is, however, featureless in magnetic anomaly pattern. In the northern Ryukyu Arc, Miocene to Pleistocene volcanic edifices are located in the inner part of the Quaternary volcanoes, i.e. Nakano-sima, Suwanose-sima and Io-Tori-sima islands belong to the recent volcanic group and Gazya-sima, Takara-sima and Akuseki-sima islands to the old volcanic group. These volcanoes are mainly composed of pyroxene andesite, which is consistent with magnetic anomalies with intermediate amplitude. In the central zone west offing of Okinawa-sima island, several oval uplifts of the West Ryukyu knolls are located in the western margin of the insular shelf (see Fig.5.8). However, no appreciable magnetic anomalies are observed over these uplifts, reflecting probably acidic rocks of weak magnetization contrast. Acidic pumices dredged from several uplifts in this zone may support the above interpretation (Kato et al., 1982). The reversed magnetic anomaly pattern lies over the Daiyon-Kume knoll (N26°11', E126°26'). These features enable us to trace back the volcanic activity of the West Ryukyu knolls at least to the Matuyama reverse epoch (before 0.7Ma).

The southern zone south of the Kerama Gap is characterized by conspicuous dipole magnetic anomaly pattern corresponding to knolls in the southern margin of the Okinawa Trough. The depth to uplift, peak to peak amplitude and distance are as follows: Daiiti Miyako knoll (H, 865m, 710nT, 5.5km), Daini Miyako knoll (J, 1630m, 390nT, 7.5km), Daisan Miyako knoll (K, 943m, 490nT, 3.0km), Daigo Miyako knoll (L, 1800m, 490nT, 4.5km), Irabu knoll (M, 1890

m, 840nT, 8.0km) etc, as shown by Ueda (1986). These magnetic anomalies show the dipole pattern suggesting normal magnetization of the source bodies. The relatively large amplitude anomalies may favour the basaltic composition of the source body instead of andesitic rocks.

As mentioned above, the northern zone is characterized by the short-wavelength and intermediate amplitude anomaly, the central zone by the featureless magnetic anomaly pattern reflecting acidic rocks and the southern zone by the conspicuous magnetic anomaly pattern due to the basaltic composition of the volcanic edifices.

The above along-arc variation of the Quaternary volcanic zone is well represented in the magnetic basement map, i.e. the distinguishable NE trending basement highs (V1) along the Tokara volcanic chain from Nakano-sima to Io-Tori-sima islands, featureless magnetic basement relief along the West Ryukyu knolls in the central zone, and the discrete basement highs (V2) in good correspondence with the West Ryukyu knolls in the southern zone.

III : Palaeo-Ryukyu volcanic zone of Miocene to Pliocene of age.

This anomaly zone is characterized by the positive anomaly extending in SW direction from the vicinity of Igyosone bank (N27°29', E128°06') to the surroundings of Kume-sima island (L2). The andesitic pyroclastic materials of Miocene age outcrop in Kume-sima and Aguni-sima islands, which are indicative of green tuff activity in the Miocene age. The magnetic anomaly overlying Kume-sima island amounts to 1000nT, which suggest the existence of basic materials of high magnetization contrast beneath the edifice. Above positive anomaly extends in WSW direc-

tion across the Kerama Gap, and another positive peak occurs on the insular shelf facing the Kerama Gap. The magnetic basement high corresponding to this anomaly zone (V3) is about 250 km length in NE direction and about 75 km in width. Aguni and Kume-sima islands are located in the southeastern part of the magnetic basement high. The general features of the magnetic basement high resemble to that in the eastern margin of the Tunghai shelf.

It should be noted that the old volcanic zone of Miocene to Pliocene age is situated here in the outer region against the Quaternary volcanic front of the West Ryukyu knolls; i. e. the opposite geographical arrangement between the old and new volcanic zones occurs in the central Ryukyu south of the Igyosone bank. These features may imply the southeastward drift of this magnetic block against the northern arc.

IV : Okinawa Trough

The magnetic features of the Okinawa Trough are different among three areas of the southern, central and the northern parts in correspondence with topographic/geological characteristics. In the southern part of the Okinawa Trough, the most significant feature of the magnetic anomaly is the WE trending paired anomaly overlying the Yayeyama graben (L4 in Fig.5.6). Besides the magnetic anomalies arising from intrusive or buried edifices are also recognized (U). Miyako seamount (21 in Fig.5.6) located at $N24.6^{\circ}$, $E125.1^{\circ}$, shows a summit depth of 812m from the surrounding depth of about 2000m and has the horizontal dimension of $12\text{km} \times 50\text{km}$. A negative anomaly overlies the edifice, however whose amplitude is subdued reflecting low magnetization intensity of the body.

The magnetic basement of the southern part of the Okinawa Trough is depressed beneath the Yaeyama graben (D0) and separated into several blocks by the N-S trending basement highs (R1, R2) and lows (D1 to D4). The above segmentation can be traced from the Tunghai shelf area to the southern Ryukyu Arc as denoted by depressions of D1, D2 superimposed on the magnetic basement map.

In the central part of the Okinawa Trough, the depression zone of the magnetic basement is not located beneath the central axis of the trough but shifted in the NE direction by about 40 km to 80 km. The marked magnetic anomalies are recognized in association with the Iheya knolls group (Y). It is noteworthy that the eastern end of these magnetic anomalies coincides with the displacement zone of the positive anomaly belt (L2). Besides, topographic depression of the Yoron basin occurs on the seaward extension of the above displacement zone. This displacement zone is named as the Yoron depression zone as mentioned in the description of the magnetic anomaly zone of II. These features are also well represented in the magnetic basement map.

Another anomaly (A) associated with Daiiti ($N26^{\circ}51'$, $E126^{\circ}52'$) and Daini ($N26^{\circ}53'$, $E126^{\circ}47'$) Tori-sima knolls also shows the elongation oblique to the Ryukyu Arc. The above trend coincides with the general direction of the echelon arrangement of the grabens appearing in the southern part of the Okinawa Trough. The magnetic basement corresponding to these anomalies is uplifted in association with Daiiti and Daini Tori-sima knolls and Iheya knolls (R3, R4). The eastward elongation of the magnetic basement high of the Iheya knolls coincides with the northern end of the magnetic basement high of

V3. Oshima et al. (1988) ascribed the magnetic anomalies associated with the Iheya knolls to the topographic effect, however the present analysis shows the considerable magnetic basement relief attributable to the buried intrusive igneous body.

In the northern part of the Okinawa Trough, the appreciable magnetic anomalies are recognized inside of the old volcanic chain, contrary to the featureless configuration of the bathymetry. Among them, two magnetic belts (L5, L6) slightly oblique to the Tokara islands chain are recognized over the inner region west of the Quaternary volcanic front. The magnetic anomalies along the former belt are comparable in amplitudes and wavelengths with those of the Quaternary volcanic edifices. Now that Kusagaki, Uzi and Kosiki-zima islands, which were intruded by andesitic to granitic rocks of Miocene age, are situated on the NE extension of L5, this belt seems to correspond to the palaeo-volcanic chain older than inner ones. Another belt L6 is not so evident as L5 in extension, however the small uplifts and buried basement highs can be recognized along this belt, i.e. Kita-ense knoll in the south-southwestern end and traced in NNE direction as the uplifts of Nisi-gazya, Oki-uzi and Minami-uzi knolls, respectively. This belt (L6) seem to be older than L5 because of thicker sedimentary layer covering the edifices. The patched anomalies (P1, P2) west of L6 show similar features in amplitude and wavelength as those on the Tunghai shelf break. This may imply that the buried bodies producing patched anomalies are originally continuous to the magnetic basement of the Tunghai shelf and then separated as it is.

The derived magnetic basement model also shows the lineated magnetic basement highs (R5,

R6) corresponding to magnetic zones of L5, L6. These magnetic basement highs terminate on the north of the magnetic basement low marked by D7, whose seaward extension coincides with the Yoron depression zone as seen in Fig. 5.9a. The magnetic basement model also shows another elongation oblique to R5, R6 as shown by the basement high of R7 and basement lows denoted by D8, D9. The southward extension of D8 coincides with the topographic depression of the Tokara channel. This NNW-SSE trend seems to agree with the strike of the lateral fault caused by the southeastward drift of the north Ryukyu due to opening of the Japan Sea (Katsura, 1992). It is also should be noted that the magnetic basement low (D5) seems to separate the magnetic basement high of R8 from that of the Tunghai shelf.

V : No remarkable anomalies are recognized within this zone except the anomaly denoted by Q, reflecting the thick sedimentary layer of the Shimajiri formation and the low magnetization contrast composing the pre-Miocene basement complex. The granitic rocks of Eocene age intruding the palaeogene complex outcrop in Amami-O-sima and Tokuno-sima islands and the Miocene granitic rocks are also recognized in the Motobu peninsula of Okinawa-sima island and Tonaki-sima islands, respectively. The broad and low amplitude anomalies marked by A1, A2 may correspond to the above granitic rocks. The anomaly overlying Daini-Amami bank marked by Q occurs within the Motobu belt, which is characterized by the intrusive rocks of grano-diorite and granite of Mesozoic to Cenozoic age.

The magnetic basement highs (H1, H2, HQ) occur in corresponding to magnetic anomalies of A1, A2 and Q. Amami-O-sima island is just locat-

ed on the uplifted magnetic basement. The depression zone of the magnetic basement (FB) is also recognized in the outer zone of the Ryukyu geanticline in nearly parallel to the Ryukyu trench. This depression zone may represent the sedimentary basin of the forearc region of the Ryukyu Arc.

VI : This zone corresponds to the southern Ryukyu Arc including Miyako and Yaeyama islands. Several conspicuous anomalies are recognized on the geanticline of the southern Ryukyu Arc such as NE elongated anomaly marked by E and EW trending anomalies of R and S. These anomalies may be correlated to the Eocene green tuff activity as revealed by pyroclastic rocks and andesite flows of Eocene age outcropping in Isigaki island (Ueda, 1986; Oshida et al., 1992). The Miocene granitic rocks outcropping in Isigaki-sima island is an alternative candidate for the magnetic source. However, information about the magnetic property of the granitic rocks is necessary to obtain the corroborant conclusion. The magnetic basement highs of the south Ryukyu can be separated into two zones of B7 and B8 by the topographic depression of the Isigaki saddle, the former magnetic basement high loads Isigaki and Iriomote islands and the latter Tarama-sima and Miyako islands. It is noteworthy that the topographic depressions of the Isigaki and Miyako saddles is in good correspondence with the magnetic basement lows marked by D1, D2 which may imply the structural origin of these topographic depressions.

VII : This zone covers the area from the continental slope to the Philippine Basin including the Daito ridge and the Amami plateau. The most

outstanding features of the magnetic anomaly are the aspects that the elongated anomalies corresponding to the Amami plateau and the Daito ridge (M1, M2) extend to the forearc region across the Ryukyu trench (Kasuga et al., 1992). These features are more apparent in the magnetic basement map (basement highs of S1, S2). The above facts suggest the ongoing accretional process of the ridge to the Ryukyu Arc. In contrast to above features, the negative anomaly zone occurs over the trench as marked by M3. This negative anomaly zone may be originated from the sharp depression of the magnetic basement (F1 in Fig.5.9). Multi-channel seismic profiling transecting the Nanseiyoto Trench also reveals the normal faults of the oceanic crust on the seaward trench slope in consistent with the magnetic features mentioned above (Kato, 1991). Conspicuous magnetic anomalies occur in coincidence with topographic uplifts of the Amami plateau and the Daito ridge. These ridges are thought to be old-island arcs accompanied by thick continental crust composed of acidic rocks, but magnetic features suggest the composition of basic materials of high magnetization intensity. As to this matter, the analysis of the Daito ridge mentioned in the following section may be helpful for understanding the origin of these magnetic anomalies.

5.5 Pseudo-gravity analysis

Pseudo-gravity was calculated as for three areas (A, B, C) shown in Fig.5.18. and compared with the short-wavelength Bouguer gravity anomaly to obtain the ρ/J (g/emu) ratio of the representative magnetic basement highs in the area of SW01, SW02 and SW03, respectively.

5.5.1 Pseudo-gravity analysis for SW01

The short-wavelength Bouguer gravity anomaly

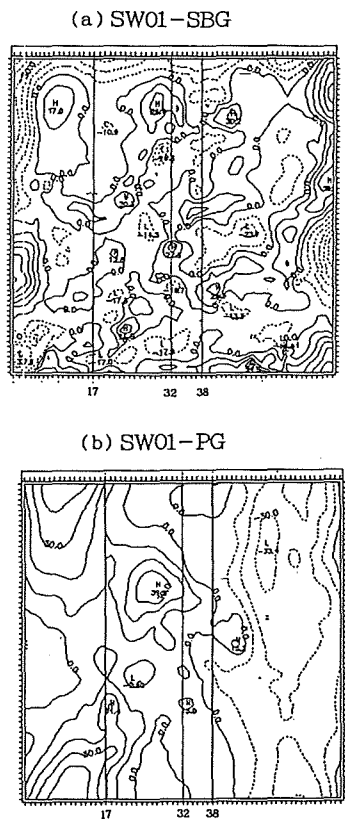


Fig.5.10 Short-wavelength Bouguer gravity anomaly (a) and the pseudo-gravity (b) of the area SW01.

The assumed ρ/J ratio for calculation of pseudo-gravity is 100 g/emu. Contour interval is 10mgal. Analyzed area is marked by A as shown in Fig.5.18.

and the calculated pseudo-gravity for the area of A (SW01) are shown in Fig.5.10 and the representative cross-sections are illustrated in Fig.5.11 together with magnetic basement relieves. These cross-sections make apparent the existence of the buried magnetic basement highs beneath the Okinawa Trough. The section-17 shows the considerable size of the buried magnetic body of the Isigaki knoll. A section-32 crossing over the Sekibi reef shows no appreciable Bouguer gravity anomaly in association

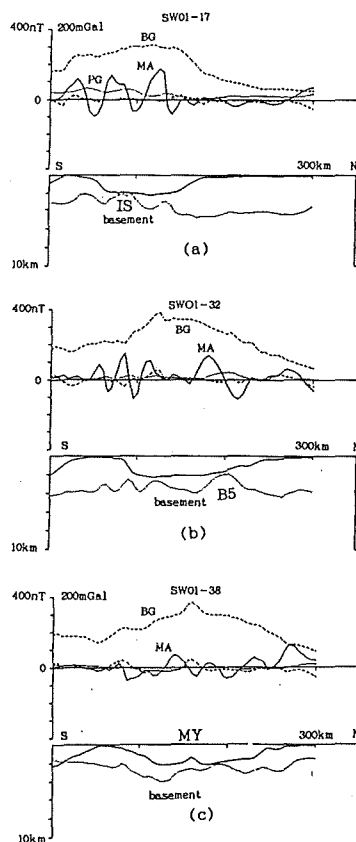


Fig.5.11 Cross-sections of magnetic basement model and the related geophysical data of the area SW01. BG:Bouguer gravity anomaly (dot), SBG:Short-wavelength Bouguer gravity anomaly (broken), PG:Pseudo-gravity (dot), MA:Observed magnetic anomaly (solid). Derived magnetic basements are shown by dot lines in the lower part. IS: (a):section-17, (b): section-32, (c): section-38.

with it. These features imply that the ρ/J ratio corresponding to the magnetic basement high of the Sekibi reef is too small to produce appreciable gravity anomaly, which is consistent with the granitic composition of the Senkaku ridge. A section-38 crossing over Miyako seamount also reveals the magnetic basement high with considerable horizontal dimension sustains the non-magnetic uplift of Miyako seamount, but the local Bouguer gravity high implies the large den-

sity contrast composing the seamount.

5.5.2 Pseudo-gravity analysis for SW02

The short-wavelength Bouguer gravity anomaly and the calculated pseudo-gravity for the area of B (SW02) are shown in Fig.5.12 and the representative cross-sections are illustrated in Fig.5.13 together with the magnetic basement relieves. The short-wavelength Bouguer gravity anomaly map shows the significant positive zone over the geanticline of the Ryukyu Arc, but no appreciable pseudo-gravity occurs reflecting the

low magnetization contrast. The positive short-wavelength Bouguer anomaly amounting to ten and several mgals occurs on the Tunghai shelf, however their amplitudes are very small relative to the pseudo-gravity. Above features are more apparent in sections shown in Fig.5.13. In section-25 and section-38, two magnetic basement highs correlative to the Goto ridge and the Miocene green tuff zone are recognized. The ρ/J

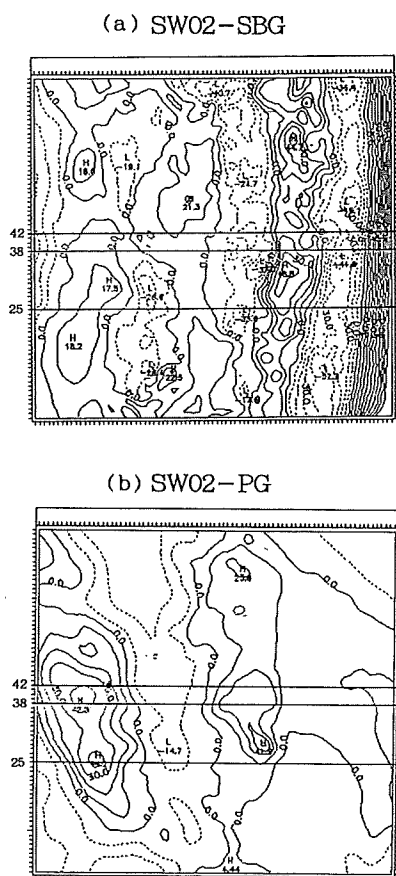


Fig.5.12 Short-wavelength Bouguer gravity anomaly (a) and the pseudo-gravity (b) of the area SW02.

The assumed ρ/J ratio for calculation of pseudo-gravity is 100 g/emu. Contour interval is 10mgal. Analyzed area is marked by B as shown in Fig.5.18.

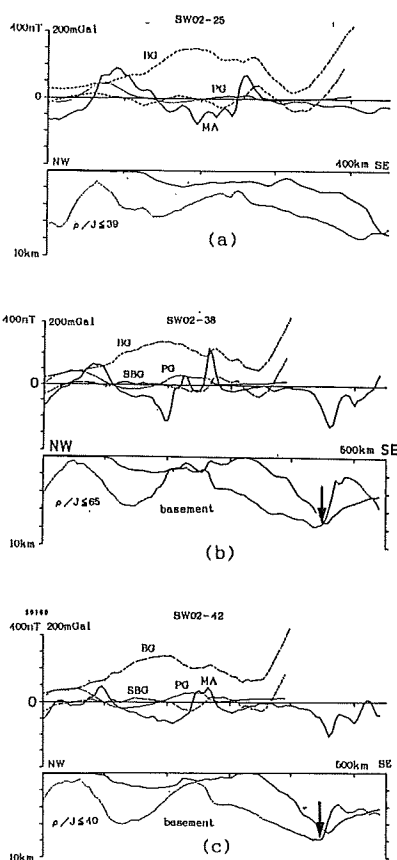


Fig.5.13 Cross-sections of magnetic basement model and the related geophysical data of the area SW02. BG:Bouguer gravity anomaly (dot), SBG:Short-wavelength Bouguer gravity anomaly(broken), PG:Pseudo-gravity (dot), MA:Observed magnetic anomaly (solid). Derived magnetic basements are shown by dot lines in the lower column. (a): section-25, (b): section-38, (c): section-42.

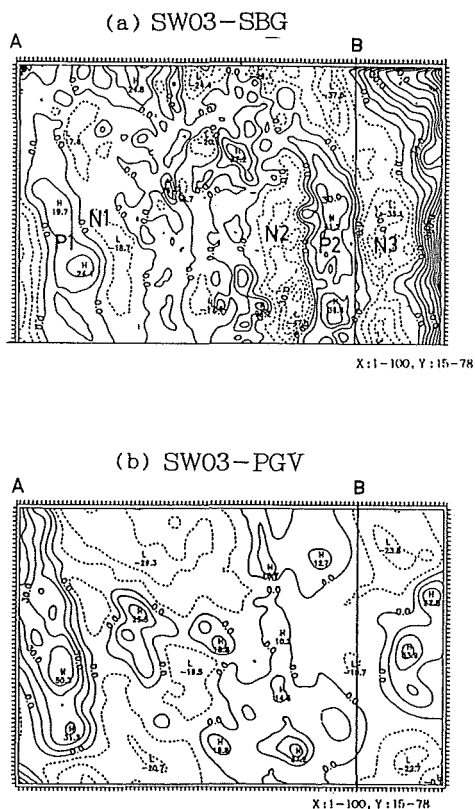


Fig.5.14 Short-wavelength Bouguer gravity anomaly (a) and the pseudo-gravity (b) of the area SW03.

The assumed ρ/J ratio for calculation of pseudo-gravity is 100 g/emu. Contour interval is 10mGals. Analyzed area is marked by C as shown in Fig.5.18. P1 and P2 mean positive anomaly zones and N1, N2, and N3 negative ones. Correlation analysis is conducted for the area between A and B as shown in Fig.5.16.

ratio of the Goto ridge becomes 39 for section-25 and 65 for section-38, respectively. These values may become smaller when the raw Bouguer gravity anomaly were adopted for correlation analysis because of the featureless Bouguer gravity anomaly pattern over the Tunghai shelf. On the contrary, the reverse correlation between the short-wavelength Bouguer anomaly and pseudo-gravity anomaly is recognized for the magnetic basement

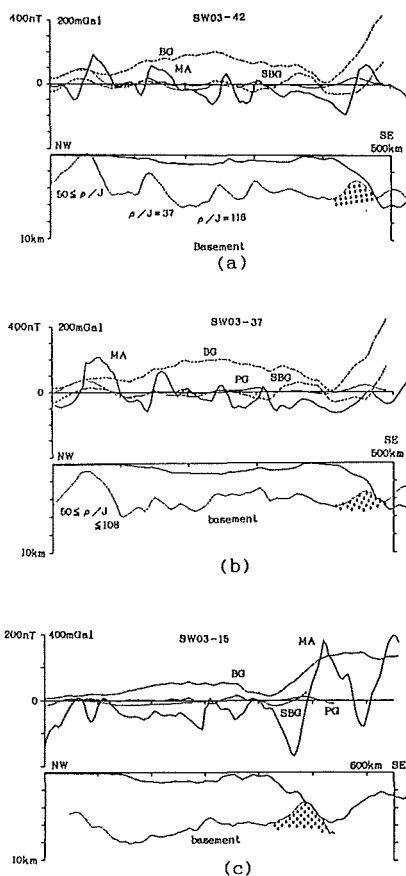


Fig.5.15 Cross-sections of magnetic basement model and the related geophysical data of the area SW03. BG:Bouguer gravity anomaly (dot), SBG:Short-wavelength Bouguer gravity anomaly (broken), PG:Pseudo-gravity (dot), MA:Observed magnetic anomaly (solid). Derived magnetic basements are shown by dot lines in the lower column. The dotted basement highs show the accreted magnetic bodies across the trench. (a): section-42, (b): section-37, (c): section-15.

high correlative to the Miocene green tuff zone. This reverse correlation may manifest the negative density contrast of the magnetic basement high or skewness effect resulting from different magnetization direction. If the assumed magnetization direction is true, we should accept the considerably small ρ/J ratio of the magnetic basement high corresponding to the Miocene

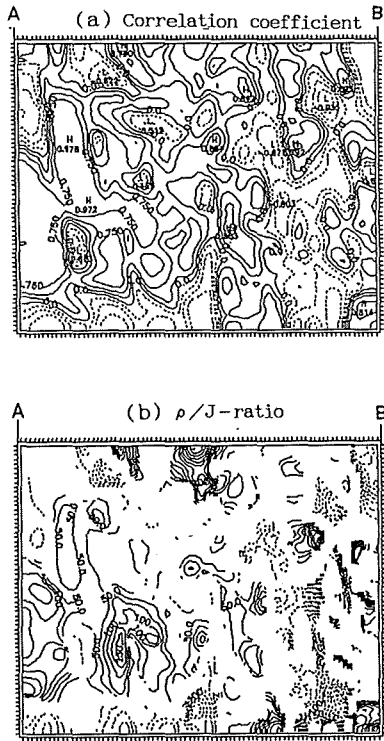


Fig.5.16 Correlation coefficients(a) and estimated ρ/J ratio(b) of the area A—B in Fig.5.14. Correlation analysis was conducted between the short-wavelength Bouguer gravity anomaly and the pseudo-gravity in SW03 shown in Fig.5.14.

(a): correlation coefficients, (b): estimated ρ/J ratio.

volcanic body. The reverse correlation also appears on the Quaternary volcanic edifices in the northern Ryukyu Arc as seen in the associated Bouguer gravity anomaly low (L3 in Fig.5.5). In the trenchward side of section-38 and section-42, we see the depressions of the magnetic basement just over the trench axis. These features represent the normal faulting of the Oceanic crust as mentioned before.

5.5.3 Pseudo-gravity analysis for SW03

The short-wavelength Bouguer gravity anomaly and the calculated pseudo-gravity for the area of C (SW03) are shown in Fig.5.14 and the the

representative cross-sections are illustrated in Fig.5.15 together with the magnetic basement relieves. The short-wavelength Bouguer gravity anomaly reveals the NE trending positive and negative anomaly zones. The westernmost positive and negative zones (P1, N1) are well correlated to those of the pseudo-gravityfringing the eastern margin of the Tunghai shelf. The easternmost negative zone (N3) seems to correspond to the forearc sedimentary basin. The negative Bouguer anomaly zone (N2) occurs over the Quaternary volcanic zone and the positive one (P2) over the Ryukyu geanticline.

The ρ/J ratio of the Goto ridge falls in the range from 50 to 108 as seen in the section-37 and 42. In these sections, the accreted magnetic basement highs are recognized beneath the landward trench slope. These accreted magnetic bodies are considerably large relative to magnetic basement highs corresponding to the Quaternary volcanic edifices. In section-42, we see the basement highs of considerable size beneath the oceanic floor of the northern part of the Okinawa Trough. These upheaved magnetic basements are well correlated to the local Bouguer gravity highs. The ρ/J ratio of these basement highs are scattered from 37 to 116. The westernmost magnetic basement high corresponding to the Goto ridge has the ρ/J ratio ranging from 50 to 108. These values are somewhat large relative to those of the central area (Fig.5.13). Two-dimensional area lcorrelation analysis between the short-wavelength Bouguer gravity anomaly and the pseudo-gravity, however, gives the value around 50 for the Goto ridge, as seen in Fig. 5.16. This value is also in favour of the magnetic source of low ρ/J ratio as revealed from the analysis of SW01 and SW02.

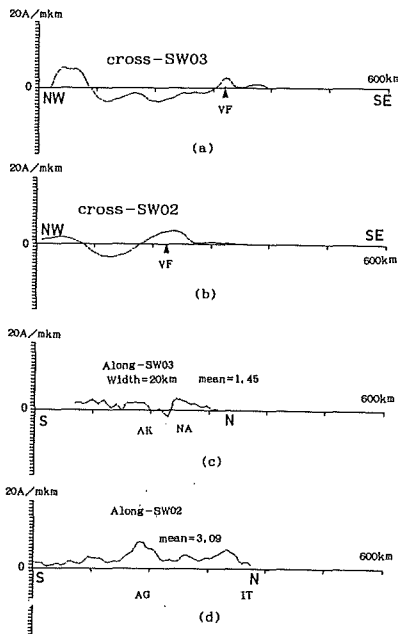


Fig.5.17 Cross-arc(a,b) and along-arc(c,d) variation of the bulk magnetization of the Ryukyu Arc. Unit of bulk-magnetization per km^2 is $\text{A/m}\cdot\text{km}$

- (a): cross-arc of SW03, (b): cross-arc of SW02,
 (c): along the volcanic frontal area of SW03. This figure represents the mean value for the zone of 20km width orthogonal to the arc. Total mean becomes $1.45\text{A/m}\cdot\text{km}$.
 (d): along the volcanic frontal area of SW02. This figure represents the mean value for the zone of 20km width orthogonal to the arc.

5.6 Bulk magnetization of the Ryukyu Arc

The mean bulk-magnetization per unit square (BMR: $\text{A/m}\cdot\text{km}$) is estimated based on the magnetic basement models for the SW02 and SW03 with the same method described in section 4.4.4. An cross-arc variation, transecting the arc orthogonally to the general trend of the arc, was estimated as shown in Fig.5.17 (a), (b). The result for SW02 shows the bimodal peaks, the western peak corresponds to the Goto ridge and the eastern one to the Miocene volcanic zone of

the central Ryukyu. It should be emphasized that the bulk magnetization (BMR) of the latter zone is comparable to that of the Goto ridge. These features may imply that the volcanic activity creating the Miocene magnetic block (V3) is similar to that forming the Goto ridge. The bulk magnetization of the northern Ryukyu Arc (SW03) shows the significantly large BMR of the Goto ridge in comparison with that of the Quaternary volcanic front. These features forced us to imagine the unusual volcanic activity producing the magnetic edifices of the Goto ridge. In the lower parts of Figs.5.17 (c), (d) are shown the along-arc variation of the bulk magnetization of the volcanic zone. The result for SW02 shows the relatively large mean BMR of 3.09, however, this value does not represent the BMR of Quaternary volcanic edifices but of the Miocene magnetic basement high; that is, no considerable magnetic edifices are seen along the volcanic front of the central Ryukyu to the south of Iotori-sima island, reflecting the acidic volcanism of weak magnetization intensity. The mean BMR for northern Ryukyu (to the north of Iotori-sima) becomes 1.45. This value is less than that of the northern Izu-Ogasawara Arc (1.74). The above difference may result from different magma production rate and the different petrological composition of the Quaternary volcanic edifices between the Ryukyu Arc and the northern part of the Izu-Ogasawara Arc.

In Table 5.4, are listed the bulk magnetization values ($\text{A/m}\cdot\text{km}^3$) for the respective magnetic basement highs together with the corresponding Bouguer gravity anomaly values. The bulk magnetization of volcanic edifices of the south Ryukyu are significantly larger than those of the north Ryukyu. These values, however, are small

relative to those of the Izu-Ogasawara Arc.

5.7 Two-dimensional magneto-gravity response analysis

To investigate the magnetic property of the Moho boundary, two-dimensional magnetic and gravity analyses were performed on the sections shown in Fig.5.18. These results are significant for consideration of the deep seated magnetic source producing relatively long-wavelength magnetic and gravity anomalies.

5.7.1 Results on SW01

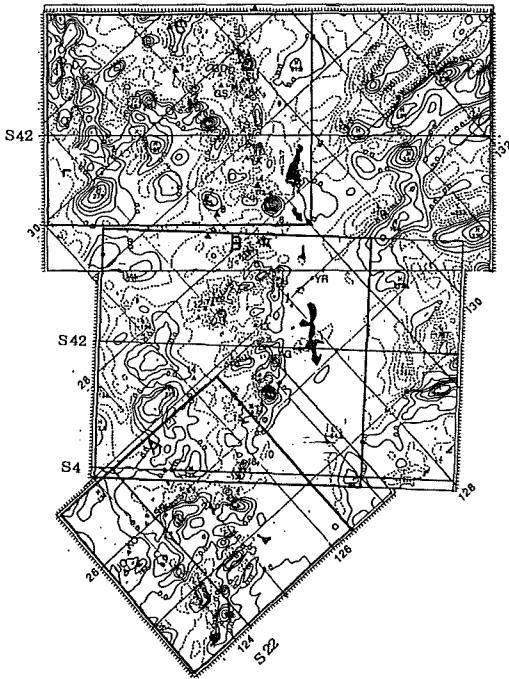


Fig.5.18 Target areas for three-dimensional pseudo-gravity analyses (Fig.5.10, Fig.5.12, Fig.5.14) and cross-sections for two-dimensional magneto-gravity response analysis (Fig.5.20 to Fig.5.23).

A: area shown in Fig.5.11, B: area shown in Fig.5.13, C: area shown in Fig.5.14. The cross-sections S22 in SW01, S4 and S42 in SW02, and S42 in SW03 are analyzed by magneto-gravity response function method.

Table 5.4 Bulk magnetization of the volcanic edifices of the Ryukyu Arc.

1 SW01	name	Bulk magnetization	BGA ($\lambda \geq 160\text{km}$)
Abbr.		($\text{A/m}\cdot\text{km}^2$)	(mGal)
18	Daisan Miyako Kalkyu	2270	143
19	Daiti Miyako Kalkyu	2210	147
22	Isigaki Kalkyu	5769	146
2 SW03			
HA	Nakano Sima	1538	66
SU	Suvanose Sima	273	66
YK	Yokoate Sima	1051	79
IT	Io-Tori Sima	469	13

In response to the recent progress of the sea-bottom surveys, Oshida et al. (1992) present the magnetic structural model crossing the southern Okinawa Trough in NS direction. Their model is based on the seismic P-wave velocity structure obtained by Hirata et al. (1991), and ascribes the observed magnetic anomaly to the magnetization of the upper crust having the P-wave velocity of 3.6~6.4km/sec. In Fig.5.19 is shown the P-wave velocity model together with the magnetic structure derived by Oshida et al. (1992). This magnetic structural model well explains the observed magnetic anomaly, but the gravity features are not taken into account. The flat bottom of the Moho boundary as shown in Fig.5.19 conflicts with the Bouguer gravity high overlying the Okinawa Trough. To avoid above contradiction, synthetic analysis of magnetic and gravity anomalies was attempted as shown in Fig.5.20 for the section-22 in SW01 (Fig.5.18). The location of this section is nearly the same as that of Oshida's model. The upper part ascribes the magnetic anomalies to the upper magnetic layer. Thus obtained magnetic basement relief is similar to Oshida's model except for the central basement high corresponding to the Yaeyama central knoll.

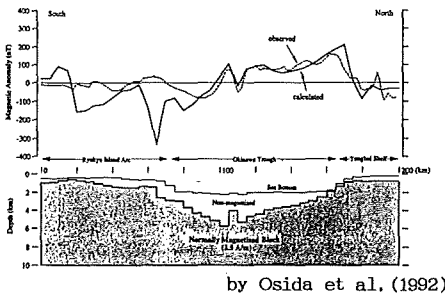
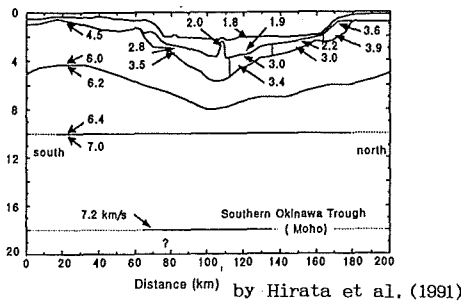


Fig.5.19 Crustal structure of the Okinawa Trough. Upper: Seismic velocity structure of the Okinawa Trough (after Hirata et al.1991). Lower: Magnetic structure of the Okinawa Trough (after Oshida et al.1992).

The pseudo-gravity is, however, depressed over the Okinawa Trough in contrast to the Bouguer gravity high. On the other hand, the lower model, which ascribes the long-wavelength magnetic anomalies to the lower boundary of the magnetic layer, well explains the magnetic and gravity features over the Okinawa Trough. As the lower boundary thus obtained corresponds to the negative density boundary, the Moho boundary is likely as the magnetic lower boundary. The ρ/J ratio of this boundary becomes -154 , so the density contrast becomes 0.45g/m^3 for the assumed magnetization intensity of 3.0A/m . These values seem to be acceptable for the Moho boundary. As mentioned above, the present model suggests the high magnetization contrast at the Moho boundary instead of the upper crust

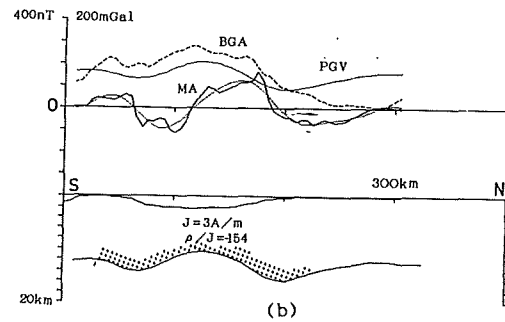
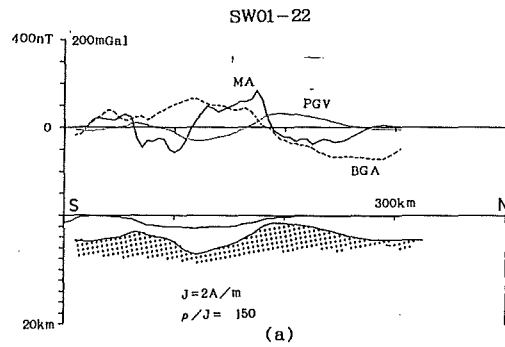


Fig.5.20 Results of magneto-gravity response analysis on section 22 of SW01.

MA:magnetic anomaly, BGA:Bouguer gravity anomaly, PGV:Pseudo-gravity for the ρ/J ratio shown in figure.

- (a): magnetic anomalies are ascribed to upper relief of magnetic layer.
- (b): magnetic anomalies are ascribed to the undulation of the lower magnetic boundary corresponding to the Moho boundary.

of Oshida's model.

5.7.2 Results on SW02

The magneto-gravity response analysis is conducted for the section-04 of SW02 (Fig.5.18) and the result is shown in Fig.5.21. The effective inclination of magnetization vector is shifted about 180° from that of the present magnetic field, besides coherence is enhanced in the wavelength longer than 80km . These features may imply that the long-wavelength anomalies can be ascribed to the magnetic lower boundary of negative density contrast. In the lower part of

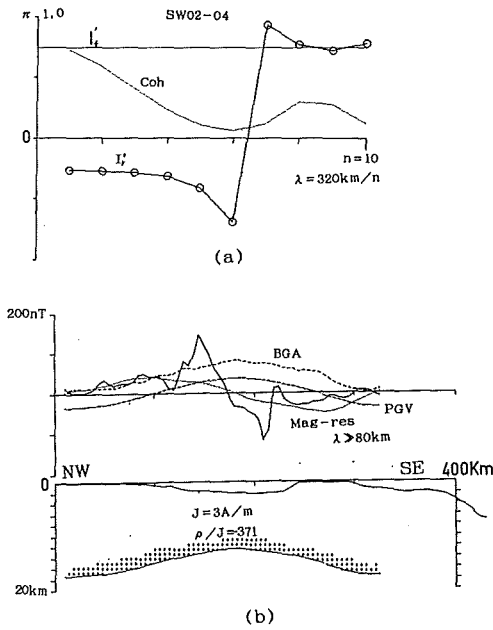


Fig.5.21 Results of magneto-gravity response analysis on section 04 of SW02.

- (a): Coherence (coh) and effective inclination (I_r') of magnetization vector against the wave-number of the magnetic anomalies.
- (b): Magnetic lower boundary (dotted pattern) derived from gravity-correlated magnetic anomaly (magnetic response) of wavelengths longer than $\lambda_c = 80\text{km}$. Magnetization direction is assumed to be present field direction.

Fig.5.21, is shown the magnetic structure derived from the magneto-gravity response filter. The correlation between the pseudo-gravity and the Bouguer gravity anomaly is 0.99 and the ρ/J_{eff} ratio becomes -371 . These results also suggest that the Moho boundary plays the role of magnetic boundary in the vicinity of this section.

The same analysis was also applied for section-42 of SW02, but the coherence is less than 0.5 even in the long-wavelength zone, besides normal magnetization assumption does not hold true as noted from the derived effective inclination considerably different from the conjugate value of

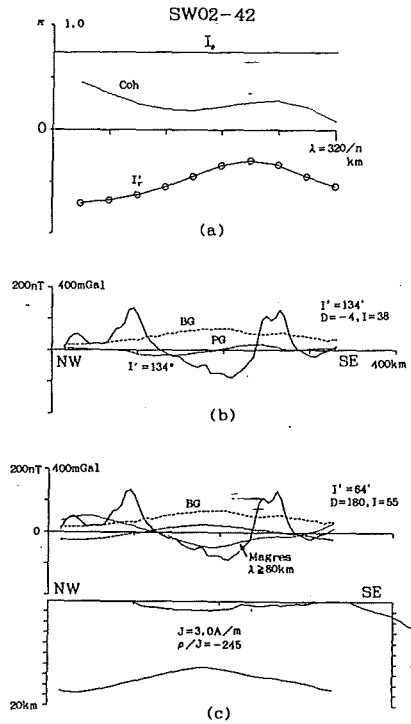


Fig.5.22 Results of magneto-gravity response analysis on section 42 of SW02.

- (a): Coherence (coh) and effective inclination (I_r') of magnetization vector against the wave-number of the magnetic anomalies.
- (b): Calculated pseudo-gravity under the present magnetic field direction ($I_r' = 134^\circ$).
- (c): Magnetic lower boundary derived from gravity-correlated magnetic anomaly (magnetic response) and the calculated pseudo-gravity for effective inclination of $I_r' = 64^\circ$, which is significantly different from present magnetic field direction.

$I_r' - 180^\circ$ (Fig.5.22). The above circumstance is reflected as the disagreement of the peak positions between the pseudo-gravity and the Bouguer gravity anomaly. This fact may arise from the situation that the Curie isotherm is upheaved above the Moho boundary beneath this section. The elevated Curie isotherm here seems to be consistent with the active hydrothermal and magmatic activities discovered in the Izena hole

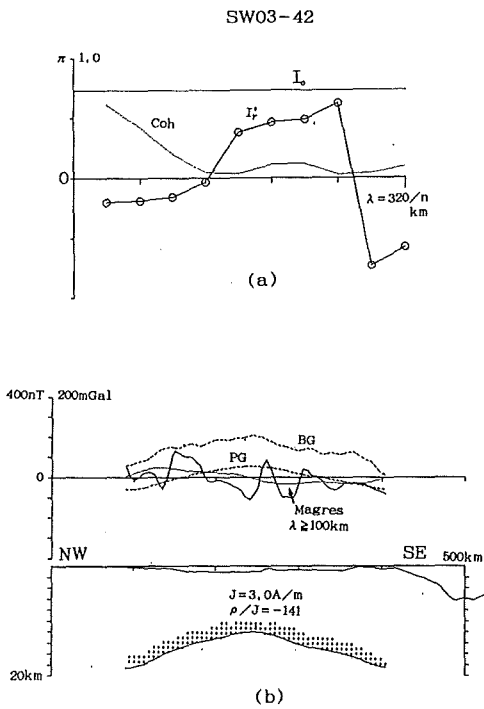


Fig.5.23 Results of magneto-gravity response analysis on section 42 of SW03.

- (a): Coherence (coh) and effective inclination (I_e') of magnetization vector against the wave-number of the magnetic anomalies.
- (b): Magnetic lower boundary derived from magnetic response components. Magnetization direction is assumed to be present field direction.

and in the Iheya knolls in the central Okinawa Trough.

5.7.3 Results on SW03

In Fig.5.23, are shown the results of magneto-gravity response function analysis on section-42 of SW03. This result indicates that the derived effective inclinations for the long-wavelength anomalies are shifted about 180° from that of the present field direction. Besides the coherences are enhanced with increasing wavelengths of the anomaly. The magnetic response of the long-wavelength component shows the positive trend in the NW side of the section (left) and the

negative one in the SE side (right). This trend is to be ascribed to the upheaved Moho boundary playing the role of the magnetic boundary as shown in the derived model. The ρ/J ratio at the Moho boundary becomes -141 for section-42. The results mentioned above may suggest that the Moho boundary is located above Curie isotherm in the northern Okinawa Trough in contrast to the case in the central Okinawa Trough.

5.8 Discussions and concluding remarks of chapter V

The present study reveals the magnetic basement structure of the Ryukyu Arc and its adjacent seas including the Tunghai shelf. Through the present study, following new aspects become apparent for each tectonic zone.

- (1) Segmented magnetic structure of the Goto and Senkaku ridge.

The magnetic basement model shows that the Tunghai shelf break is not a continuous folded zone trending in NE direction but is composed of several blocks segmented by magnetic basement depressions. Some of the above depressions can be traced toward the forearc region of the Ryukyu Arc across the Okinawa Trough in good corresponding with topographic features; i.e. Ishigaki and Miyako saddles in the south Ryukyu, the Yoron depression zone in the central Ryukyu, and the Tokara channel in the northern Ryukyu Arc. The above segmented structure is well developed in the southern Ryukyu Arc, where the outline of each segmented block shows the jigsaw fitting in considerable degree. These features seem to be consistent with the assumption of southward drift of the south Ryukyu (Konish, 1965).

- (2) Enormous bulk magnetization and relatively

low ρ/J ratio of the Goto-Senkaku ridge.

The bulk magnetization of the Goto and Senkaku ridges are much larger than that of the Quaternary volcanic zone. These features suggest the occurrence of unusual igneous activity creating the huge magnetic basement ridge of the Goto-Senkaku folded belt. The ρ/J ratio of the Goto-Senkaku folded belt is generally less than 50. Especially, no appreciable ρ/J ratio is estimated on the Senkaku ridge. The low ρ/J ratio may imply that the granitic to andesitic bodies of magnetite series compose the basement of this belt.

(3) The Yoron depression zone as the tectonic boundary

The Tokara channel has been thought to be left lateral fault segmenting the Ryukyu Arc (Kizaki, 1978). The magnetic anomaly and derived magnetic basement structure, however, indicates that the Yoron depression zone characterized by the Yoron and Okinoerabu basins is a significant boundary segmenting the Ryukyu Arc; i.e. ① the displacement of the Miocene volcanic zones occurs along this depression zone, besides the intense hydrothermal and igneous activities of the Iheya knolls seem to occur in the western extension of this depression zone, ② two linear arrangements of the old volcanic zones (R5, R6 in Fig. 5.9) terminate in the north of this depression zone, ③ the magnetic features of the Quaternary volcanic edifices change significantly at the Yoron depression zone.

In accordance with above features, the author proposes that the Yoron depression zone is an active tectonic boundary segmenting the Ryukyu Arc.

(4) Systematic change of the magnetic basement highs corresponding to the Quaternary volcanic

zone.

The magnetic basement structure along the Quaternary volcanic zone changes significantly at the Yoron depression zone and the Kerama Gap, i.e. the NE trending continuous magnetic basement high to the north of Yoron depression zone, discrete magnetic basement highs to the south of the Kerama Gap and in between no appreciable basement highs correlative to Quaternary volcanic edifices. The above along-arc variation may be attributable to the different petrological composition of the volcanic edifices; that is, andesitic volcanic activity in the northern Ryukyu Arc, acidic one in the central Ryukyu Arc and basaltic one in the southern Ryukyu Arc, respectively. The above systematic change may arise from ① the different crustal thickness which may be related to the efficiency of magma ascent and crustal anatexis, ② the different tectonic stress field between the north-central Ryukyu and the south Ryukyu; i.e. compressive stress field due to the collision of the buoyant ridge against the Ryukyu Arc in the northern and central Ryukyu Arcs, and extensional stress field prevailing in the southern Okinawa Trough, ③ the different subducting angle of the Philippine Sea plate resulting from fingering of the subducting slab as proposed by Nagamune (1987) for explanation of the different subduction angle between the north-central Ryukyu Arc and the southern Ryukyu Arc.

One or combination of the above causes may bring about the along-arc systematic change of the volcanic front. The distinct change, however, seems to be in favour of the third origin, in which case the Yoron depression zone, may correspond to the fingering zone of the subducting slab.

(5) Reversed arrangement of the Miocene volcanic zone in the central Ryukyu Arc.

In the area north of Io-Tori-sima island, the Miocene volcanic zone is situated in the inner region of the Quaternary volcanic front. But, the above lateral arrangement is reversed in the central Ryukyu Arc; i.e. the Miocene volcanic zone is located in the outer region of the Quaternary volcanic front. These features may imply that the central Ryukyu Arc has migrated south-eastward against the northern Ryukyu Arc.

(6) Accretional process and normal faulting revealed by magnetic basement structure.

Magnetic basement highs are recognized beneath the lower continental slope of the north to central Ryukyu Arcs. These magnetic basement highs extending to the Amami plateau and Daito ridge across the trench show the ongoing accretional process of the buoyant ridge. On the other hand, the magnetic basement depression is recognized over the southern part of the Nansaiyoto Trench, in consistent with seismic profiling indicative of normal faulting due to bending effect of the subducting plate.

(7) ρ/J ratio of the Moho boundary derived from magneto-gravity response analysis.

The magnetic anomaly over the Okinawa Trough shows the positive trend in the NW side and negative one in the SE side of the trough. This trend is attributable to the magnetic effect of the upheaved Moho boundary. In the southern part of the Okinawa Trough, the ρ/J ratio of the Moho boundary becomes about -150 . A similar value is also expected for the northern Okinawa Trough, whereas the reliable results showing the magnetization of the Moho boundary are not obtained for the central Okinawa Trough. The above features seem to be consistent with high

hydrothermal activity of the central Okinawa Trough, resulting in the elevation of the Curie isotherm above the Moho boundary.

CHAPTER VI. CRUSTAL STRUCTURE OF THE DAITO RIDGE AS REVEALED FROM MAGNETIC AND GRAVITY FIELD ANALYSIS

6.1 Background

The Daito ridge is about 500km length in EW direction and about 100km in width. The Kita-Daito and Minami-Daito islands are located on the western summit of the ridge. The maximum elevation amounts to about 5000m from surrounding depth of seafloor. The origin of the ridge is still in controversial, however, the crystalline schist and other acidic and plutonic rocks dredged from the ridge suggest that the ridge is not a palaeo-spreading ridge but a kind of palaeo-island arc (Shiki et al., 1979; Aoki and Ishikawa, 1985). Seismic and geological studies also indicate the continental origin of the ridge as proposed by Mizuno et al. (1975), and by Okuda et al. (1976). On the contrary, the low K content and low Sr^{87}/Sr^{86} ratio of the dredged tonalites are significantly different from the acidic rocks of the Japanese granitoids. The isotopic age of the igneous rocks shows late Cretaceous to Early Cenozoic age (Shiki et al., 1985). It is also should be pointed out that the Eocene Nummulites and large Foraminifera were sampled from many locations of the Daito ridge, which may imply shallow water-environment during Eocene age. The palaeomagnetic measurements on the sediment cores from DSDP Site 445 reveals that the Daito ridge was located in the equatorial region in Eocene age and then migrated northward by about 2000km (Kino-

shita, 1980).

To clarify the magnetization of the Daito ridge is thought to be a significant subject for elucidation of the origin of the associated conspicuous magnetic anomalies and tectonic framework of the Philippine Sea Plate. A magneto-gravity response analysis seems to be applicable to determine the inclination of magnetization vector of the Daito ridge because of its EW elongation of the uplift.

6.2 Data description

The data used in this study is based on the continental shelf surveys conducted by JHD in 1983 and 1984. Some of the results of above surveys were reported by Kasuga et al. (1986). The MGD77 files of above survey data are now supplied from JODC on request. The MGD77 data were projected on a X-Y plane based on Mercator projection and then grid data of 10km mesh intervals in X and Y direction were calculated by the iteration method of the 2nd order polynomial fitting.

In Fig.6.1, are shown the machine contoured maps of bathymetry, total intensity magnetic anomaly and free-air gravity anomaly. A positive correlation between bathymetry and free-air gravity is recognized. The positive free-air gravity anomaly amounting more than 100mgal overlies the summit area of the ridge. On the other hand, broad negative anomalies less than -40 mgal appear over the Minami-Daito basin. Although the depth of the Kita-Daito basin is nearly the same as that of the Minami-Daito basin, free-air anomaly of the Kita-Daito basin is characterized by the zero level of the free-air gravity anomaly.

The EW trending high amplitude magnetic

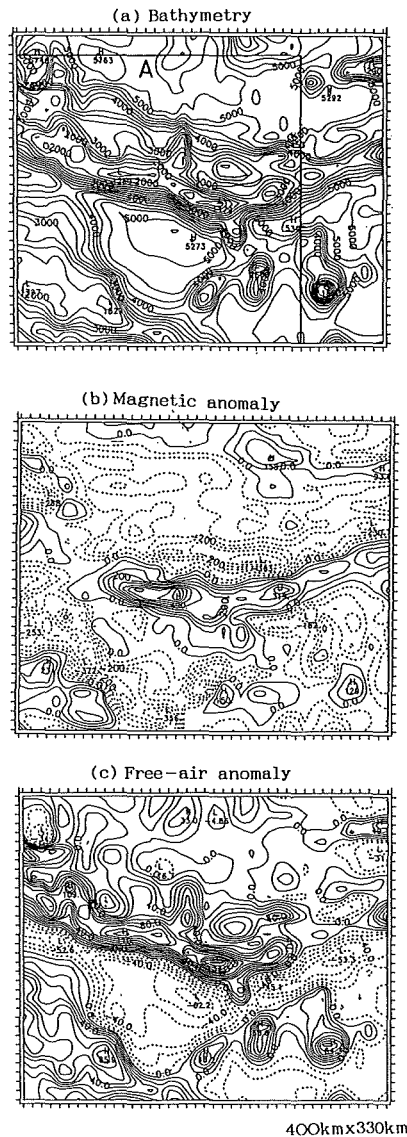


Fig.6.1 Bathymetry(a), total intensity magnetic anomaly(b) and free-air gravity anomaly(c) of the Daito ridge. Contour intervals are 250 m, 50nT and 10mgal respectively. The southwestern corner of the map is $N24^{\circ}$, $E131^{\circ}$, and the coverage is 400km in the EW and 330km in the NS direction. The area A ($310\text{km} \times 310\text{km}$) enclosed by thick lines was analysed as shown in Figs.6.3 and 6.6.

anomaly larger than 700nT (peak to peak of the anomaly) occurs in good correspondence with the topographic uplift of the ridge. Such a high ampli-

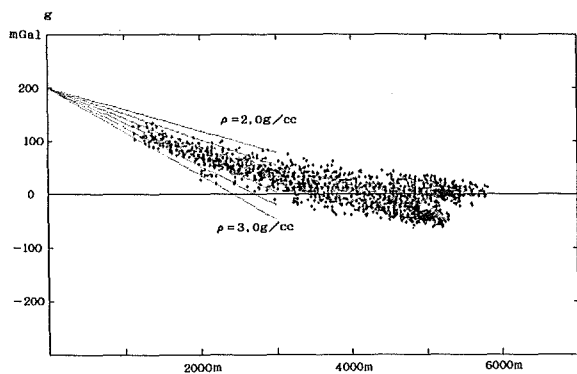


Fig. 6.2 Relation between depth and free-air gravity anomaly of the Daito ridge. The regressive gradient corresponds to 2.18g/cm^3 .

tude magnetic anomaly is also recognized in correspondence with the Amami plateau (Kasuga et al., 1992). Elucidation of the origin of such high amplitude anomalies associated with continental crust are thought to be significant subject for understanding the structure of these continental crust.

Prior to the calculation of Bouguer corrections, free-air anomaly values were plotted against water depth as shown in Fig. 6.2 in order to estimate a mean density contrast of the uplift in conventional way. The regressive line shown in Fig. 6.2 shows a probable mean density contrast of the ridge to be 2.18 g/cm^3 , which is significantly less than the usual value of 2.67 g/cm^3 . This may arise from two causes, one is relatively low density contrast of thick coral materials covering the ridge, the other is isostatic compensation by the thickening of the continental crust. Gravity anomalies caused by topographic relief (terrain effect) were calculated by Parker's inversion technique under the assumed density of 2.18g/cm^3 and subtracted from the observed free-air gravity anomalies as shown in Fig. 6.3. The terrain corrected gravity anomaly reveals

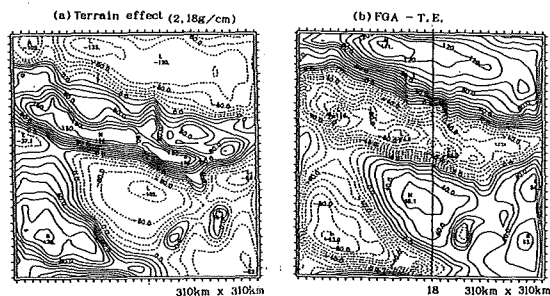


Fig. 6.3 Calculated gravity field (a) by the topography of the Daito ridge and reduced gravity anomaly (b) obtained by removal of the terrain effect from the observed free-air gravity anomaly.

the concave-shaped features over the ridge, which may be correlated to isostasy of the Daito ridge. Besides, the enhanced Bouguer gravity anomaly of the Kita-Daito basin manifests the upheaved structure or denser contrast of the Moho boundary relative to that beneath the Minami-Daito basin. Bouguer gravity anomalies associated with seamounts show two type of anomalies, one is accompanied by negative Bouguer anomalies indicative of isostasy, the other is featureless gravity anomalies suggesting the elastic sustentation of the seamount's weight without root structure. These features are significant for consideration of the structure of the seamounts.

6.3 Gravity-topography response analysis

To estimate the degree of isostatic compensation of the uplift, the response function between observed free-air gravity anomaly and topographic relief was calculated by Eq. (65) to obtain the wavelength dependence of the density contrast of the ridge. If the ridge is not accompanied with isostatic compensation, the derived density contrast is to be equal to the real density contrast of the ridge. On the contrary, when the ridge is subjected to isostatic compensation, the derived

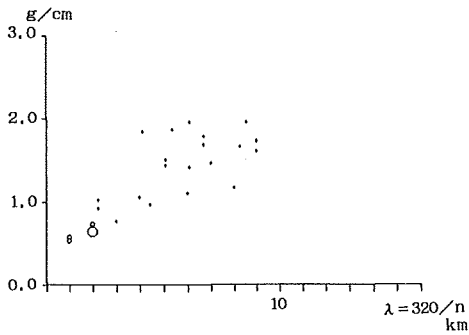


Fig.6.4 Calculated density contrasts obtained by gravity-topography response analysis against the wavelengths of free-air gravity anomaly.

density contrast may be reduced in accordance with degree of isostatic compensation. The calculated result shown in Fig.6.4 shows considerably low density contrast for the wavelengths longer than 80km. This feature implies mature stage of the isostasy of the Daito ridge in consistent with crustal structural model derived by Segawa (1976).

6.4 Magneto-gravity response analysis

The Daito ridge has a considerably strong magnetization as inferred from associated high amplitude magnetic anomalies. To derive magnetization direction is a significant subject for consideration of palaeomagnetic constrain and the magnetic source of the ridge. The response analysis between magnetic and free-air gravity anomalies shows magnetization direction corresponding to the uplift of the ridge, on the other hand, that between magnetic and Bouguer gravity anomalies gives the magnetization direction of the deep-seated source producing Bouguer gravity anomalies. In Fig.6.5a, is shown the effective magnetization inclination derived from response function between magnetic and free-air gravity anomalies. This figure indicates normal

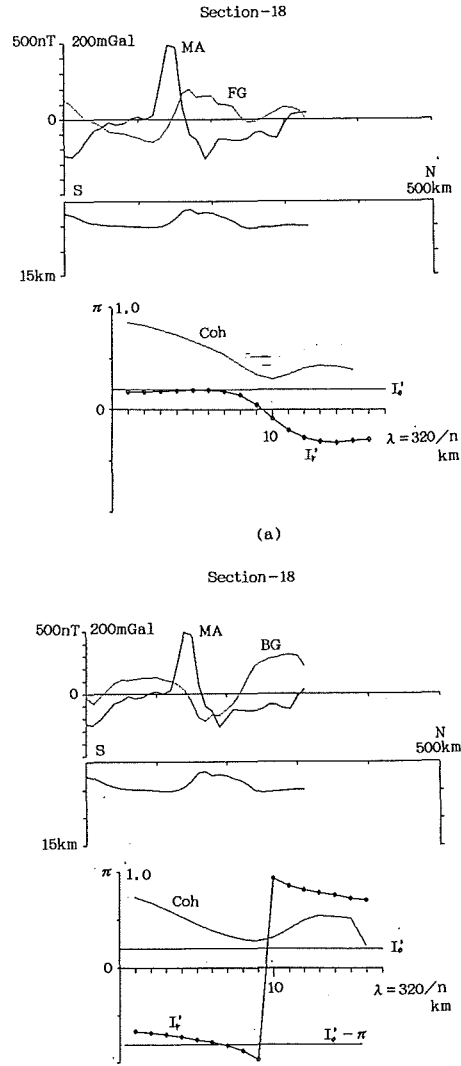


Fig.6.5 Results of magneto-gravity response analysis on the Daito ridge.

Upper column: the cross-sectional data along section-18 shown in Fig.6.3.

Lower column: coherence and effective inclination against the wave number of the gravity field.

MA: magnetic anomaly, FG: free-air anomaly, BG: Bouguer anomaly.

(a): response between magnetic anomaly and free-air gravity anomaly.

(b): response between magnetic anomaly and Bouguer gravity anomaly.

magnetization direction in the wavelengths longer than 45km, contrary to the shallow inclination suggested by palaeomagnetic measurement of DSDP sediment cores (Kinoshita, 1980). Effective inclinations obtained from magnetic and Bouguer gravity anomalies are shifted about 180° from the effective inclination of the present field as shown in Fig.6.5(b), which indicates a normal magnetization direction in the wavelengths longer than 45km in consistent with Fig.6.5(a). These aspects imply that the magnetic anomalies of the Daito ridge are originated from induced magnetization or viscous remanent magnetization instead of thermal remanent magnetization. The required large magnetization intensity as indicated in following section may be in favour of the viscous remanent magnetization of the crust.

6.5 Three-dimensional gravity and magnetic basements of the Daito ridge

In the wavelengths longer than about 80km, coherences between magnetic and Bouguer gravity anomalies become larger than 0.5 as seen in Fig.6.5(b). The above features suggest that Bouguer gravity anomalies whose wavelengths longer than 80km are well correlated to long-wavelength magnetic anomalies. Based on these results, the lower density boundary corresponding to the Moho boundary was estimated from Bouguer gravity anomalies of wavelengths longer than 80km under two-layer assumption as illustrated in Fig.6.6(a). The magnetic lower boundary was also calculated from magnetic anomalies with wavelengths longer than 80km as shown in Fig.6.6(b). A good correspondence between the above two boundaries is recognized; depressed beneath the eastern part of the Daito ridge and elevated beneath the Kita- and Minami-Daito

basins. However no appreciable correlation is seen over the areas marked by A to C. This may manifest the lateral variation of the magnetization of the lower crust. Fig.6.7 shows a NS transection of the derived lower boundaries. The

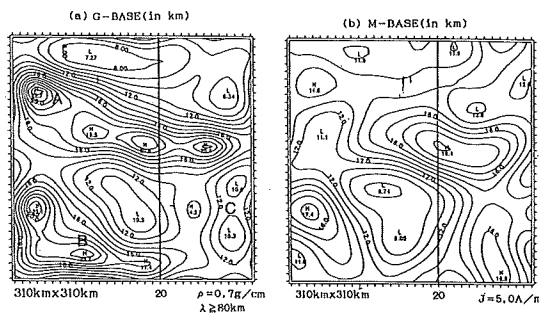


Fig.6.6 Relief of the Moho boundary estimated from gravity and magnetic anomalies of the Daito ridge. Unit in km below sea level. No appreciable correlation between magnetic and gravity basement is recognized on the zones of A, B, and C.

- (a): Lower density boundary derived from Bouguer gravity anomalies. Assumed density contrast is 0.7g/cm^3 .
- (b): Lower magnetic boundary derived from magnetic anomalies. Magnetization contrast is 5.0A/m and magnetization direction is assumed to coincide with the present field direction.

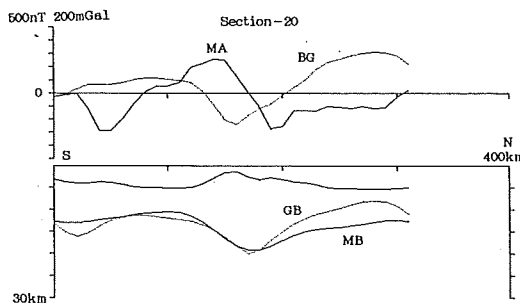


Fig.6.7 N-S cross-section at x-coordinate of 20 of Fig.6.6.

MA: magnetic anomaly, BG: Bouguer gravity anomaly, MB: magnetic lower boundary, GB: the lower density boundary.

good agreement between the above lower boundaries is seen beneath the area from the Minami Daito basin to the Daito ridge. On the other hand, the lower density boundary is much elevated above the magnetic boundary beneath the Kita-Daito basin, reflecting the enhanced Bouguer gravity anomalies over the Kita-Daito basin (Fig. 6.3(b)). This disagreement may be solved by assigning relatively high density contrast or relatively weak magnetization intensity contrast at the lower boundary beneath the Minami-Daito basin.

6.6 Concluding remarks

The magneto-gravity response analysis on the Daito ridge reveals that the effective inclination of magnetization vector coincides with that of the present field direction in the wavelengths longer than 45km, although the palaeomagnetic measurements on DSDP sediment cores shows shallow magnetization inclination suggesting the equatorial region at the formative period. This aspect implies that the viscous remanent magnetization of the crust is the main cause of the observed magnetic anomalies in place of remanent one. Besides, the crust of the Daito ridge is thought to be highly magnetic. The origin of the magnetic crust is not clarified at present, however, seems to be significant features related to the formative process of the continental crust of the Daito ridge. The magneto-gravity response analysis between magnetic and free-air gravity anomalies (Fig. 6.5(a)) also suggests that the upper crust of the Daito ridge is also magnetic. The magnetic upper crust, as inferred from the above results, may be attributable to granitic rocks of magnetite series. The rapid subsidence of the Daito ridge may also result from the

magnetic crust of probably high density contrast relative to usual continental crust.

CHAPTER VII. DISCUSSIONS AND CONCLUSIONS

(1) Inversion methods to derive a magnetic basement relief from observed magnetic anomalies are described. Some of the methods are newly developed by the author with numerical examples. Plausibility and accuracy of three-dimensional inversion method based on iteration algorithm, which was developed by using Oldenburg's (1974) two-dimensional formula, are confirmed to be applicable to areal grid data.

Synthetic analysis methods of magnetic and gravity anomalies are proposed to obtain more reliable structural models. This method incorporates a new idea of magneto-gravity response function to determine magnetization direction of the source body and of magneto-gravity response filter to extract the magnetic anomalies correlative to the gravity anomalies. In addition, the correlation analyses in space domain are also described to determine ρ/J ratio and magnetization intensity of the source body. These methods should enable us to construct a model consistent with magnetic and gravity anomalies.

(2) Magnetic anomaly profiles covering the Japanese islands are prepared based on airborne magnetic surveys conducted by JHD. Using the above magnetic profiles and the Bouguer gravity anomaly profiles, the magnetic structural models consistent with gravity anomalies are constructed with respect to several transections of Honsyu Arc and a single transection of Kurile Arc of southeastern part of Hokkaido. By this analysis a good correspondence between the magnetic basement and seismic velocity structure is shown

for the case of the northeast and central Honsyu. The former corresponds to the Conrad boundary in the crust and the latter to the seismic velocity structure having seismic velocity of 6.0 to 6.3 km/s. The Conrad boundary beneath the Kurile Arc in the southeast Hokkaido seems magnetic. The magnetic anomaly over the inner region of southwest Honsyu is to be attributable to the magnetic body of low ρ/J ratio, which may correspond to granitic rocks of magnetite series. A lithological model of northeast Honsyu (Takahashi, 1978) derived from xenolith samples is consistent with the present magnetic models of northeast Honsyu. The relatively large magnetization intensity of the magnetic source with low ρ/J ratio beneath the inner part of southwest Honsyu suggests the enhanced magnetic susceptibility. Besides, the viscous remanent magnetization may also be responsible for the observed large amplitude magnetic anomaly.

(3) Grid data files of topography, total intensity magnetic anomaly, free-air and Bouguer gravity anomalies are calculated and mapped for the Izu-Ogasawara Arc and Ryukyu Arc based on areal survey data released from JODC. The pseudo-gravity and high-pass filtered gravity maps are also compiled for correlation analysis in space domain. Magnetic basement models of the Izu-Ogasawara and Ryukyu Arcs are constructed based on the calculated grid data for quantitative interpretation of the magnetic anomalies. Bulk magnetizations, vertical integration of magnetization intensity, are estimated for the magnetic bodies at the volcanic front and for the representative magnetic basement blocks. This estimation indicates that the bulk magnetization of the volcanic front of the Izu-Ogasawara Arc is larger than that of the Ryukyu Arc by about 30%, which

may have resulted from different productivity of magnetic materials at the volcanic front. The southern volcanic front of the Izu-Ogasawara Arc shows the maximum productivity, which is consistent with the huge size of the volcanic edifices of the arc.

In addition, the derived magnetic basement models provide important information for understanding the geological structures and related tectonics, as discussed in each chapter.

(4) The Magneto-gravity response analyses on the Daito ridge reveal that the Daito ridge is magnetized in the present field direction contrary to the shallow inclination of magnetization suggested by DSDP sediment cores. Besides, the lower magnetic boundary derived from long-wavelength magnetic anomalies shows a close resemblance to the estimated undulation of the Moho boundary. This resemblance implies that the lower crust of the Daito ridge is polarized in the present field direction. The origin of high magnetization intensity in the present field direction is reasonably ascribed to the enhanced magnetic susceptibility and/or viscous remanent magnetization of the magnetic source of the Daito ridge.

(5) The ρ/J ratio at the Moho boundary is estimated for the Izu-Ogasawara Arc by the correlation analysis between the long-wavelength Bouguer gravity anomaly and pseudo-gravity anomaly. This result discloses the edge effect due to upheaval of the Moho boundary over the western margin of the northern part of the Izu-Ogasawara Arc. On the contrary, appreciable ρ/J ratio zone is restricted beneath the Ogasawara Trough in the southern arc. These features imply that the magnetization of the lower crust and the Curie isotherm depth are different between the

northern and southern arc of the Izu-Ogasawara Arc. Magneto-gravity response analysis in the Okinawa Trough also reveals the long-wavelength magnetic anomalies related with convex features of the Bouguer gravity anomalies in the southern and northern part of the trough. The magnetic anomalies corresponding to the undulation of the Moho boundary may imply that it is elevated above Curie point isotherm due to thin continental crust of the regions concerned.

Throughout the present study, the existence of the magnetic source having low ρ/J ratio has become apparent. Two types of low ρ/J ratio are confirmed, one is granitic to andesitic rock of magnetite series, the other is serpentinite suite of low density contrast. Typical cases of the latter are found in the Kamuikotan belt and the Honsyu-Kurile linear magnetic anomaly, south offing of the southeastern part of Hokkaido. The former source is recognized in the inner part of southwest Honsyu Arc, in the forearc region of the northern Izu-Ogasawara Arc, and along the Tunghai shelf break to the west of the Ryukyu Arc. Magnetic sources of the Kyusyu-Palau ridge may also be classified into low ρ/J ratio, as shown by the magnetic and Bouguer gravity anomaly maps compiled by Kasuga et al. (1992).

Ishihara (1979) reported that the volume of magnetite series increases toward the marginal seaside and he ascribed them to the tensile tectonic environment, which allowed the deeply-originating magma to ascend without crustal contamination. This may have resulted in the formation of granitoids rich in magnetite. In addition, the present study has revealed low ρ/J ratio sources in the forearc region of the northern part of the Izu-Ogasawara Arc. Taking into

account the above distribution, another origin of the low ρ/J source may be in the forearc magnetism related to the initial stage of subduction. The deeply-generated magma may also ascend without contamination of the crust under the above condition. This situation may form the granitic to andesitic rocks of magnetite series as seen in the Kyusyu-Palau ridge and the forearc region of the Izu-Ogasawara Arc. In addition to the above situation, a hydrous column in the forearc region, as suggested by Tatsumi (1989), may also keep the crust in oxidation state, resulting in the formation of titanomagnetites rich in Fe_3O_4 content.

Moreover, the magneto-gravity response analysis (Fig. 6.5(a)) on the Daito ridge suggests the existence of the magnetic source of low density contrast within the crust. Tonalites recovered from the Daito ridge are characterized by low $\text{Sr}^{87}/\text{Sr}^{86}$ ratio, which is in favour of the magma without crustal contamination. Accretion of the palaeo-island arc such as the Daito ridge against the palaeo-Asian continental margin may also form the magnetic zone with low ρ/J ratio source. In general, the radiometric age and magnetite content of the granitic rock decreases toward trench side. This trend is, however, reversed in the northeast Japan (Kinoshita and Ito, 1988), that is, granitic rocks of magnetite series in northeast Japan show a reciprocal distribution in regard to radiometric age and magnetite content. However, this reciprocal pattern may be attributable to the accretion of the palaeo-island arc with low ρ/J ratio such as the Daito ridge. The upward magnetization vector calculated from the the short-wavelength magnetic anomaly components of the Sanriku-Isikari linear anomaly (SILA) may also favours this inter-

pretation.

The present study also suggests the significant contribution of the enhanced induced magnetization of the deep-seated magnetic sources to the observed magnetic anomalies. The magnetic susceptibility of the low ρ/J ratio sources, calculated from the synthetic analysis of magnetic and gravity anomalies, exceeds the observed mean susceptibility value of the granitic rocks of magnetite series as shown in Table 3.1. Such enhancement of susceptibility may be attributable to the enhanced initial susceptibility and to the contribution of the viscous remanent magnetization due to increasing temperature in the deep crust (Shimizu, 1960; Wasilewski et al., 1979). These magnetizations are related to in-situ fugacity (O_2)-temperature equilibrium condition in the crust. Further advance in the field of experimental study on the rock magnetism concerning the enhanced magnetic susceptibility may be required for the construction of the more convincing magnetic structural model.

Acknowledgements

The author would like to express his hearty thanks to Prof. Jiro Segawa for his valuable suggestions and continuing encouragements during the course of this study. His useful comments

and guidance on the manuscript are indispensable to the success of this study. He also acknowledges Dr. Motohiko Kato for the useful discussions on the subject described in Chapter II of this study. He is also much indebted to colleagues of the Hydrographic Department, especially to Messrs. Hisaho Nakagawa, Ryoichi Horii, Koichi Kumagawa, Yoshiharu Nagaya, and Tetsuhiro Yabuki, who helped the author in the magnetic surveys and desk works for mapping data. He also pays his respects to the staffs of the continental shelf surveys office of JHD who took part in marine surveys and compilation works for their continuous effort and enthusiasm. He is also grateful to the personnel of JODC who kindly provided MGD77 data for the present study. The author also pays his respect to the captain and crews of YS-11 and the staffs of the Haneda Air Base of the third Regional Head Quarter for the cooperation in the case of the airborne magnetic surveys. He finally expresses his gratitude to Dr. Yoshio Iwabuchi, Chief Hydrographer of JHD, for allowing the author to use the original survey data of JHD for the present study.

This paper is the major part of the author's dissertation submitted to the University of Tokyo.

和 文 要 旨

日本列島は千島弧、本州弧、琉球弧、伊豆-小笠原弧から構成され、それぞれの島弧はプレートの沈み込み境界である海溝を伴い、活発な地震、火山、地熱活動の場となっている。これらの島弧は厚い大陸性地殻の存在で特徴づけられる。大東海嶺もまた、厚い大陸性地殻の存在が知られており、古島弧と考えられている。プレートテクトニクスにより、これらの島弧の起源について、グローバルな視点からの理解が得られるようになったが、

それぞれの島弧の地殻構造の特徴やその起源については、まだ十分に解明されていない。このような島弧の地殻構造を明らかにすることは、島弧の地質構造やテクトニクスの理解だけでなく、地殻の岩石学的モデルの構築、地殻深部の磁気的性質の解明、地殻深部の物理的、化学的条件等の解明にとっても重要な課題である。

近年、日本列島とその周辺島弧に関する地形・地磁気・重力異常に関するデータは、水路部をはじめ、大学・研究機関などの調査成果が日本海洋データセンターの

データベースに集約され、地球物理学的研究への利用が図られている。これにより、日本列島とその周辺海域の地形や地磁気・重力異常等の図がまとめられ、それぞれの特徴が明らかにされつつある。しかし、今後は、このようなデータを総合的に解析し、それぞれの異種間データに全体として調和的な地殻構造を求めることが重要な課題と考えられる。

本論文は、このような地形・地磁気・重力異常データを総合的に解析する方法を提示するとともに、本方法を、島弧の地殻構造の解析に適用することにより求められた結果を述べたものである。

本論文は、まえがき（第1章）に引続き、第2章：本論文で用いた磁気・重力異常の総合的解析法、第3章：航空磁気測量のプロファイルデータの解析結果にもとづく千島弧、本州弧、の地殻構造、第4章：磁気・重力異常による伊豆-小笠原弧の地殻構造、第5章：磁気・重力異常による琉球弧とその周辺海域の地殻構造、第6章：磁気・重力異常による大東海嶺の地殻構造、第7章：結論の全7章から構成される。

第2章では、フーリエ級数法にもとづく2次元磁気基盤構造解析法、フーリエ変換の繰返し法(Parker(1972), Oldenburg(1974))による3次元磁気基盤構造解析法、磁・重力応答関数法による磁化方向の決定法、磁気異常から重力と相関のある磁気異常を抽出するための磁・重力応答フィルター、について具体的な数値実験の例を示してそれらの適用方法について述べた。さらに、このようなインバージョン法により求められた磁気基盤構造、擬重力異常と、地形・重力異常との空間領域での相関解析により、解析対象の磁化強度、 ρ/J 比をもとめるアルゴリズムを確立した。

第3章の千島弧、本州弧の解析では、北海道北部の神居古潭帯、北海道南東岸沖の釧路-根室磁気異常帯(KNLA)、東北日本の三陸-石狩磁気異常帯(SILA)、中部日本の負異常帯、西南日本の日本海側の東西にのびる正異常帯(SWHLA)の各断面について、磁気基盤構造を求めた。SILAの北緯41度付近のプロファイルに対応する磁気基盤モデルは、コンラッド面の起伏とほぼ一致する結果が得られた。また、KNLAの磁気基盤構造も、地殻

内部の密度境界に対応しており、これらの結果から、下部地殻が磁性の強い岩体で構成されていることが推定される。中部日本の負異常帯に対応する磁気基盤の起伏もまた、爆破地震により得られた地殻構造モデルと良い対応を示すが、磁化強度は、前記2例に比べ約半分程度の値となる。このような結果は沈み込むプレートの性質の違いを反映しているものと推察される。一方、神居古潭帯やSWHLAについては、磁気異常の振幅は300nT以上に及び、その原因岩体も大規模な構造を有すると推定されるが、ブーゲー重力異常は平坦である。以上の結果から、大陸性地殻起源の磁気異常の主要な原因岩体としては、地殻内部の密度境界に対応するものと(SILA, KNLA)上部地殻での低密度、高磁気モーメント(低 ρ/J 比)の岩体によるものに区分できることがわかった。後者は、磁鉄鉱系の花崗岩もしくは、蛇紋岩がその原因と思われる。

第4章では、伊豆-小笠原弧の磁気基盤モデルを作成し、同島弧の地殻構造の特徴を求めた。それによると、同島弧は婦孺岩構造線を境に南北でその様相が異なる。北部では、①ほぼ南北につらなる西七島海嶺の磁気基盤構造、②火山フロント付近の隆起部とその背弧側での磁気基盤の落込み、③前弧域における大規模なブロック状の磁気基盤隆起帯とさらにその外側の南北に延びる磁気基盤隆起帯、などが特徴的である。前弧域の磁性岩体の ρ/J 比は負の値を示すものがあり、逆磁化か周囲よりも軽い岩体で構成されている可能性がある。西七島海嶺の磁気異常は、地形との相関からほぼ現在の磁場方向で説明できると推定される。同海嶺の磁気基盤の隆起部は現在の火山フロントに併走しており、その磁性岩体の規模も火山フロントのそれにほぼ等しい。このことから、西七島海嶺はかつての伊豆弧の火山フロントであった可能性が考えられる。

一方、婦孺岩構造線以南では北部の①や③に対応する構造は顕著ではないが、火山フロントに沿った磁気基盤の規模は北部の約2.3倍と大きい。また、小笠原弧に対応する磁気基盤の隆起部は、地形との相関から東向き磁化を示すグループ(父島)と現在の磁場方向の磁化を示すグループ(母島)とに区分することが可能である。この

ような結果は東向き磁化を示す小笠原弧の古地磁気学的研究結果と矛盾するが、熱残留磁化と誘導磁化の違いを反映している可能性も考えられる。

第5章では、琉球弧とその周辺海域の磁気基盤モデルを作成し、地質構造との対比からそれを7つの構造区に区分し、それぞれの磁気基盤の特徴を求めた。

それによると、東海陸棚外縁部に沿って大規模な磁性岩体がブロック状に配列していること、琉球弧の火山フロントにそって、北部、中部、南部で磁気基盤構造が系統的に変化していること、中部では、中新世の磁気基盤構造に対比できる幅60km、長さ250kmにも及ぶ磁気基盤隆起帯が存在することが明らかとなった。東海陸棚外縁部の磁気基盤の ρ/J 比は50-70程度であり、低 ρ/J 比を示す。また、中部にみられる磁気基盤隆起帯は、現在の火山フロントに対し海溝側に位置し、北部での新旧火山帯の位置関係とは逆転している。このことから、本隆起帯の南東側への相対的変移があったことが推察される。大陸斜面から海側にかけての磁気基盤構造によると、中部から北部にかけて奄美海台、大東海嶺の延長部が、琉球弧に付加しており、また、中部では、海溝軸付近の海洋地殻が断層により落込んでいる様子が確かめられた。

第6章では、大東海嶺の磁気異常がほぼ現在の磁場方向で説明できること、また、長波長成分の異常からもとめた、磁化層とモホ面深度との起伏が比較的良好一致することを示した。この結果、大東海嶺の磁気異常は、誘導磁化もしくは、粘性残留磁化によるものであることが推論される。また、磁化層の原因岩体としては、磁鉄鉱系の花崗岩と推察される。

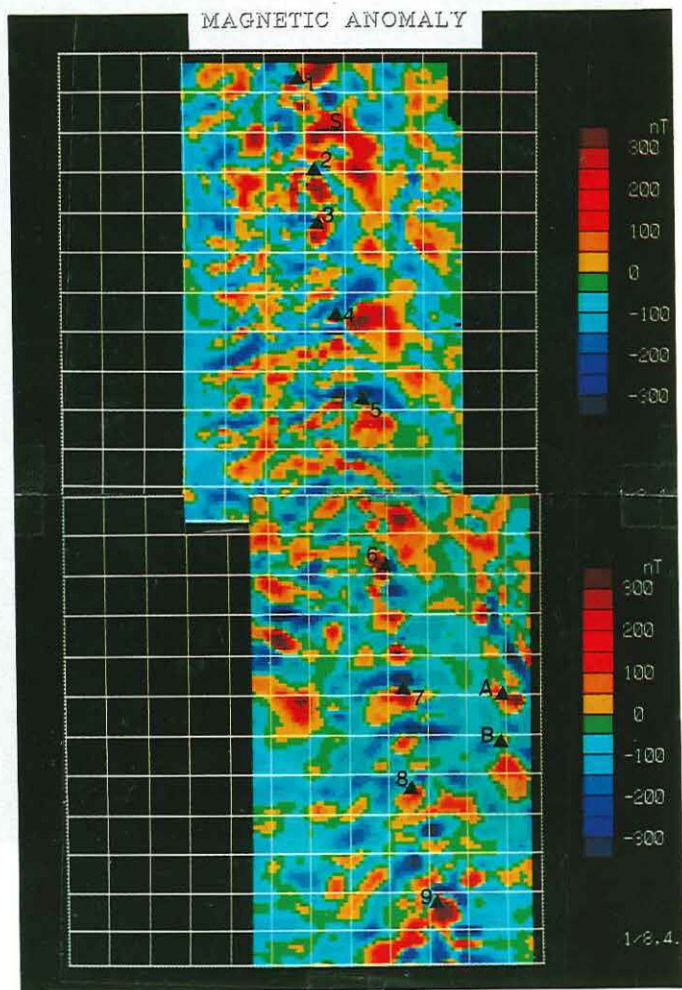
今回の研究により、地形、地磁気、重力異常、から求めた日本列島とその周辺島弧の地殻構造の特徴がより明確に捉えられた。特に、低 ρ/J 比の磁性岩体の分布が、西南日本の内帯、伊豆-小笠原弧の前弧域、東海陸棚外縁隆起帯、などに存在することが推察され、また、大東海嶺の地殻も低 ρ/J 比の岩体から構成されることがわかった。このような低 ρ/J 比の岩体は、磁鉄鉱系の花崗岩に対応するものと考えられる。従来の岩石磁気学的研究では、このような、磁鉄鉱系の花崗岩は島弧-海溝系

での縁海側に形成されると考えられていたが、今回の研究は、前弧域でもこのような磁鉄鉱系の岩体が形成されることを示唆するものである。前弧域は沈み込むプレートからの水が供給される場所でもあり、このような脱水過程が前弧域での磁鉄鉱系花崗岩の形成と関連する可能性も考えられる。

伊豆-小笠原弧、琉球弧の磁・重力の解析結果からは、モホ面の起伏が長波長成分の磁気・重力異常の原因と推定される。特に、伊豆小笠原弧北部の四国海盆に面した境界付近や、沖縄トラフ南部にこのような特徴が顕著である。このことは、それぞれの部分では、地殻の厚さが比較的薄く、そのためモホ面がキューリー等温面深度で浅に位置するためと推察される。今回の研究により、本州弧・千島弧での代表的な磁気異常が正磁化のモデルにより説明できることから、地殻深部の磁性岩体の磁化は熱残留磁化よりも、むしろ誘導磁化や粘性残留磁化に起因すると考えられる。しかし、このような機構で、磁気異常を説明するには、温度の影響による磁化率や粘性残留磁化の上昇機構を考える必要がある。

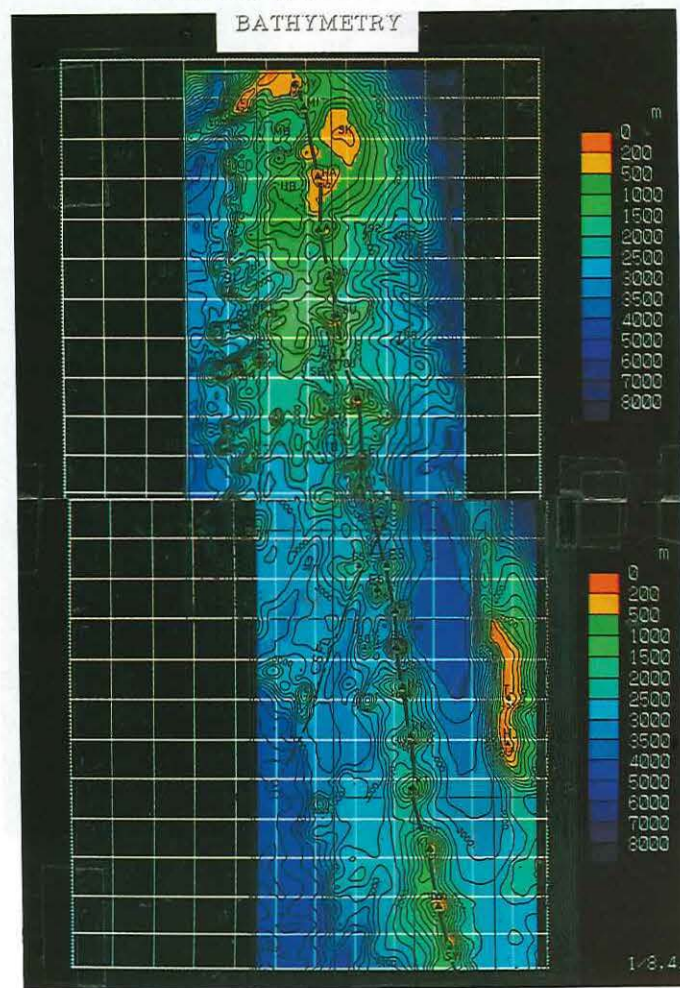
Annex-1: Colour image maps of the geophysical data on the Izu-Ogasawara (Bonin) Arc. Grid interval is 50km.

(b) Total intensity magnetic anomaly (IGRF1985).

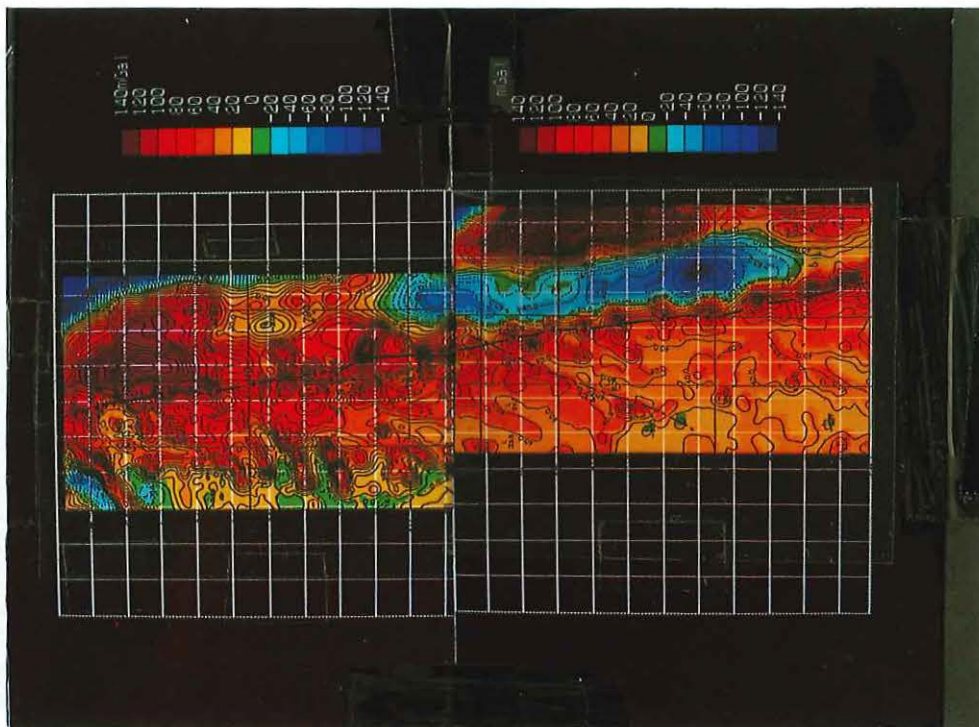
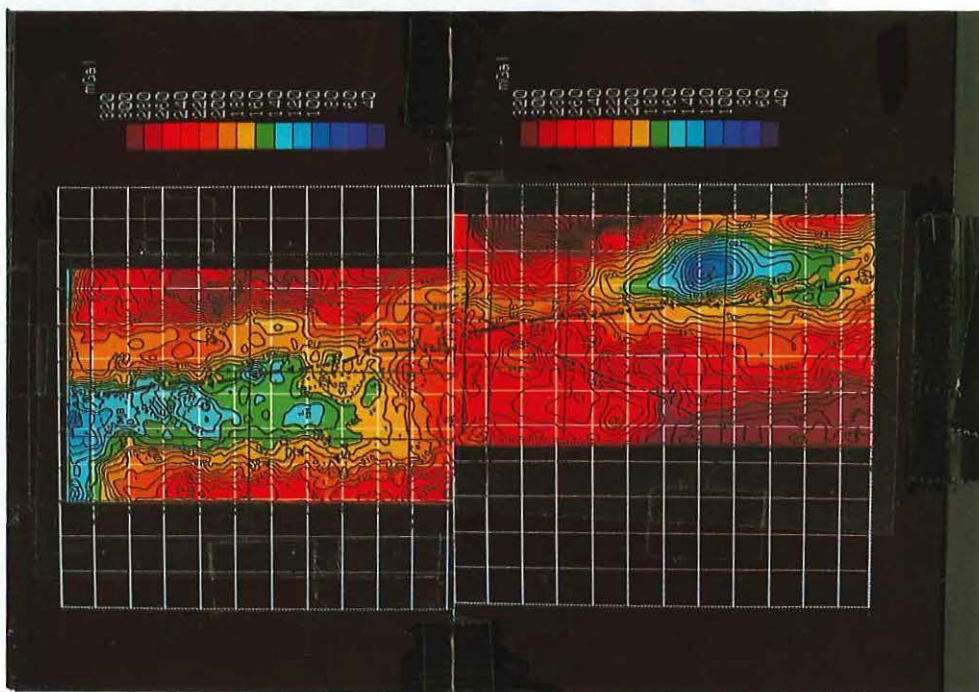


(a) Bathymetry of the Izu-Ogasawara Arc.

- 1: Miyake sima, 2: Hatizyo sima,
 3: Aogasima, 4: Tori sima,
 5: Nisino sima, 6: Kaitoku Smt., 7: Io sima.

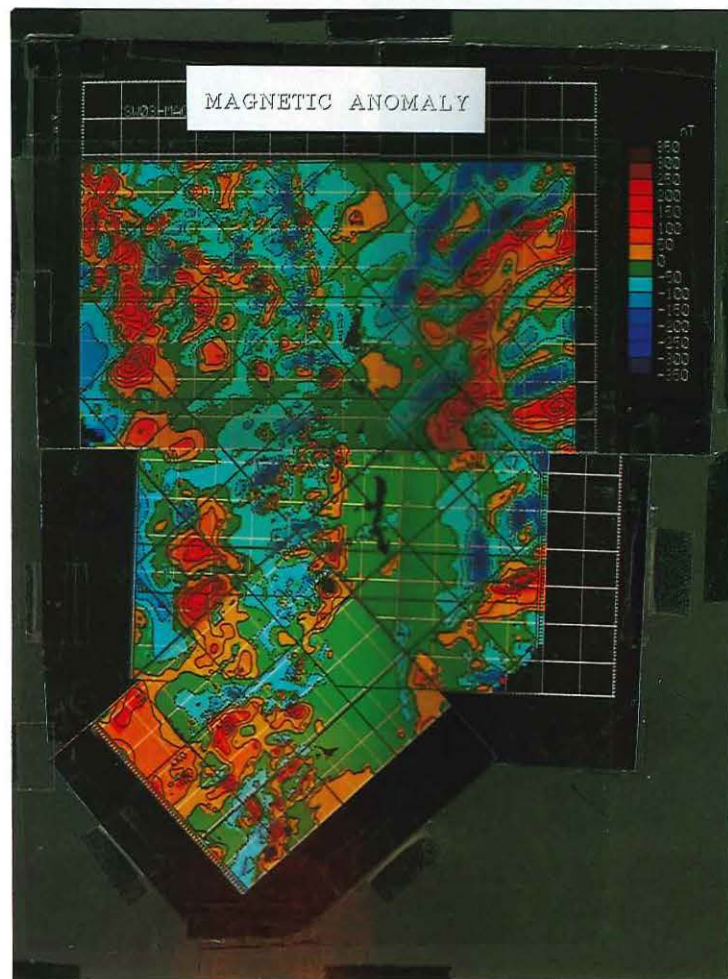


(c) Free-air gravity anomaly.

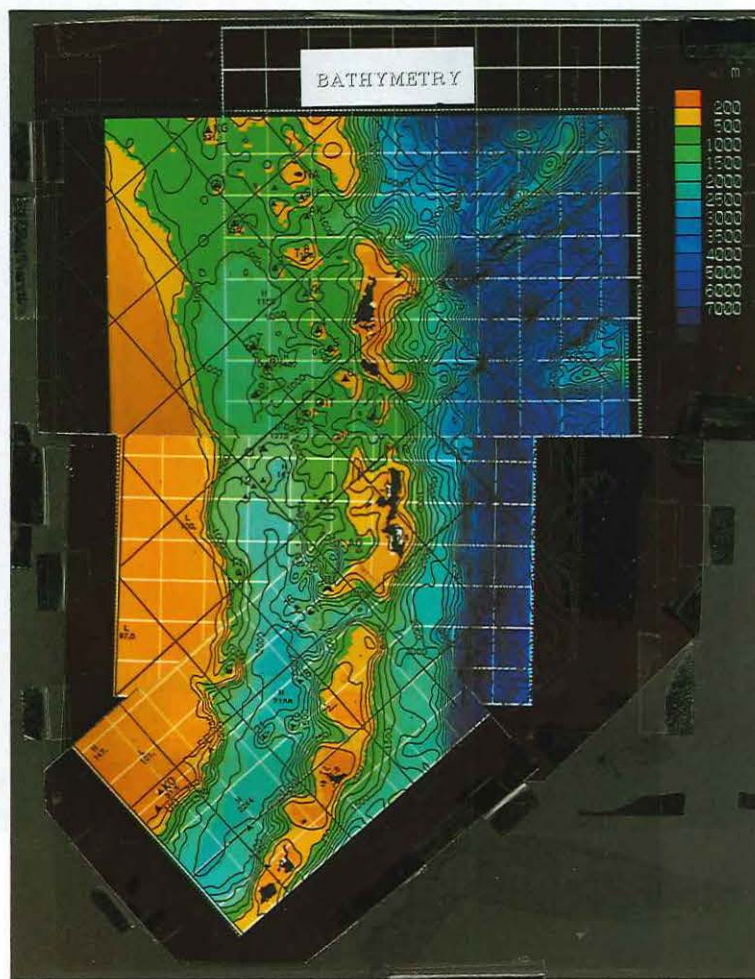
(d) Bouguer gravity anomaly ($\rho=2.67\text{g/cm}^3$)

Annex-2 Colour image maps of the geophysical data on/around Nansei-Syoto. Grid interval is 50km.

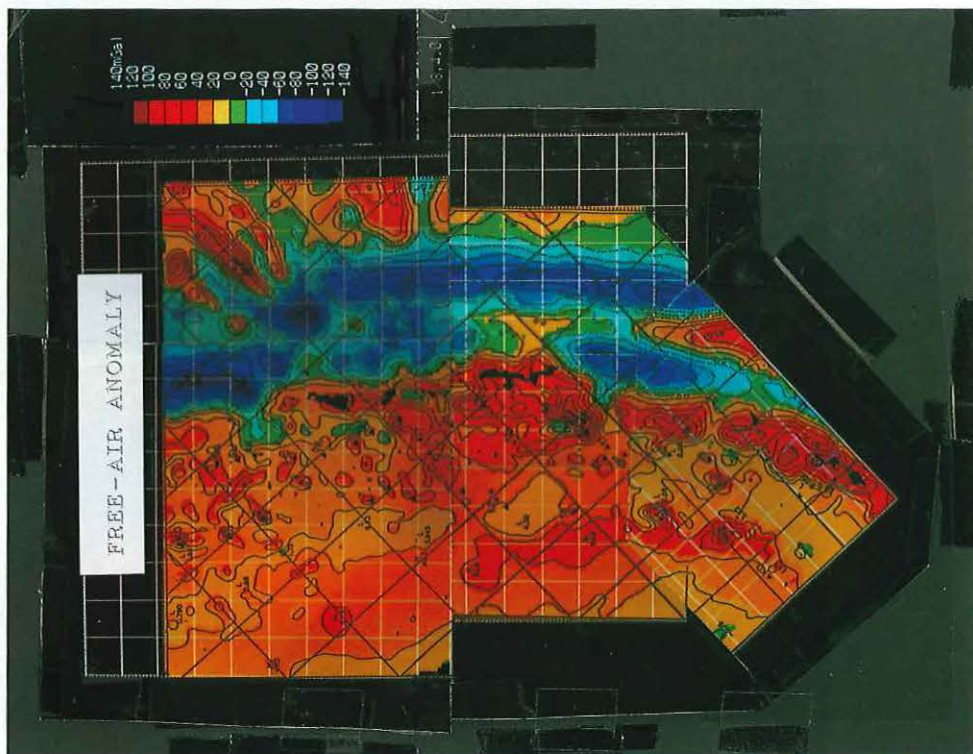
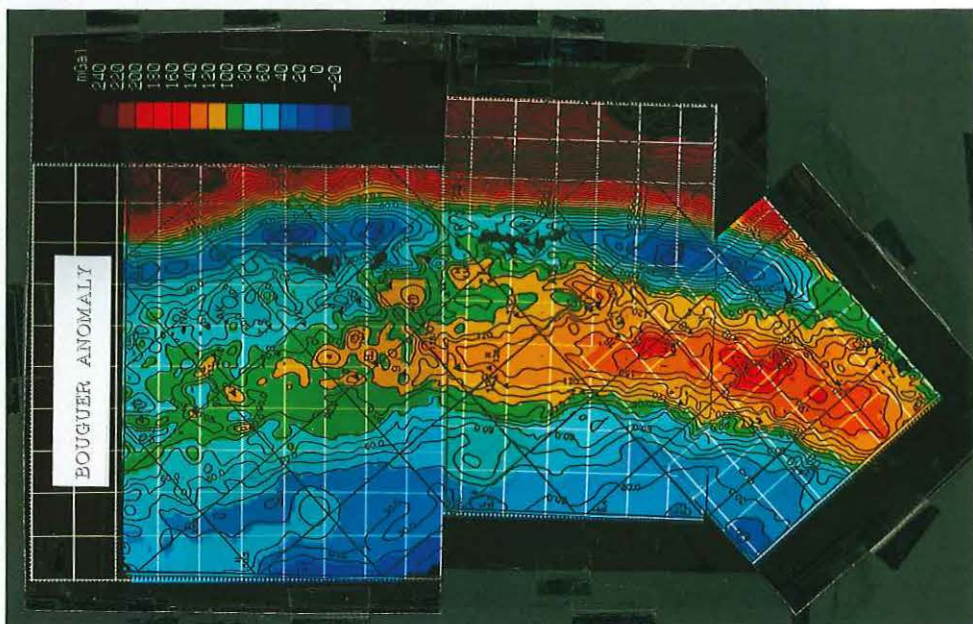
(b): Total intensity magnetic anomaly map (IGRF1985).



(a): Bathymetry.



(c): Free - air gravity anomaly.

(d): Bouguer gravity anomaly ($\rho=2.67g/cm^3$).

REFERENCES

- Aiba, J. and E. Sekiya: Distribution and characteristics of the Neogene sedimentary basins around the Nansei-shoto (Ryukyu Islands), *J. Japanese Assoc. Petroleum Technologists*, **44**, 229–340, (1979 in Japanese with English abstract)
- Aoki, H., T. Tada, Y. Sasaki, T. Ooida, I. Muramatu, H. Shimamura and I. Furuya: Crustal structure in the profile across central Japan as derived from explosion seismic observation, *J. Phys. Earth*, **20**, 197–223, (1972)
- Aoki, H. and A. Ishikawa: On the igneous rocks dredged in the Daito ridge group and the Kyushu-Palau ridge in the GDP cruises, *Geology of the Northern Philippine Sea*, Tokai univ. press, 42–49, (1985)
- Clarke, G. C.: Linear filters to suppress terrain effects on geophysical maps, *Geophysics*, **36**, 963–966, (1971)
- Fujioka, K., B. Taylor, A. Nishimura, M. Koyama, K. Kaiho, K. Tazaki, T. Janecek and scientific party of leg 126: Drilling across the Izu-Bonin Arc, results of ODP Leg 126 cruise, *J. Geography*, **98**, 886–910, (1989 in Japanese with English abstract)
- Fujii, K. and M. Sogabe: Tectonic movement occurred in Hokkaido during the late Miocene and Pliocene time, *Bull. Geol. Surv. Japan*, **29**, 631–644, (1978) in Japanese with English abstract)
- Ganeko, Y. and Y. Harada: Gravity anomalies around Japan, *Rept. Hydrogr. Res.*, **17**, 163–180, (1982)
- Geographical Survey Institute: A new bouguer anomaly map of Japan, *Bull. Geogr. Surv. Inst.*, **29**, 102–103, (1985)
- Geological Survey of Japan, *Geological Atlas of Japan*, (1982)
- Grauch, V. J. S.: A new variable-magnetization terrain correction method for aeromagnetic data, *Geophysics*, **52**, 94–107, (1987)
- Hagiwara, Y.: Relationship between short-wavelength Bouguer anomaly and Earthquake activities in the northeast Japan, *J. Geod. Soc. Japan*, **25**, 209–210, (1979 in Japanese with English abstract)
- Hagiwara, Y.: Pseudomagnetic anomaly derived from gravity observations in Central Japan, *Bull. Earthq. Res. Inst.*, **55**, 27–41, (1980)
- Hagiwara, Y.: Effects of the Pacific and Philippine sea plates on the gravity field in central Japan, *J. Geod. Soc., Japan*, **32**, 12–22, (1986 in Japanese with English abstract)
- Haston, R. B. and M. Fuller: Paleomagnetic data from the Philippine Sea Plate and their tectonic significance, *J. Geophys. Res.*, **96**, 6073–6098, (1991)
- Hatae, N.: On the geology of the Uji Group (Uji Gunto) and the Kusagaki Group of Islands (Kusagaki jima), *J. Geography*, **64**, 14–26, (1955 in Japanese with English abstract)
- Hilde, T. W. C., N. Isezaki and J. M. Wageman.: Mesozoic seafloor spreading in the north Pacific, the Geophysics of the Pacific Ocean Basin and its margin. *Am. Geophys. Union. Geophys. Monogr.*, **19**, 205–226, (1976)
- Hirata, N., H. Kinoshita, H. Katao, H. Baba, Y. Kaiho, S. Koresawa, Y. Ono and K. Hayashi: Report on DELP 1988 Cruises in the Okinawa Trough, Part III: Crustal Structure of the Southern Okinawa Trough, *Bull. Earthq. Res. Inst., Univ. Tokyo*, **66**, 37–70, (1991)
- Hittelman, A. M., R. C. Groman, R. T. Haworth, T. L. Hocombe, G. McHendrie and S. M. Smith: The marine geophysical data exchange

- format—MGD77 (bathymetry, magnetics and gravity), KGRD, No.10, 18pp., Natl. Geophys. and Solar—Terr. Data Cent., NOAA, Boulder, Colo., (1981)
- Hotta, H.: A crustal section across the Izu—Ogasawara Arc and Trench, *J. Phys. Earth*, **18**, 125—141, (1970)
- Hurukawa, N.: Pn Velocity and Moho—offset at the west of Lake Biwa in the Kinki district, Japan, *J. Phys. Earth*, **31**, 33—46, (1983)
- IAGA Division I Working Group 1: International Geomagnetic Reference Field revision 1987, *J. Geomag. Geoelectr.*, **39**, 773—779, (1987)
- Isezaki, N. and H. Miki: A compilation of magnetic data in the northwestern Pacific and in the north Philippine sea, in *Advances in earth and planetary sciences No.6, Geodynamics of the Western Pacific*, J.S.S.P., Tokyo, 403—407, (1979)
- Isezaki, N.: A magnetic anomaly map of the Japan Sea, *J. Geomag. Geoelectr.*, **38**, 403—410, (1986)
- Ishihara, S., Lateral variation of magnetic susceptibility of Japanese granitoids, *J. Geol. Soc., Japan*, **85**, 509—523, (1979)
- Ishihara, T.: Gravity anomalies of the seamounts in the Ogasawara arc, *The Earth Monthly*, **78**, 689—693, (1985 in Japanese)
- JHD (Hydrographic Department of Japan), Magnetic survey of Japan 1984—1985, Data Report of Hydrographic Observations, Series of magnetic survey, **5**, (1988)
- JHD(Hydrographic Department of Japan), the Southern Seas of Nippon, 120th anniversary, (1991)
- Johnson, W. W.: A leastsquares method of interpreting magnetic anomalies caused by two-dimensional structures, *Geophysics*, **34**, 65—74, (1969)
- Kaizuka, S.: Landforms in and around the South Fossa Magna and their tectonic processes of growth, *Quaternary Res.*, **23**, 55—70, (1984 in Japanese with English abstract)
- Kanamori, H.: Seismic and aseismic slip along subduction zones and their tectonic implications, *Island Arcs, Deep Sea Trenches and Back—Arc Basins*, Amer. Geophys. Union, Washington, D.C., 163—174, (1977)
- Kaneoka, I., N. Isshiki and S. Zashu: K—Ar ages of the Izu—Bonin Islands, *Geochem. Jour.*, **4**, 53—60, (1970)
- Karig, D. E.: Structural history of the Mariana Island Arc system, *Geol. Soc. Amer. Bull.*, **82**, 323—344, (1971)
- Kasuga, S., K. Koyama and Y. Kaneko, Geomagnetic and gravity anomalies around the Daito ridge, *Rept. Hydrogr. Res.*, **21**, 65—76, (1986 in Japanese with English abstract)
- Kasuga, S., Y. Kato, S. Kimura, K. Okino, and members of continental shelf survey office: Characteristics of arc-trench system and back-arc basins in the Southern waters of Japan—outline of geophysical survey by Hydrographic Department of Japan, *Rept. Hydrogr. Res.*, **28**, 19—54, (1992 in Japanese with English abstract)
- Katsura, T.: Submarine geology in the vicinity of Tsushima—Goto Retto region, *Rept. Hydrogr. Res.*, **28**, 55—138, (1992 in Japanese with English abstract)
- Kato, M.: Analysis of the gravitational field and the total magnetic field and the subterranean structure corresponding to them, *Rept. Tech. Res. Cent., J.P.D.C.*, **21**, 1—60, (1975a in Japanese with English abstract)
- Kato, M.: the gravitational field, the magnetic field and the subterranean model, *Butsuri—Tansa*, **28**, 210—219 & 220—233, (1975b in Japanese with

- English abstract).
- Kato, S., T. Katsura and K. Hirano: submarine geology off Okinawa Island, Rept. Hydrogr. Res., **17**, 31–70, (1982 in Japanese with English abstract)
- Kato, S.: A geomorphological study on the classification and evolution of trenches around Japan, Rep. Hydrogr. Res., **27**, 1–57, (1991)
- Kawai, N., T. Nakajima and K. Hirooka: The evolution of the Island arc of Japan and the formation of granite in the Circum-Pacific belt, J. Geomag. Geoelec., **23**, 269–293, (1971)
- Kimura, G.: Subduction in the Cretaceous Hokkaido, Kagaku, **55**, 24–31, (1985 in Japanese)
- Kinoshita, H.: Paleomagnetism of sediment cores from Deep Sea Drilling Project Leg 58, Philippine Sea, Init. Repts. DSDP, 58: Washington (U.S. Govt. Printing Office), 765–768, (1980)
- Kinoshita, O. and H. Ito: Cretaceous magmatism in Southwest and Northeast Japan related to two ridge subduction and Mesozoic magmatism along East Asia continental margin, J. Geol. Soc. Japan, **94**, 925–944, (1988 in Japanese with English abstract)
- Kizaki, K.: Tectonics of the Ryukyu Islands Arc., J. Phys. Earth., **26**, Suppl., S302–S307, (1978)
- Kizaki, K.: Geology and tectonics of the Ryukyu islands, Tectonophysics, **125**, 193–207, (1986)
- Kobayashi, K. and M. Nakada: Magnetic anomalies and tectonic evolution of the Shikoku inter-arc Basin, in Advances in earth and planetary sciences No.6, Geodynamics of the Western Pacific, J.S.S.P., Tokyo, 391–402, (1979)
- Konishi, K.: Geotectonic framework of the Ryukyu Islands (Nansei-shoto), J. Geol. Soc. Japan, **71**, 437–457, (1965 in Japanese with English abstract)
- Kubota, R., Sano, S. and Nomura, M.: On the analysis of gravity and magnetic anomalies by a two dimensional Fast Fourier Transform method, abstract at the 1st meeting of Marine survey and technology society, 25–26, (1989 in Japanese)
- Langel, R. A. and R. H. Estes: A geomagnetic field spectrum, Geophys. Res. Lett., **9**, 250–253, (1982)
- Lowrie, W.: Magnetic properties of DSDP basalts, EOS, **54**, 1026–1027, (1973)
- Ludwig, W.J., S. Murauchi, N. Den, P. Buhl, H. Hotta, M. Ewing, T. Asanuma, T. Yoshii and N. Sakajiri: Structure of East China Sea–West. Philippine Sea margin off southern Kyushu, Japan, J. Geophys. Res., **78**, 2526–2536, (1973)
- Maekawa, H. and M. Shozui, T. Ishii: Fore-arc Ophiolite, J. Geography, **98**, 241–251, (1989 in Japanese with English abstract)
- Mizuno, A., Y. Okuda, K. Tamaki, Y. Kinoshita, M. Nohara, M. Yuasa, M. Nakajima, F. Murakami, S. Terashima and K. Ishibashi: Marine geology and geological history of the Daito ridge area, northwestern Philippine Sea, Mar. Sci./Monthly, **7**, 484–491, 543–548, (1975 in Japanese)
- Murauchi, S., N. Den, S. Asano, H. Hotta, T. Yoshii, T. Asanuma, K. Hagiwara, K. Ichikawa, T. Sato, W. J. Ludwig, J. I. Ewing, N. T. Edgar and R. E. Houtz: Crustal structure of the Philippine Sea, J. Geophys. Res., **73**, 3143–3171, (1968)
- Nagamune, T.: Intermediate-depth earthquakes and tectonics of the Kyushu–Ryukyu region, Zisin, **40**, 417–423, (1987 in Japanese with English abstract)
- Ogawa, K. and J. Suyama: Distribution of aeromagnetic anomalies, Volcanoes and Tectonosphere, Tokai. Univ. Press, 207–215, (1975)

- Okubo, Y., M. Urai, H. Tsu, S. Takagi and K. Ogawa: Aeromagnetic anomalies of whole of Japan, *Chishitsu news*, **374**, 48–57, (1985 in Japanese)
- Okuda, Y., Mizuno, A., Tamaki, K. and Nagayama, K.: Tectonic development of the Daito ridges, *Mar.Sci. /Monthly*, **8**, 414–422, (1976 in Japanese)
- Okuma, S., T. Nakatsuka, M. Makino and R. Morijiri: Determination of basement structure offshore of the western Nansei Islands from aeromagnetic data, *Butsuri-Tansa*, **44**, 202–214, (1991 in Japanese with English abstract)
- Oldenburg, D. W.: the inversion and interpretation of gravity anomalies, *Geophysics*, **39**, 526–536, (1974)
- Oosaki, T.: An introduction to spectrum analysis of seismic vibration, *Kashima Pub.*, 260pp, (1976 in Japanese)
- Oshida, A., K. Tamaki and M. Kimura: Origin of the magnetic anomalies in the Southern Okinawa Trough, *J. Geomag. Geoelectr.*, **44**, 345–359, (1992)
- Oshima, S., T. Kondo, T. Tukamoto and K. Onodera: Magnetic anomalies at sea around the northern part of Japan, *Rept. Hydrogr. Res.*, **10**, 39–44, (1975 in Japanese with English abstract)
- Oshima S., T. Kaneko, K. Onodera, H. Nakagawa, T. Tozaki, M. Mishina and J. Ossaka: Geomagnetic anomaly distribution of Iwo-zima, *J. Geography*, **94**, 502–515, (1985 in Japanese with English abstract)
- Oshima, S.: Characteristic features of geomagnetic anomaly distribution around Japan, *Rept. Hydrogr. Res.*, **22**, 41–73, (1987 in Japanese with English abstract)
- Oshima, S., M. Takanashi, S. Kato, M. Uchida, I. Okazaki, S. Kasuga, C. Kawashiri, Y. Kaneko, M. Ogawa, K. Kawai, H. Seta and Y. Kato: Geological and Geophysical survey in the Okinawa Trough and the adjoining seas of Nansei Syoto, *Rept. Hydrogr. Res.*, **24**, 19–44, (1988 in Japanese with English abstract)
- Otofuji, Y., T. Matsuda and S. Nohda: Paleomagnetic evidence for the Miocene counter-clockwise rotation of Northeast Japan—rifting process of the Japan Arc, *Earth Planet. Sci. Lett.*, **75**, 265–277, (1985)
- Otofuji, Y., T. Matsuda and S. Nohda: Brief review of Miocene Opening of the Japan Sea: Paleomagnetic evidence from the Japan Arc, *J. Geomag. Geoelectr.*, **38**, 287–294, (1988)
- Parker, R.L.: the Rapid calculation of potential anomalies, *Geophys. J. R. astr. Soc.*, **31**, 447–455, (1972)
- Petroleum Development Corporation Agency (PDCA), Japan, Report of the test drilling "Sorachi", (1971 in Japanese)
- Petroleum Development Corporation Agency (PDCA), Japan, Report of the test drilling "Nanporo", (1973, in Japanese).
- Quinn, J. M., D. J. Kerridge and D. R. Barraclough: World magnetic charts for 1985—spherical harmonic models of the geomagnetic field and its secular variation, *Geophys. J. R. astr. Soc.*, **87**, 1143–1157, (1986)
- Schouten, H. and K. McCamy: Filtering marine magnetic anomalies, *J. Geophys. Res.*, **77**, 7089–7099, (1972)
- Segawa, J. and S. Oshima: Buried Mesozoic volcanic—plutonic fronts of the northwestern Pacific island arcs and their tectonic implications, *Nature*, **256**, 15–19, (1975)
- Segawa, J.: Gravity anomaly, Crust and Mantle in the Philippine Sea and the surrounding Island

- Arcs, *Mar. Sci./Monthly*, 8, 62–68, (1976 in Japanese)
- Segawa, J. and T. Furuta: Geophysical study of the mafic belts along the margins of the Japanese islands, *Tectonophysics*, 44, 1–26, (1978)
- Seno, T. and S. Maruyama: Paleogeographic reconstruction and origin of the Philippine Sea. *Tectonophysics*, 102, 53–84, (1984)
- Shiki, T., Y. Mizusawa and I. Konda: The Daito ridge group and the Kyusyu-Palau ridge—with special reference to the tectonics of the Philippine Sea—, *J. Phys. Earth*, 27, S113–S124, (1979)
- Shiki, T., A. Mizuno and K. Kobayashi: Data listing of the bottom materials dredged and cored from the Northern Philippine Sea, *Geology of the Northern Philippine Sea*, Tokai univ. press, 23–47, (1985)
- Shiono, K., T. Mikumo and Y. Ishikawa: Tectonics of the Kyushu-Ryukyu Arc as evidenced from seismicity and focal mechanism of shallow to intermediate depth earthquakes, *J. Phys. Earth.*, 28, 17–43, (1980)
- Shimizu, Y.: Magnetic viscosity of magnetite, *J. Geomag. Geoelectr.*, 11, 125–138, (1960)
- Takahashi, E.: Petrologic model of the crust and upper mantle of the Japanese island arc, *Bull. Volcanol.*, 41, 529–547, (1978)
- Tamaki, K. and T. Miyazaki: Rifting in the Bonin Arc, in *Abstracts, International Symposium on recent crustal movement of the Pacific region: Wellington*, Royal Society of New Zealand, 57, (1984)
- Tanaka, M., K. Hiroishi and S. Matsumura: Magnetic anomalies in and around Japan based on aeromagnetic surveys, *J. Geomag. Geoelectr.*, 36, 463–470, (1984)
- Tanaka, M., K. Hiroishi, S. Ando, and S. Matsumura: Aeromagnetic surveys by the Geographical Survey Institute and the magnetic anomalies in and around Japan, *Bull. Geogr. Surv. Inst.*, 30, 1–14, (1986)
- Tatsumi, Y.: Migration of fluid phases and genesis of basalt magmas in subduction zones, *J. Geophys. Res.*, 94, 4697–4707, (1989)
- Tomoda, Y. and Fujimoto, H.: Maps of gravity anomalies and bottom topography in the western Pacific and reference book for gravity and bathymetric data, *Bull. Ocean Res. Inst.*, University of Tokyo, 14, 1–158, (1982)
- Tsunakawa, H.: K-Ar dating of volcanic rocks in the Bonin Islands and its tectonic implication, *Tectonophysics*, 95, 221–232, (1983)
- Ueda, Y.: Geomagnetic anomalies around the Nansei Syoto (Ryukyu Islands) and their tectonic implications, *Bull. Volcanol. Soc. Japan*, 33, 177–192, (1986 in Japanese with English abstract)
- Ueda, Y.: Preliminary study of the geomagnetic structure of the Japanese islands arcs as inferred from aeromagnetic anomalies, *Rept. Hydrogr. Res.*, 26, 189–240, (1990 in Japanese with English abstract)
- Ueda, Y.: A comprehensive analysis method of magnetic and gravity anomalies using response function and its applications, *J. Japan Soc. for Mar. Surv. and Technol.*, 2, 49–60, (1990 in Japanese with English abstract)
- Ueda, Y. and M. Kato: An inversion method for estimation of top and bottom undulations of magnetic layer and its application to aeromagnetic profiles, *J. Geomag. Geoelectr.*, 43, 505–524, (1991)
- Ueda, Y.: Analyses on the continental linear magnetic anomaly based on magneto-gravity response function method, *The earth monthly*, 159, 558–564, (1992 in Japanese)
- Uyeda, S. and M. Richards: Magnetization of four

- Pacific seamounts near the Japanese Islands, Bull. Earthq. Res. Inst., Univ. Tokyo, **44**, 179–213, (1966)
- Uyeda, S. and A. Miyashiro: Plate Tectonics and the Japanese Islands: A synthesis, Geol. Soc. Am. Bull., **85**, 1159–1170, (1974)
- Wagemen, J. M., T. W. C. Hilde and K. O. Emery: Structural framework of East China Sea and Yellow Sea, A.A.P.G. Bull., **54**, 1611–1643, (1970)
- Wasilewski, P. J. and M. A. Mayhew: Crustal xenolith magnetic properties and long wavelength anomaly source, Geophys. Res. Lett., **9**, 329–332, (1982)
- Wasilewski, P. J., H. H. Thomas and M. A. Mayhew: The moho as a magnetic boundary, Geophys. Res. Lett., **6**, 541–544, (1979)
- Watanabe, T.: Heat flow in ocean floor, in Marine Geophysics ed. M. Hoshino, Tokai University press, Tokyo (in Japanese), 57–65, (1972)
- Yamazaki, T., T. Ishihara and F. Murakami: Magnetic anomalies over the Izu-Ogasawara (Bonin) Arc, Mariana Arc and Mariana Trough, Bull. Geol. Surv. Japan, **42**, 655–686, (1991)
- Yoshii, T. and S. Asano: Time-term analyses of explosion seismic data, J. Phys. Earth, **20**, 47–57, (1972)
- Yuasa, M. and F. Murakami: Geology and geomorphology of the Ogasawara arc and the Sofugan tectonic line, J. Geography, **94**, 115–134, (1985 in Japanese with English abstract)
- Yuasa, M. and M. Nohara: Petrographic and geochemical along-arc variations of volcanic rocks on the volcanic front of the Izu-Ogasawara (Bonin) Arc, Bull. Geol. Surv. Japan, **43**, 421–456, (1992)
- Yuasa, M.: Origin of along-arc geologic variations on the volcanic front of the Izu-Ogasawara (Bonin) Arc, Bull. Geol. Surv. Japan, **43**, 457–466, (1992)